Spatial and temporal Modeling of Air Pollutant Source Impacts

A Dissertation
Presented to
The Academic Faculty

by

Xinxin Zhai

In Partial Fulfillment
of the Requirements for the Degree
Doctor of Philosophy in the
School of Civil and Environmental Engineering

Georgia Institute of Technology
December 2017

Spatial and temporal Modeling of Air Pollutant Source Impacts

Approved by:

Dr. James A. Mulholland, Advisor
School of Civil and Environmental Engineering
Georgia Institute of Technology

Dr. Armistead G. Russell, Co-advisor
School of Civil and Environmental Engineering
Georgia Institute of Technology

Dr. Rodney J. Weber
School of Earth and Atmospheric Sciences
Georgia Institute of Technology

Dr. Yongtao Hu
School of Civil and Environmental Engineering
Georgia Institute of Technology

Dr. Heather A. Holmes
Department of Physics
University of Nevada, Reno

Date Approved: 10/30/2017

ACKNOWLEDGEMENTS

I sincerely acknowledge all the wonderful people I have met during my graduate study in Georgia Tech. I would like to thank my advisors, Dr. James Mulholland and Dr. Armistead Russell, for their guidance and mentoring in my PhD research. I would also like to thank my committee members, Dr. Heather Holmes, Dr. Yongtao Hu, and Dr. Rodney Webber, for their suggestions and comments to my research, especially Heather for mentoring me at the beginning of my research. I would like to thank all the members in Dr. Mulholland and Dr. Russell groups in past and present for the collaborations, discussions, and companions in work and life.

I would also like to thank my family and friends for their support during my graduate studies. I would like to thank my parents for being supportive in the past years while I was away from them and not able to visit a lot. I would like to thank my boyfriend, Yufei Zou, for the companion and the help during the hard times and during all times, and for building a better life together with me than I ever had. I would like to thank my best friends, Tianye and Zhuyun, for listening to me and encouraging me the whole time. I would like to than my friends in Atlanta, Fei, Xiaofei, Ran, Sunni, and many others, for all the encouragement, support, and fun in life. Thank Dobby for coming to my life and brings all the fun and love.

TABLE OF CONTENTS

LIST OF TABLES

LIST OF FIGURES

LIST OF SYMBOLS AND ABBREVIATIONS

AMBSLF	ammonium bisulfate
AMNITR	ammonium nitrate
AMSULF	ammonium sulfate
AQS	Air Quality System
ARC	Atlanta Regional Commission's
AREES	Atlanta Roadside Emissions Exposure Study
ASOS	Automated Surface Observing Stations
BC	Black Carbon
BURN	biomass burning
CC	coal combustion
CMAQ	Community Multi-Scale Air Quality
CMB	Chemical Mass Balance
CMB-GC	Chemical Mass Balance with Gas Constraints
CO	carbon monoxide
CSN	Chemical Speciation Network
CTM	chemical transport model
DV	diesel vehicle
EC	Elemental Carbon
EPA	Environmental Protection Agency
FP	fuzzy points
GV	gasoline vehicle
HDDV	heavy duty diesel vehicle
IMPROVE	Interagency Monitoring of Protected Visual Environments Network
IMSI	**Integrated Mobile Source Indicator Method**

JST	Jefferson Street Site
LDGV	light duty
LSPM	Lomb-Scargle Periodogram Method
LUR	land-use regression model
MOVES	Motor Vehicle Emission Simulator
NAAQS	National Ambient Air Quality Standards
NEI	National Emissions Inventory
NMB	normalized mean bias
NOx	nitrogen oxides
NRMSE	normalized root mean square error
OC	organic carbon
OTHROC	unapportioned organic carbon
PM2.5	fine particulate matter
PMF	positive matrix factorization
PSD	passive sampler detector
R-LINE	Research-Line Model
SDK	South DeKalb site
SDUST	suspended dust
SEARCH	Southeast Aerosol Research and Characterization
SMOKE	Sparse Matrix Operator Kernel Emissions System
SOC	secondary organic carbon
STAR	STability ARray
tor	thermal optical reflection
tot	thermal optical transmittance
TRAPs	traffic-related air pollutants
VOCs	volatile organic compounds
YRK	Yorkville site

SUMMARY

Ambient air pollution is found to be associated with human mortality and morbidity. In this study, I developed and employed multiple air quality modeling techniques provide temporally and spatially resolved information on source impacts and pollutant concentrations.

I applied the Chemical Mass Balance (CMB) receptor model that uses observational data to quantify source impacts in the State of Georgia. The results show that $PM_{2.5}$ total mass concentrations decreased from 13.8 $\mu g/m^3$ to 9.2 $\mu g/m^3$ averaged across all sites from 2002 to 2013. The secondary sulfate and nitrate species decreased by 58% and 44%, respectively. Total mobile source impacts decreased more at urban sites (39%) than rural sites (23%)。 Biomass burning impacts decreased more at rural sites (34%) than urban sites (27%). The observation-based estimates provide source impact trends and levels but are limited by the spatial and temporal coverage. In addition, the mobile source is found to be a major primary source and more information about mobile sources can help understand their impacts on human health.

To understand mobile source impacts on $PM_{2.5}$ at finer spatially and temporally scales, I developed an approach using EC, CO, and NO_x measurements as indicators of mobile source impacts based on an integrated mobile source indicator (IMSI) method. I extended the method in three aspects for better spatial resolution, 1) using 24-hr average pollutant concentrations estimated at 4km and 12km resolutions, 2) using spatially-resolved emissions instead of county-level emissions in the IMSI formulation, 3) spatially

calibrating the unitless indicators based on annual average mobile source impacts estimated by CMB. The generated total mobile and separate vehicle source impacts agree well with daily CMB results for 2002 to 2010 in Georgia, with high temporal correlations and low biases. Overall, this approach provides mobile source impacts that are similar to observation-based estimates but at finer spatial and temporal resolutions. The daily mobile source impacts generated in this study are being used to improve assessment of air pollution health effects.

At city-level, source and pollutant exposure assessment requires much finer resolution data. A common method to estimate the city-scale and fine resolution primary pollutant concentration is dispersion model, such as the newly developed Research LINE-source (RLINE) dispersion model for near-surface emission releases. I developed a procedure that generates observation-calibrated hourly concentrations of $PM_{2.5}$, CO, and NO_x from mobile sources using RLINE at 250m resolution in the 20-county Atlanta area. In the procedure, I used a computationally efficient annual average approach and calibrated RLINE concentrations with observational data. Our results show that RLINE overestimated the annual averages of CO and NO_x daily 1-hour maximum concentrations by factors of 1.3 and 4.2 on average, respectively, and $PM_{2.5}$ mobile source impacts by a factor of 1.8 compared with estimates by CMB with gas constraints. Based on observational data, I calibrated the RLINE estimates of CO, NO_x, and $PM_{2.5}$ emitted by mobile sources from 2002 to 2011 at multiple sites. The calibration largely reduced modeling biases. The calibrated results agree well with the pollutant fields from observation-blended 12-km resolution Community Multi-scale Air Quality (CMAQ) model fields of CO and NO_x with Pearson correlation R^2 values of 0.55 for CO and 0.54 for NO_x, respectively. The calibrated

fields of $PM_{2.5}$ were compared with 4-km resolution mobile source impact fields by the extended IMSI method with an R^2 value of 0.53. The method has been applied in air quality planning efforts. The pollutant concentration fields were used in health exposure studies and helped evaluating the health impact of air pollution exposure for pregnant women and pediatric respiratory disease.

In the trafficked and populated areas of cities, the accuracy of spatial gradients of ambient air pollutant concentrations near roadways are critical for fine scale exposure assessment. In this study, I measured and simulated the spatial gradients near-road and evaluated the estimate of the RLINE modeling results. I first characterized the spatial gradients of two-week averaged near-road pollution for NO_x, CO, $PM_{2.5}$, and eight volatile organic compounds (VOCs) using passive sampler detectors (PSD) and dispersion model RLINE in Atlanta, GA. I found that the spatial gradients show a decrease of up to 3.1 fold from highway adjacent areas (<100m away from highway) to remote areas (>1500m away from highway) for all pollutants in the PSD measurements and up to 4.2 fold in RLINE estimates. As there was no measurement for CO or $PM_{2.5}$ by PSD, I compared the correlation of paired pollutants from same sources to check the simulation performance of RLINE. The comparisons show good correlations for NOx estimated by RLINE with NOx measured by PSD, CO by RLINE with benzene by PSD, and $PM_{2.5}$ by RLINE with m-xylene by PSD, indicating RLINE captures the spatial variations well. However, the comparison of NOx shows RLINE yielded larger spatial gradients and higher concentration levels. After calibrating RLINE estimation using the PSD measurements, the near-road spatial gradients of NO_x were well captured. This study reveals the near-road spatial gradients for NO_x and VOCs and calibrates the RLINE estimates of NO_x to observation levels for use in health

exposure studies. In addition to the two-week average near-road gradients, I also evaluated sampling representativeness of fixed monitors for the surrounding areas by comparing spatio-temporal variations of NOx, NO_2, black carbon (BC), and $PM_{2.5}$ measured by nephelometer. The results show that the fixed monitors can represent the pollution condition in surrounding ~600m radius areas.

Overall, this research developed and evaluated multiple modeling techniques that simulate concentrations and source impacts at different temporal resolutions and spatial scales with a focus on the mobile sources. These approaches help improve the estimation of fine-scale concentration fields by calibrating modeling results to observational levels with better spatial and temporal coverage. The methods are being applied in studies in different areas and years, and the generated concentration fields have helped evaluating the health impacts of air pollution on the cohort in Georgia.

CHAPTER 1. INTRODUCTION

The association between ambient air pollution and human mortality and morbidity has become a concern worldwide (Brook et al., 2010; Gill et al., 2011; Lim et al., 2012; Stanek et al., 2011). While air pollution has been regulated and controlled in many regions of the world, mortality attributable to air pollution is still increasing (Lim et al., 2012). In particular, the fine particulate matter ($PM_{2.5}$ with size $\leq$2.5μm) is of the most concern as its concentrations are still increasing in many regions of the world with broad health impacts on pregnant women, children, and all other vulnerable populations (Chen et al., 2015; Pennington et al., 2017a; Strickland et al., 2010). It's been found that exposures to $PM_{2.5}$ in short terms (e.g., from hours to weeks) and long-terms (e.g., years) are associated with cardiorespiratory disease and mortality (Brauer et al., 2016; Cohen et al., 2005; Kioumourtzoglou et al., 2016; Lelieveld et al., 2015; Pennington et al., 2017a; Strickland et al., 2010). The health impact of $PM_{2.5}$ can be tracked to specific emission sources and in return help in source control policy. This leads to increasing interest in the source impact study of $PM_{2.5}$ (Andersson et al., 2015; Liu et al., 2016; Wang et al., 2014) and the link of source impacts with health effects. For further investigation of the linkage in health and source impacts, accurate estimates of the spatial and temporal distributions of source impacts are needed.

Typically, source impacts on $PM_{2.5}$ can be estimated using source apportionment receptor-based models, such as the chemical mass balance (CMB) model (EPA, 2004a) and the positive matrix factorization (PMF) method (Paatero and Tapper, 1994). Receptor-based models use the measurements of $PM_{2.5}$ species to retrieve the source contributions to total

mass. The Chemical Mass Balance (CMB) model is a wide used receptor model based on specified source profiles (EPA, 2004a; Watson et al., 1984). The receptor models are assumed to capture the actual level of source impacts but their applications are limited by the availability of the field measurements. For better spatial and temporal coverage, emission-based source apportionment models are also used for source impact analysis such as Community Multiscale Air Quality model with Decoupled Direct Method (CMAQ-DDM) (Dunker et al., 2002; Napelenok et al., 2006; Zhang et al., 2012). The conceptual models use simulated emissions and meteorology information and can subject to large errors because of the uncertainties in the simulations. To combine the advantage of observation-based receptor models and the emission-based models, several methods have been developed that assimilate model simulations and field measurements for both concentrations and source impacts (Beckerman et al., 2013; Friberg et al., 2016a; Ivey et al., 2015; Redman et al., 2016; Sturtz et al., 2014; Zhai et al., 2016).

The health impact of traffic related air pollution is of particular interest because mobile vehicles are the most common sources in highly populated regions and has been found to be associated with asthma in children and other diseases (Brauer et al., 2008; Gehring et al., 2010; Pennington et al., 2017a). Motor vehicles are major sources of elemental carbon (EC) and organic carbon (OC) in $PM_{2.5}$ emissions, and gas phase pollutants such as carbon monoxide (CO) and nitrogen oxides (NOx). These pollutants have been used as surrogate of mobile vehicle impact and been found to be associated with adverse health effects in several studies (Chen et al., 2013; Delfino et al., 2006; Nordling et al., 2008). The impact of mobile source on human health are being investigated using and pollutant concentration metrics and source impact metrics. Other than the receptor models and emission-based

source apportionment models, multi-pollutant metrics and dispersion models are also used to estimate the mobile source related impacts for different regions at multiple resolutions (Oakes et al., 2014b; Pachon et al., 2012; Zhai et al., 2016). Multipollutant metrics can be more related with potential health effects than direct source impacts in some cases (Dominici et al., 2010; Hidy and Pennell, 2010; Johns et al., 2012). An emission-based Integrated Mobile Source Indicator (IMSI) using observed concentrations and estimated emissions of CO, NO_x, and EC was developed to generate a unitless indicator of mobile source impacts. The mobile indicator by this method was found to be significantly correlated with health outcomes at multiple locations (Oakes et al., 2014b; Pachon et al., 2012), but it does not reflect the actual spatial variation levels in source impacts. For capture of the source impact levels, further calibration is needed.

For the city-level and neighborhood-level simulations of traffic source impacts, the spatially sparse observations limit the ability of receptor models in capturing the spatial coverage, while the accuracy and relatively coarse resolution of chemical transport models (CTM) limit the utility in capturing the highly variated actual exposure to traffic sources. For such fine scale and high-resolution exposure information, dispersion model Research-Line (R-LINE) can be used (Batterman et al., 2015; Chang et al., 2015; Zhai et al., 2016). R-LINE is a steady-state plume model and designed for line sources with a new plume meandering algorithm for light wind conditions (Snyder et al., 2013; Venkatram et al., 2013). However, dispersion models in general are found to overestimate the pollutant concentrations (Venkatram et al., 2004). The evaluation of the R-LINE is needed for it's accuracy in capturing the spatial variation and concentration levels.

The objective of this research is to reduce the limitations in air quality models by extending the spatial resolutions for different spatial scales and calibrating the biased modeling results to observational levels for better accuracy. This research provides multiple modeling techniques with focus on mobile sources. The proposed methods are able to generate fine-resolution concentrations and source impacts with relatively low bias. The long-term data generated from this research allow for the spatial analysis of health data to assess pollutant exposure risks of susceptible and vulnerable populations. The methods help reveal spatial and temporal air pollution characteristics for better understanding of air quality and its impact on human health.

Chapter 2 presents the source impacts on $PM_{2.5}$ for 9 sources using receptor model CMB at 13 sites in Georgia for 2002 to 2013. The analysis shows the contributions of each source in the decrease over time and the long-term and short-term trends of the sources. Chapter 2 shows that mobile sources are important primary sources and in Chapter 3, I further investigated the source impacts of mobile vehicles by developing an extended IMSI approach. This approach extends the original IMSI to a spatial application and calibrates the unitless indicators with CMB estimated mobile source impacts on $PM_{2.5}$. I applied the approach and generated daily mobile source impacts for Georgia from 2002 to 2008 in 12km resolution and 2008 to 2010 in 4km resolution. In Chapter 4, finer resolution annual average concentration fields are generated using an annual average approach based on R-LINE estimation and field observations. The comparison of R-LINE with observations in Atlanta shows that R-LINE overestimates the spatio-temporal distributions but captures the variation well. I developed a calibration method for R-LINE using the observations and generated 250m resolution annual concentration fields for NOx, CO, and $PM_{2.5}$ for 2002 to

2011. The results show decreased bias compared to observations but higher spatial resolution. In Chapter 5, I characterized the near-road spatial gradients using R-LINE and near-road measurements by passive detector samplers for two-week averages. The results of modeling and measurements both show high spatial gradients from near-road to far-road, with good agreement in the variations of the two methods. However, the spatial gradients and concentrations are both overestimated by R-LINE. After calibrating R-LINE to the measurements, R-LINE can capture the spatial gradients well. In addition, I compared the fixed monitor observations with the mobile platform measurements surrounding the monitor and found that the monitors are representative of the air pollution in the surrounding areas. Overall, this study uses multiple modeling techniques for estimation of traffic related air pollution in spatial scales from state-level to neighborhood-level. The generated concentration fields lay the foundation of the health impact study of air pollution exposure.

CHAPTER 2. SPATIAL AND TEMPORAL SOURCE APPORTIONMENT OF PM2.5 IN GEORGIA, 2002 TO 2013

As published in Atmospheric Environment 161 (2017): 112-121.

Abstract

The Chemical Mass Balance (CMB) receptor model was applied to estimate $PM_{2.5}$ source impacts over Georgia from 2002 to 2013 using ambient $PM_{2.5}$ species concentration data from 13 sites. Measurements of 19 $PM_{2.5}$ species were used as inputs along with measurement-based source profiles to estimate the impacts of nine sources, including both primary components (from heavy duty diesel vehicle, light duty gasoline vehicle, biomass burning, coal combustion, and suspended dust sources) and secondary pollutants (ammonium sulfate, ammonium bisulfate, ammonium nitrate, and secondary organic carbon). From 2002 to 2013, $PM_{2.5}$ total mass decreased from 13.8 $\mu g/m^3$ to 9.2 $\mu g/m^3$ averaged across all sites, a 33% decrease. Largest decreases were observed for secondary sulfate and nitrate species (58% and 44%, respectively). The amount of neutralization by ammonium did not change substantially over the time period in spite of substantial decreases in sulfate and nitrate concentrations. Total mobile source impacts decreased more at urban sites (39%) than rural sites (23%), whereas biomass burning decreased more at rural sites (34%) than urban sites (27%). The estimated central-site source impacts are found to spatially represent large areas for secondary pollutants, smaller areas for biomass burning and dust, and very local areas for mobile sources and coal combustion. Trends from the National Emissions Inventory were compared with the annual trends of mobile

source impacts, coal combustion impacts, and sulfate concentrations, resulting in statistically significant positive trends with Pearson R^2 of 0.80, 0.64, and 0.79, respectively. Results presented here suggest that $PM_{2.5}$ reductions in Georgia and the Southeast have been achieved by control of both stationary and mobile sources, and that $PM_{2.5}$ is comprised of increasing fractions of biomass burning emissions and suspended dust. The temporal trends of source impacts at each site adds information about source changes beyond the every-three-year emission inventories for evaluation of emission-based model results.

2.1 Introduction

Ambient air quality has been found to be associated with adverse increased health effects (Brook et al., 2010; Gill et al., 2011; Lim et al., 2012; Stanek et al., 2011). Short-term exposures to fine particulate matter ($PM_{2.5}$) (e.g., from hours to weeks) are found to be associated with acute cardiorespiratory morbidity (Brook et al., 2010; Miller et al., 2007; Sarnat et al., 2008), and long-term exposure (e.g., years) is associated with mortality (Lelieveld et al., 2015; Mar et al., 2006). In particular, elevated $PM_{2.5}$ levels are found to impact the health of children, as children have higher exposures than adults due to longer duration of outdoor activities (Bateson and Schwartz, 2008; Salvi, 2007). While air quality has improved in many regions of the world, deaths attributable to ambient particulate matter worldwide increased from about 2.9 million in 1990 to 3.2 million in 2010 (Lim et al., 2012). In addition to the impacts on human health, $PM_{2.5}$ affects the broader environment such as atmospheric visibility (e.g., (Kim et al., 2006; Lin et al., 2014; Poschl, 2005; Schichtel et al., 2001; Shen et al., 2015)) and interacts with climate (e.g., (Poschl, 2005; Zou et al., 2017)). The interactions of $PM_{2.5}$ with health, visibility and climate are

highly source specific, which has led to increased interest in investigating the source impacts of $PM_{2.5}$ (Andersson et al., 2015; Liu et al., 2016; Wang et al., 2014).

$PM_{2.5}$ is a complex mixture of components that are emitted by different sources. Epidemiologic studies have investigated the associations of adverse health effects with total $PM_{2.5}$ (Lelieveld et al., 2015; Wesson et al., 2010), $PM_{2.5}$ source contributions (Brauer et al., 2008; Chen et al., 2013; Nordling et al., 2008), and combinations of $PM_{2.5}$ constituents with other pollutants (Oakes et al., 2014a; Pachon et al., 2012). Increasingly, attention is being drawn to link the health effects of source impacts to emission controls and regulations, driving a desire for accurate estimates of the spatial and temporal distributions of source impacts.

Emissions, such as those provided by the National Emissions Inventory (NEI) (Environmental Protection Agency, 2016) at the county level, reflect the source changes over time and space. For several sources, emission trends are found to be correlated with concentrations of tracer species (Hidy et al., 2014). Such tracer species concentrations can be used to evaluate the emission changes for certain sources. However, they are still not quantitatively reflecting direct source impacts.

Source impacts on $PM_{2.5}$ are typically estimated using receptor-based and emission-based source apportionment models (Chan et al., 2008; Held et al., 2005; Ito et al., 2004; Lee et al., 2008b; Liu et al., 2010b; Marmur et al., 2006; Querol et al., 2007; Shi et al., 2009; Shi et al., 2011; Viana et al., 2008; Wang et al., 2012b; Watson et al., 2015; Zheng et al., 2002). Receptor-based models use the components of $PM_{2.5}$ to infer the contributions of sources to total $PM_{2.5}$ concentrations. A widely used receptor model, the Chemical Mass Balance

(CMB) model, is based on specified source profiles and measured concentrations (EPA, 2004a; Watson et al., 1984). The estimated source impacts are assumed to reflect the actual level of impact but the model's dependence on measurements limits the application to locations with speciated $PM_{2.5}$ measurements. When receptor-based results at central monitors are used to represent a region in exposure studies, their spatial representativeness needs evaluation.

Emissions-based source apportionment models are also used to estimate source impacts (Dunker et al., 2002; Napelenok et al., 2006; Odman et al., 2002). The models typically provide much more complete results than measurements, both spatially and temporally, but these results are subject to potentially large errors due to uncertainties in the simulated meteorology, chemistry, and emissions data. A number of methods have been developed that combine model simulations and field measurements for both concentrations and source impacts (Beckerman et al., 2013; Friberg et al., 2016a; Ivey et al., 2015; Redman et al., 2016; Sturtz et al., 2014).

In this research, we estimated the daily source impacts on $PM_{2.5}$ using CMB for nine sources at 13 monitoring locations in Georgia over 2002 to 2013. We investigated the long-term changes of $PM_{2.5}$ composition and $PM_{2.5}$ source impact changes and compared the trends of sources with data from the National Emissions Inventory (Environmental Protection Agency, 2016). For use in health studies, we characterized the spatial representativeness of the sites for each source. The source impact results support ongoing studies of source exposure impacts on acute health effects. The trends analysis is being used to support policy outcome assessment studies for air quality management.

2.2 Methods

We applied CMB version 8.2 (EPA, 2004a) with measurement-based source profiles (Marmur et al., 2005) for 9 sources at 13 $PM_{2.5}$ speciation monitoring sites in Georgia as described below using data from 2002 to 2013.

2.2.1 $PM_{2.5}$ Species Data

The CMB application used measured concentrations of $PM_{2.5}$ species, including the major five species sulfate (SO_4^{2-}), nitrate (NO_3^-), ammonium (NH_4^+), elemental carbon (EC), and organic carbon (OC), and 14 trace metal species (Al, Br, Ca, Cu, Fe, K, Mn, Pb, Sb, Se, Si, Sn, Ti, and Zn). We used 24-hr ambient concentrations of $PM_{2.5}$ total mass and these 19 species available from 2002 to 2013 at 11 sites in Georgia and 2 sites at the borders of Georgia with Florida and Tennessee (Fig. 1). Nine sites are from the Chemical Speciation Network (CSN) (EPA, 2011), two sites from the Interagency Monitoring of Protected Visual Environments (IMPROVE) monitoring network (Malm, Schichtel, and Pitchford 2011), and two sites from the Southeast Aerosol Research and Characterization (SEARCH) network (Edgerton et al., 2006; Malm et al., 2011). CSN sites are located in urban areas and provide data every three days at the South DeKalb (SDK) site in Atlanta and every six days at the other sites in Georgia (Athens, Columbus, Macon, Augusta, Rome, and Douglas) as well as in Chattanooga near the Georgia-Tennessee border and Tallahassee near the Georgia-Florida border. The IMPROVE sites provide data every three days at two rural locations in Georgia (Murray and Charlton). Data are available daily from two SEARCH sites in Georgia, one an urban site at Jefferson Street (JST) in midtown Atlanta and the other a rural site in Yorkville (YRK). The two IMPROVE sites do not provide

measurements of NH_4^+, Sb, and Sn. The two SEARCH sites do not provide measurements of Sb and Sn. The NH_4^+ concentrations at IMPROVE sites are estimated using linear regression relationships of SO_4^{2-} and NH_4^+ neutralized by SO_4^{2-} at nearby sites (details are in Fig. A8).

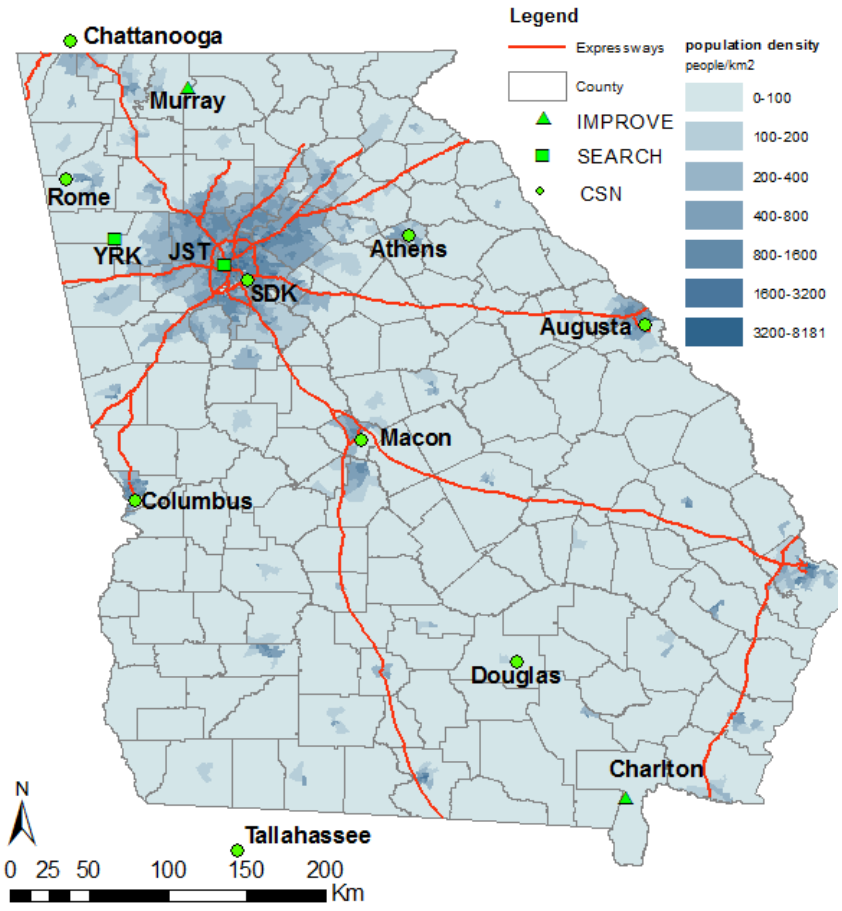

Figure 1 Monitors with PM2.5 species concentrations in Georgia.

OC and EC were measured by either thermal optical transmittance (TOT) or thermal optical reflection (TOR) (Chow et al., 1993). The two methods split the organic carbon and elemental carbon differently (Malm et al., 2011). The TOT method was used for OC/EC measurement until April 2007 at two CSN sites, Columbus and Macon, and then by the TOR method. The other CSN sites switched from the TOT method to the TOR method in

April 2009. The two IMPROVE sites and two SEARCH sites used the TOR method throughout 2002 to 2013. We converted the concentrations measured by the TOT method to TOR equivalent levels using the method developed by Malm et al 2011 (Malm et al., 2011) that accounts for seasonal differences. The converted OC concentrations in TOR are highly correlated with the measured OC in TOR, but with some difference in the daily variations, which leads to some difference in the daily variations of source impacts, mainly OTHEROC and HDDV. The OC/EC concentrations are blank-adjusted, as described in SI.

CMB requires uncertainties as weighting factors for optimization. The IMPROVE network reported uncertainties for EC and OC thermal fractions, based on which the uncertainty of total EC and OC are calculated. When uncertainties were not directly reported, we followed the EPA guidance for evaluating uncertainties using detection limit information and concentrations (EPA, 2011; Taylor and Kuyatt, 1994).

2.2.2 CMB Model

In the CMB modeling approach, species concentrations of $PM_{2.5}$ at receptor locations and predetermined source profiles based on emission information are used to solve mass conservation equations (EPA, 2004a). The choice of source profiles introduces uncertainties since the number and composition of sources may change with region and season. Selecting a representative source profile is important for the accuracy of results. Different techniques have been applied to provide source profiles, such as measurements (Chow et al., 2004), Bayesian-based ensemble method (Balachandran et al., 2013) and optimization methods (Balachandran et al., 2012; Blanchard et al., 2012; Cesari et al., 2016; Marmur et al., 2007).

In this work, we used a set of source profiles summarized by Marmur et al. (2005) which have been developed for applications in the southeastern U.S. and have been utilized in multiple studies (Balachandran et al., 2013; Redman et al., 2016); see more details in Appendix. This approach has limitations for a large study area and a 12-year study period, but is reasonable for our goal of providing data for use in long-term health effect studies in Georgia for consistency over the time period. We wanted to avoid uncertainties and interpretation issues associated with using source profiles that vary over time and space. More discussion of the limitations of using a single set of source profiles is presented in this paper following presentation of results. Also, since Sn and Sb are not reported for SEARCH and IMPROVE sites, and because their concentrations are often near or below their detection limits, we evaluated whether including those species for data from CSN sites influenced the results significantly and found that they had a negligible impact.

The sources contributing to primary $PM_{2.5}$ included were light duty gasoline vehicle (LDGV), heavy duty diesel vehicle (HDDV), biomass burning (BURN), coal combustion (CC), and suspended dust (SDUST). Measurement profiles for LDGV and HDDV were from Chow et al. (2004). The mass fractions of secondary pollutants formed in the atmosphere are grouped as ammonium sulfate (AMSULF), ammonium bisulfate (AMBSLF), ammonium nitrate (AMNITR), and unapportioned organic carbon (OTHROC), which is assumed to be largely secondary organic carbon (SOC). These groupings are used to account for their mass fraction in $PM_{2.5}$ and are not meant to imply anything about aerosol mixture status in the atmosphere; that is, atmospheric aerosols are complex mixtures derived from sources as well as from physical and chemical atmospheric processing.

2.2.3 Spatial and Temporal Trend Analysis

Seasonal characteristics in temporal trends were investigated using Lomb-Scargle Periodogram Method (LSPM) spectral analysis (Balachandran, 2013). LSPM allows for the spectral density analysis in unevenly sampled data (Press and Rybicki, 1989); in this case, monitoring data at 11 out of the 13 sites collected every three or six days. The LSPM analysis returns the periodicity of a time series and helps identify the significant seasonality characteristics of the time series. Periods with statistical significance of 0.05 ($\alpha<0.05$) are identified.

In addition to statistical period analysis, running averages were calculated to track the actual trends within a year. For each day in a year, the value is calculated as the average of 30 days, i.e., 14 days prior and 15 days later. The days when no more than 50% of days within the 30-lag days were available were removed. We averaged the running average for 12 years (for each day in a year, 12 values from 12 years are used) to present the trends in a typical year.

Ordinary kriging was used to spatially interpolate the ratio of sulfate neutralization. Ordinary kriging is a geostatistical method that spatially interpolates data for a continuous surface of estimates (Cressie, 1988). In this study, we used MATLAB and the mGstat toolbox in MATLAB to calculate the exponential semivariograms in the kriging process. The estimated ratios are used as known data to estimate the values at each 4km by 4km grid in the Georgia domain. The generated surfaces are assumed to represent the spatial pattern of the ratio distribution.

2.3 Results and Discussion

2.3.1 $PM_{2.5}$ Species Concentration Trends

12-year averaged concentrations of $PM_{2.5}$ components varied from about 8.2 to over 13.5 $\mu g/m^3$ (Fig. 2), with the highest level found at JST in Atlanta, while the two IMPROVE sites located in rural areas had the lowest total concentrations (8.7 $\mu g/m^3$ for Murray and 8.2 $\mu g/m^3$ for Charlton). EC, largely from mobile sources, and metals were lowest at the three rural locations (YRK, Murray, and Charlton). Metal concentrations (Fig. A1 of SI), particularly calcium and zinc, were highest in Macon where there are several nearby coal-fired power plants, cement kilns, and metal processing plants.

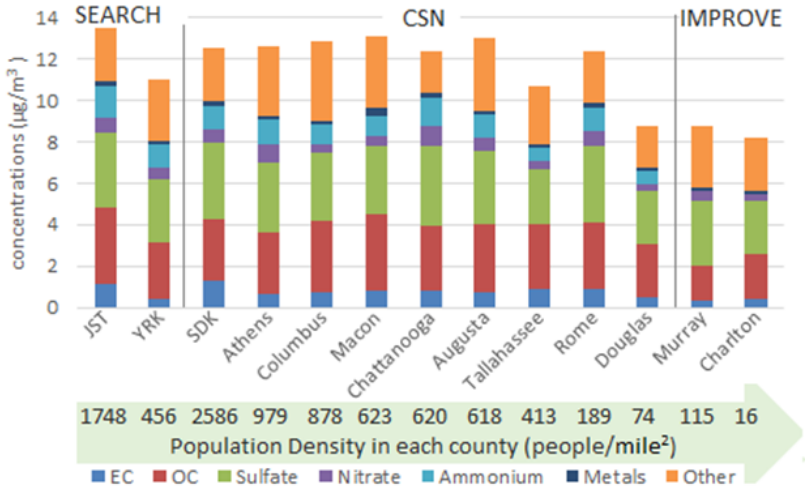

Figure 2. $PM_{2.5}$ total mass and species concentrations, averaged over 2002 to 2013 for each site. Sites are ordered by SEARCH, CSN, and IMPROVE and then county-level population density (2010). Other mass is defined as the total mass minus the sum of the listed species. Ammonium is included in other mass at the two IMPROVE sites.

The annual average $PM_{2.5}$ total mass averaged across all sites decreased significantly (p-value <0.001), from 13.8 $\mu g/m^3$ in 2002 to 9.2 $\mu g/m^3$ in 2013 (trends in species concentrations can be found in Figs. S1 and S2). On average, larger decreases were observed at urban sites (a drop of 4.8 $\mu g/m^3$ from 2002 to 2013 averaged across urban sites)

than at rural sites (a drop of 3.8 μg/m^3 averaged across rural sites). The maximum and minimum decreases occurred at JST (6.2 μg/m^3) and Charlton (2.6 μg/m^3), respectively. Over the 12 years, the difference between urban sites and rural sites is decreasing, suggesting that $PM_{2.5}$ concentrations at urban sites are approaching a background level.

As the three secondary inorganic ion concentrations have decreased substantially over time, the degree of neutralization of the particles may also have changed. The neutralization status of sulfate is sometimes estimated by molar ratio of ammonium to sulfate after removing ammonium associated with nitrate ($R_{SO4} = ([NH_4^+] - [NO_3^-]) / [SO_4^{2-}]$); here, large R_{SO4} values (near two) represent a high degree of neutralization and low R_{SO4} values (near one) represent low degrees of neutralization. When R_{SO4} is lower than 1, it may be due to insufficient ammonium to neutralize both sulfate and nitrate and/or the presence of other cations, such as sodium. This ratio is not a surrogate for aerosol pH (Weber et al., 2016), but is informative of how the three species (sulfate, nitrate, and ammonium) interact with gas phase precursors. R_{SO4} average levels over the 12-year period range from 0.5 to 1.8 across the nine CSN sites and 1.2 to 2.0 at the two SEARCH sites (Fig. A3). The different ranges at CSN and SEARCH sites are likely due to different measurement methods and treatment of artifacts (See Fig. A4 and description in SI for more information).

R_{SO4} decreased significantly over time ($p < 0.001$) at all sites, with a rate of decrease ranging from 0.026 unit/yr to 0.043 unit/yr (Fig. A3). The decreasing trend is consistent with R_{SO4} ratios found at six SEARCH sites in a broader region including four states in the southeastern US (Hidy et al., 2014), indicating that the ammonium bisulfate fraction is increasing over time in the southeastern US, corresponding to a more acidic aerosol (Weber

et al., 2016), in spite of decreasing sulfate and SO_2 emissions. This has been attributed to lower ammonium concentrations when sulfate concentrations are low, shifting the equilibrium of ammonia toward the gas phase (Weber et al., 2016). There is little evidence of nitrate replacement of sulfate in the aerosol.

Spatially, R_{SO4} is higher in north Georgia and lower in the south (Fig. A5, fields calculated using ordinary kriging method) and the pattern is consistent over the years. This spatial trend can be related to the spatial pattern of fuel combustion emissions by electricity generator units (EGUs) as EGU emissions have major impacts on components like sulfate and nitrate. $PM_{2.5}$ emissions from fuel combustion by EGUs in the 2011 NEI (Fig. A6) were higher in counties located in northern Georgia than those in the south. A similar spatial pattern was observed from six locations in the southeast US (Hidy et al., 2014) where the lowest R_{SO4} values were found at the most southern sites (Gulfport and Oak Grove, Mississippi) and highest R_{SO4} values were found at the most northern sites (JST and YRK, Georgia).

2.3.2 $PM_{2.5}$ Source Impact Trends

2.3.2.1 Source impact composition

The majority of the mass of $PM_{2.5}$ was allocated to sources using CMB (86% of $PM_{2.5}$ averaged across all sites and all years), with the rest of the mass unapportioned (Fig. 3). Of the identified sources, secondary pollutants that are formed in atmospheric reactions, i.e., ammonium sulfate, ammonium bisulfate, ammonium nitrate, and other OC, were the major

contributors to $PM_{2.5}$ mass, comprising about 57% of total mass. Sources that contribute to primary $PM_{2.5}$ were estimated to contribute 29% to the $PM_{2.5}$ mass.

Biomass burning comprised 40% of the total impact on primary $PM_{2.5}$. It is the largest contributor to primary $PM_{2.5}$ at the two rural sites, Murray (54% of primary impacts) and Charlton (55%). Mobile sources, light duty gasoline vehicle and heavy duty diesel vehicle, comprised 37% of the total primary impacts. They are the largest contributors to primary $PM_{2.5}$ at the three Atlanta sites, JST (53%), YRK (43%), and SDK (48%), as well as Chattanooga (50%). At the two rural sites, mobile sources are only 23% (Murray) and 20% (Charlton) of the primary impact. Dust contributed to 13% of total primary impacts. The largest dust contributions occurred at Athens (16%) and Douglas (16%). Coal combustion contributed to 10% of the total primary $PM_{2.5}$ impacts, and the largest impact occurred at Macon (18% of total primary impact).

The largest all-year average gasoline vehicle impact is observed at Chattanooga, with 1.7 $\pm$ 0.4 $\mu g/m^3$. This large gasoline impact is related to its location near a hospital with heavy traffic volumes. The largest diesel vehicle impact is found at SDK, with 1.2 $\pm$ 0.2 $\mu g/m^3$, as it is located 0.6 km from a major interstate highway that encircles Atlanta and has a large diesel vehicle volume as heavy duty trucks going through Atlanta without local deliveries are required to use this highway (State of Georgia, 2013). The largest coal combustion contribution was found in Macon (0.85 $\pm$ 0.2 $\mu g/m^3$), where there are several nearby coal-fired power plants.

Some of the sources may be apportioned with bias due to collinearity of sources with similar tracer species. Specifically, when the tracer species concentrations are below

detection limits, CMB can fail to differentiate sources with similar profiles. For example, source profiles for light duty gasoline vehicle and heavy duty diesel vehicle were similar and the metal species that provide differentiation between them were not always available. At the rural site Charlton, where the mobile impact is low and tracer species are often below detection limitations, about 77% of the days only light duty gasoline vehicle source impacts are identified and no heavy duty diesel vehicle result is generated. Similarly, both biomass burning and heavy duty diesel vehicle are highly correlated with EC concentrations (Fig. A7). When a tracer species for biomass burning, i.e. potassium, was below detection limit or missing, CMB would mainly depend on other indicators such as EC, leading to mismatched results in the two sources.

The representativeness of the selected source profiles can lead to uncertainty to the estimated source impact. For example, a large wildfire, i.e., the Bugaboo Scrub Fire with high OC to EC levels, occurred in southern Georgia during April to June 2007, spread around Okefenokee Swamp located near the Charlton monitor, and impacted downwind sites such as Charlton, Tallahassee, Douglas, Macon, and Columbus. On the high concentration days at these impacted sites, both large biomass burning and other OC impacts were identified. This can be caused by formation of secondary OC during the fire but the source profiles are only indicative of the primary species. It can also be caused by source profiles not capturing the characteristics of the burning mass on those days, the intensity of the fires, or types of flames under particular fire scale and weather. For example, source profiles for different woods vary (Fine et al., 2001) and the source profile used may not represent the biomass burned in a particular fire. Since biomass emissions are subject

to many changes, such as changing climate (Koppmann et al., 2005), it is not possible to capture the variation in source profiles over time and space.

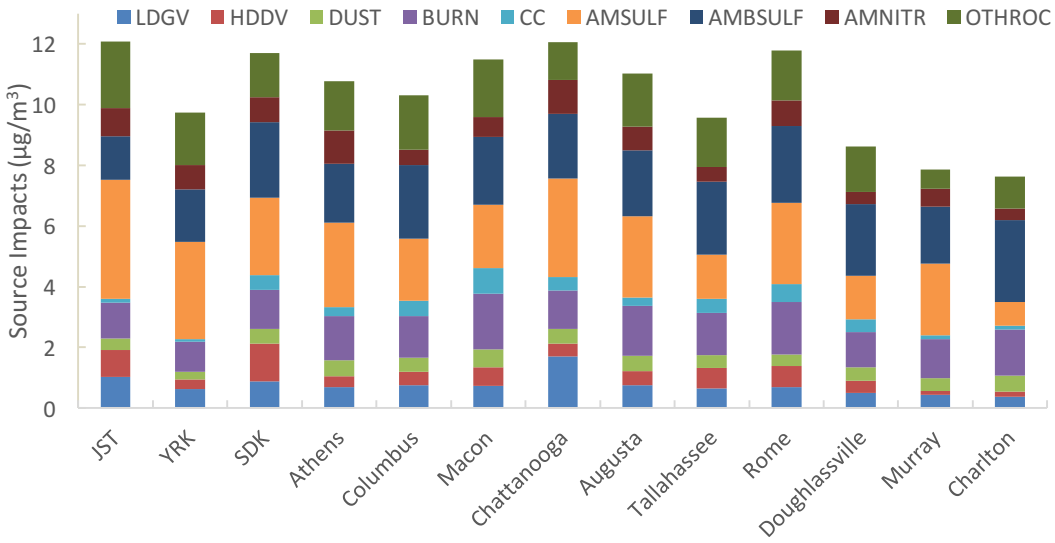

Figure 3. 12-year Averages of Source Impacts: the sites ordered same with Fig. 2. Sulfate species at the two IMPROVE sites are estimated (See description in Fig. A8 in SI).

2.3.2.2 Long-term trends

Significant decreasing trends (p-value less than 0.01) were found in six sources out of the nine sources, except for dust, coal combustion, and other OC (Fig. A9). Light duty gasoline vehicle and heavy duty diesel vehicle both decreased 0.02 µg/m^3/yr; biomass burning and ammonium nitrate both decreased 0.05 µg/m^3/yr; ammonium sulfate and ammonium bisulfate both decreased 0.19 µg/m^3/yr. Other OC also showed substantial decrease over the study period (24% decrease in 2013 compared to 2002). In total, ammonium sulfate and ammonium bisulfate contributed to more than 80% of the decrease in $PM_{2.5}$ total mass over the 12 years.

Overall, sources impact on primary $PM_{2.5}$ decreased to a lesser degree than on secondary $PM_{2.5}$ species, leading to increasing fraction of primary $PM_{2.5}$ to total $PM_{2.5}$. With secondary

pollutants decreasing and dust source impacts remaining largely constant, the dust fraction in $PM_{2.5}$ total mass are 66% larger in 2013 than in 2002. Similarly, relatively small decrease in biomass burning compared to secondary pollutants also led to an increase in its fraction in $PM_{2.5}$ total mass, with the 2013 fraction 11% larger than that in 2002. Thus, sources contributing to primary $PM_{2.5}$ such as biomass burning and dust, are becoming the major contributors to $PM_{2.5}$ total mass.

The annual trends largely follow the changes in emissions, with some variation due to meteorology. For example, precipitation has a strong effect on all source impacts, resulting in the low levels for most sources at most sites in 2009 when rainfall levels were high (Fig. A9). In addition, peaks of source impacts are observed when large emissions occurred, such as the large other OC impacts in 2007 due to the Bugaboo Scrub Fire.

2.3.2.3 Short-term trends

The trends with periods within a year are analyzed using LSPM and running averages. Results are presented for JST, YRK, SDK, Murray, and Charlton because they have more complete measurements, i.e., daily and one-in-three day measurements, and represent both rural and urban areas in Georgia. The sites with one-in-six-day data are insufficient in the running average and LSPM analyses. Spectrum results using LSPM are shown in Table A1 for periods with a statistical significance of 0.05 for daily and one-in-three day measurements. As an example, spectrum plots of JST for all sources and $PM_{2.5}$ total mass are shown in Fig. A10 as JST site is with daily measurement. Running averages are shown in Fig. A11.

Seasonality (defined as a cycle of approximately one year) was found by LSPM spectrum analysis for most sites and most sources. The peak periods were not always 365 but varied between 350 to 380 for three reasons: first, the source impact results are incomplete due to gaps in measurements and non-convergence of CMB; second, the precipitation and other conditions disturb the yearly distribution differently, which can impact the identification of the periods, and third, sampling every six days diffuses the detectable signal frequency.

Light duty gasoline vehicle was found to be larger in winter and lower in summer, with a stronger seasonal trend at urban sites (JST and SDK) than rural sites (YRK, Murray, and Charlton). The pattern is consistent with larger emissions and lower mixing heights in winter than in summer. Dust impacts peak in the summer (July to September) and are slightly lower in May, consistent with precipitation and temperature effects. Biomass burning impacts peak in March and November, and are lower during summer when there is a ban of prescribed fires (May through September).

The sulfate species, ammonium sulfate and ammonium bi-sulfate, are observed to be highest during summer time. In winter and spring, more precipitation washes out sulfate (Garland, 1978). At higher temperature in the summer, oxidation of SO_2 gas to sulfate is more favorable because of higher levels of reactive species present, such as hydroxyl radical (Seinfeld and Pandis, 2012a). Ammonium nitrate impacts have an inverse pattern as sulfate. Under longer sunlight exposure in summer, reactions that convert NO_2 to organic nitrates are more active and reduce nitrate formation, and nitrate remains volatile at high temperature in summer due to its semi-volatility. The split of ammonium sulfate and

ammonium bisulfate is subject to uncertainties as the impact of other anions and cations, such as Cl^- and Na^+, are assumed to be negligible.

For other OC, two rural sites (YRK and Murray) and urban site (JST) showed strong seasonality, at periods of 364 days (YRK), 361 days (Murray) and 358 days (JST). At the two urban sites SDK and JST, peak concentrations occurred in both summer and winter. At the rural sites YRK, Murray, and Charlton, larger impacts appeared in summer than in winter (Fig. A11). This is consistent with secondary OC being a major contributor to other OC in rural areas in Georgia whereas there may be other sources with substantial contributions to other OC in urban areas. Higher secondary OC in summer is due to high reactivity as well as more biogenic emissions.

JST is found to have strong weekly trends for light duty gasoline vehicle, heavy duty diesel vehicle, dust, and coal combustion through LSPM analysis (Fig. A12). The two mobile sources and the coal combustion source that is mostly by power plants are anthropogenic sources. In urban areas, dust impacts are associated with traffic because of traffic-induced dust. Therefore, these four sources have similar weekly trends that are consistent with more emissions on weekdays and less on weekends.

2.3.3 Comparison with NEI

We compared the annual source impacts of mobile sources and coal combustion with the NEI, as well as sulfate concentrations with SO_2 emissions. The mobile source impacts on primary $PM_{2.5}$ at JST in central Atlanta correlate with annual emissions in the 20 counties in metropolitan Atlanta area estimated by MOVES based on National Emissions Inventory

well (R^2 = 0.80 and slope of 0.075 with 95% confidence interval of 0.046 to 0.103, Fig. 4a). The intercept is 0.7 with 95% confidence interval 0.2 to1.2, indicating a small background impact of mobile sources.

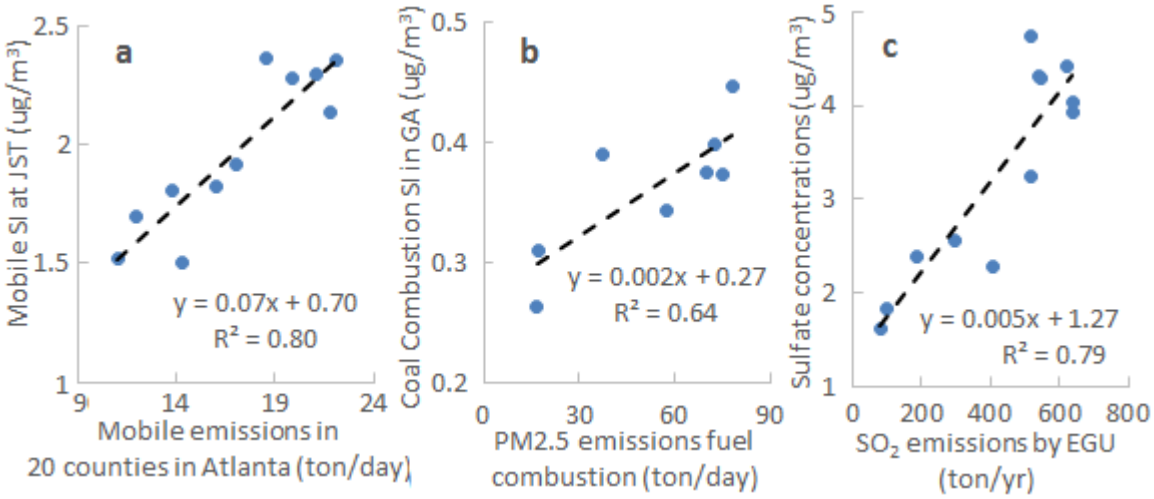

Figure 4. (a). Annual mobile source impacts at JST ($\mu g/m^3$) vs. mobile emissions at 20 counties in Metropolitan Atlanta (tons/day) estimated by MOVES based on 2011 National Emissions Inventory; (b). $PM_{2.5}$ emissions of fuel combustion by EGU vs coal combustion source impacts; (c). annual concentrations of sulfate averaged across all sites vs SO_2 emissions by EGU in GA.

Annual averages of coal combustion impacts are correlated with $PM_{2.5}$ emissions from fuel combustions (Environmental Protection Agency, 2016), with an R^2 = 0.64 and a positive slope of 0.002 (95% confidence interval of 0.0005 to 0.003, Fig. 4b). The intercept of 0.27 (95% confidence interval of 0.19 to 0.35) shows a relatively small background impact but to a similar level of the source impacts, indicating small response of source impacts to reduction in emissions. From 2002 to 2011, EGU emissions decreased 75%, while estimated coal combustion source impacts decreased 40% in the same time. The difference in the decreases in emissions and source impacts could be due to higher uncertainties in the coal combustion impact estimates because lower tracer species concentrations of coal are often below detection limit.

Annual average concentrations of sulfate averaged across all sites are compared with SO_2 emissions by EGUs in Georgia in Fig. 4c, with R^2=0.79 and a positive slope (0.005 with 95% confidence interval of 0.003 to 0.0065). The intercept (1.3 with 95% confidence interval of 0.5 to 2.1) also suggests a relatively small background impact. Coal combustion is the major source of SO_2 emissions and EGUs represent the major use of coal combustion. A decrease of 87% in EGU- generated SO_2 emissions in GA resulted in 58% sulfate concentration decrease.

The comparisons with NEI suggest that emissions changes are the main contributors to the long-term trends of the source impacts and concentrations (80% for mobile sources, 64% for coal combustions, and 79% for sulfate concentrations). The observation based source impact estimates serves as a direct assessment of the emissions control policies. The positive correlations of source impacts with emissions and their decreasing trends together provide evidence of achievements in the controls in EGUs and mobile sources. The implications for health exposure is that when estimating traffic related exposures, the spatial pattern of exposures can remain very similar over time in high traffic density areas because of the high dependence of source impacts on emissions also implies, similar to the findings in a long-term and fine spatial resolved traffic related concentration study (Zhai et al., 2016).

2.3.4 Spatial Representativeness

The spatial and temporal representativeness of the central sites for each source is evaluated here based on temporal trends (Fig. 5) and correlograms (Fig. 6). The correlograms shown

here are the relationships of the Pearson correlation coefficient of daily variations between all pairs of sites and the distance between the two sites.

Similar temporal trends were found at all sites for secondary pollutants (Fig. 5). Furthermore, daily variations in secondary pollutants are highly correlated at sites that are located close to each other as shown in the correlograms (Fig. 6). The high spatial autocorrelations of ammonium sulfate, ammonium bisulfate, and ammonium nitrate indicates homogeneity of secondary pollutants in the region.

Biomass burning and dust were also found to be correlated at nearby sites, with $R>0.6$ for the daily variations between sites within 100 km (Fig. 6). These findings demonstrate the regional effects of fires, such as the Bugaboo Scrub Fire in 2007, and dust emissions, that are related to regional weather patterns.

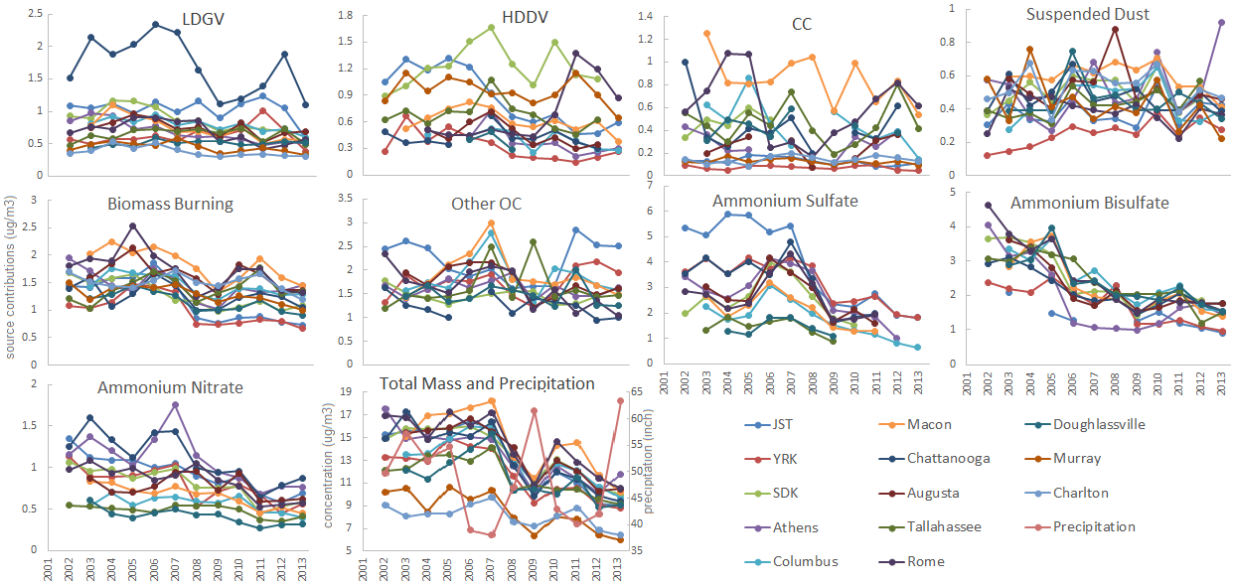

Figure 5. Temporal trends of all sources and total $PM_{2.5}$ at all sites.

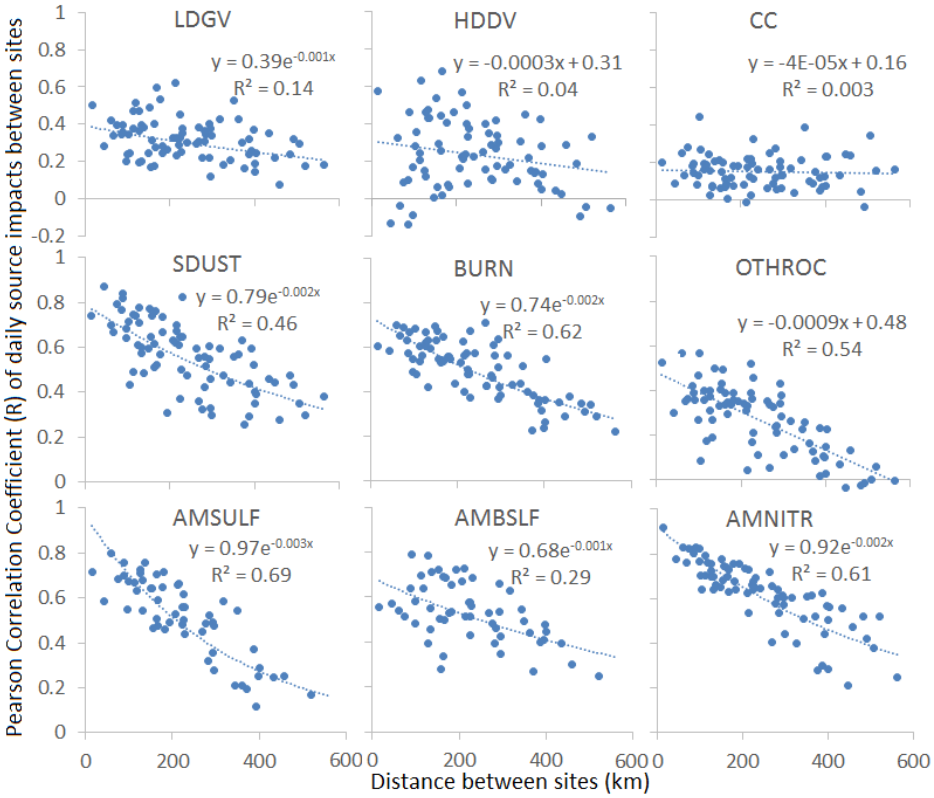

Figure 6. Correlograms of Pearson correlation coefficient (R) of daily source impact variation between all pairs of sites versus distance between the corresponding two sites.

Fitted exponential correlogram models are shown. For sources with negative correlations, linear fits are employed.

The other sources that contribute to primary $PM_{2.5}$, mobile sources and coal combustion, are local sources with various temporal trends and no significant temporal correlation even for sites within 15 km of each other. For mobile sources, the traffic density is heterogeneous over space and time. For coal combustion, which is mostly by spatial distribution of coal-fired power plants, the impact is highly affected by wind (direction and magnitude) and mixing height (mixing down plumes).

Overall, the short-term covariation (correlograms) and long-term covariation (annual average trends) indicate that the central monitors can represent larger areas for the secondary pollutants and smaller areas for regional sources, such as biomass burning and dust. For localized sources, such as mobile sources and coal combustion, the central sites can only represent small scale of surrounding environment. When used in epidemiologic studies in large metropolitan areas, central sites provide better exposure information for secondary pollutants than for biomass burning and dust. For highly localized sources, spatially resolved information is needed to improve exposure estimates.

2.3.5 Limitations

$PM_{2.5}$ source impacts cannot be measured directly and must be estimated using one of a number of source apportionment methods available. In the CMB application here, we used a set of fixed source profiles over multiple locations and years. This can result in error even when representative source profiles are used (Wang et al., 2012a; Watson et al., 2012). Here, the use of a single source profile for biomass burning led to the misclassification of

impacts from the Bugaboo Scrub Fire, as described above. The source profile used may not have been representative of the type of biomass burned in this particular wildfire. Moreover, burning conditions likely varied over time and space resulting in variation in emissions; for example, the relative amounts of OC and potassium associated with a wildfire can change substantially with burning conditions ranging from smoldering to flaming (Lee et al., 2008a).

Source profiles have been developed that are applicable and commonly used in the southeastern U.S. region (Lee and Russell, 2007; Marmur et al., 2005; Watson et al., 2015; Zheng et al., 2002). Source impacts were generated to provide long-term and regional assessment of air pollutant mixtures for health analysis. Therefore, the approach used provides a degree of consistency in the source mixtures being characterized to avoid the uncertainties introduced by varying source profiles. The uncertainty associated with how source profiles change over time (e.g. by season) can be substantial. The unapportioned mass (about 14% on annual average level) is slightly greater in summer (Fig. A13). The unapportioned mass is a result of measurements of OC which do not include the non-carbon content of this organic fraction. For primary sources, the non-carbon content is small; however, for SOC, here approximated by OTHROC, the non-carbon content can be high, with estimates of the ratio of organic matter to organic carbon varying widely and as high as two or more due in large part to the presence of oxygenated organics (Blanchard et al., 2016). In this study we did not try to estimate the non-carbon content of the organic fraction due to the uncertainties involved. The unexplained mass in this study is consistent with a ratio of organic matter to organic carbon of about 2. Furthermore, the correlation of

unapportioned mass and OTHROC is high (e.g., R=0.53 at YRK), with both peaking in the summer.

The spatial domain of this study is Georgia (including monitoring sites near to the border of Georgia) which is a regionally coherent area in terms of types of emissions and regulation. That is, the major sources identified, such as mobile sources and biomass burning, are expected to be more similar within Georgia than across regions. For example, the biomass in prescribed burns is similar across Georgia, and the range of burn and atmospheric conditions are similar over the long term (i.e., years). While short-term variations exist, the long-term trends presented in this paper are useful in investigations of long-term health effects. Although variability in emissions over space and time adds noise to our results, the lack of data to describe these differences accurately limits our study to addressing the long-term regional variations in source impacts.

Another limitation of this research is potential biases in our SOC estimates. We apportion all unidentified OC into an "other OC" category which we assume to be largely SOC. While aerosol properties can provide a mechanistic linkage to SOC, these properties are not readily available. The use of lumped categories for secondary species is a commonly used approach in receptor modeling that does not treat atmospheric chemistry explicitly. There is substantial evidence that the unapportioned OC from this approach can be interpreted largely as SOC in the southeast, with uncertainties addressed (Balachandran et al., 2012; Marmur et al., 2005; Pachon et al., 2010). The overall amount of OC that we attribute to SOC is consistent with findings that show a large fraction of OC is secondary in the southeastern U.S. (Balachandran et al., 2012).

2.4 Conclusion

Daily source impacts of nine sources at multiple sites in Georgia were estimated from 2002 to 2013. Annual $PM_{2.5}$ averaged across sites decreased from 13.8 $\mu g/m^3$ to 9.2 $\mu g/m^3$. Of the nine source impacts quantified, seven sources showed statistically significant decreasing trends. More than 80% of the $PM_{2.5}$ concentration decrease is attributed to decreases in ammonium sulfate and ammonium bisulfate. The source impact trends are consistent with NEI trends, suggesting that emission control policies are reflected in the change of ambient concentrations. Low levels of coal combustion impacts on primary $PM_{2.5}$ and large decreases in sulfate indicate that changes in coal-fired power plant impacts on $PM_{2.5}$ were largely secondary (i.e., derived from SO_2 emissions from EGUs).

Using data from multiple sites, this work provides spatial trends of source impacts on $PM_{2.5}$ over 12 years. The source apportionment results using CMB correspond well with the expected spatial and temporal distribution and can be helpful to estimate source impacts in different regions. The monitor data are found to be representative of large areas for secondary pollutants, smaller regions for biomass burning and dust, and very local areas for sources such as mobile sources and coal combustion. Information on spatial representativeness is needed to assess population exposures. The data generated from this research are being used for the spatial analysis of pollutant exposure risks in susceptible and vulnerable populations such as pregnant women. Based on such information, policy makers can make more effective regulations that help limit air pollution emissions, which might help reduce the development or worsening of diseases.

2.5 Acknowledgement

This study was conducted as part of the Southeastern Center for Air Pollution and Epidemiology (SCAPE), with support from the US EPA under grant R834799. Its contents are solely the responsibility of the grantee and do not necessarily represent the official views of the USEPA. Further, USEPA does not endorse the purchase of any commercial products or services mentioned in the publication.

CHAPTER 3. SPATIAL $PM_{2.5}$ MOBILE SOURCE IMPACTS USING A CALIBRATED INDICATOR METHOD

As submitted to Air Quality, Atmosphere & Health.

Abstract

Motor vehicles are major sources of fine particulate matter ($PM_{2.5}$), and the $PM_{2.5}$ from mobile vehicles is associated with adverse health effects. Traditional methods for estimating source impacts that employ receptor models are limited by availability of observational data. To better estimate temporally and spatially resolved mobile source impacts on $PM_{2.5}$, we developed an approach based on a method that uses EC, CO, and NO_x measurements as an indicator of mobile source impacts. We extended the original integrated mobile source indicator (IMSI) method in three aspects. First, we generated the spatially resolved indicators using 24-hr average concentrations of EC, CO, and NO_x estimated at 4km resolution by a method developed to fuse chemical transport model (CMAQ) simulations and observations. Second, we used spatially-resolved emissions instead of county-level emissions in the IMSI formulation. Third, we spatially calibrated the unitless indicators to annual average mobile source impacts estimated by the receptor model Chemical Mass Balance (CMB). When calibrating the indicators to source impacts, we compared two methods: a global IMSI method and a local IMSI method. We found that the two methods yield similar results. Daily total mobile source impacts on $PM_{2.5}$, as well as separate gasoline and diesel vehicle impacts, were generated at 12km resolution for 2002 to 2008 and 4km resolution for 2008 to 2010 in Georgia. The total mobile and

separate vehicle source impacts compared well with daily CMB results, with high temporal correlation and low error. The total mobile source impacts have higher correlation and lower error than the separate gasoline and diesel sources when compared to observation-based mobile source impacts. Overall, this approach provides spatially resolved mobile source impacts that are similar to observation-based estimates and can be used to improve assessment of health effects.

3.1 Introduction

Ambient air pollution has been associated with human morbidity and mortality (Brauer et al., 2016; Kampa and Castanas, 2008; Lelieveld et al., 2015; West et al., 2016). The relationship between adverse health effects and air pollution has been investigated using different types of pollutant exposure metrics, particularly single pollutant metrics of fine particulate matter ($PM_{2.5}$) and NO_2 (Cohen et al., 2005; Kioumourtzoglou et al., 2016; Pope et al., 2009; Zeger et al., 2008) and ozone (Chen et al., 2015; Uysal and Schapira, 2003). Single pollutant metrics are usually provided by ambient measurements, model simulations, or fusion of observation and simulation (Zhai et al., 2016). Variation in single pollutant levels may not adequately represent the actual variation in human exposure to air pollution changes because populations are exposed to a complex mixture of pollutants. Multipollutant metrics may be more representative of actual source impacts (SI) and potential health effects (Dominici et al., 2010; Hidy and Pennell, 2010; Johns et al., 2012).

Multipollutant exposure has been estimated by different grouping methods, such as chemical and/or biological reactivity, health effects, and contributing sources (Chen and Lippmann, 2009; Hart et al., 2011; Kim et al., 2007; Mauderly and Chow, 2008; Oakes et

al., 2014a; Pachon et al., 2012). Source impacts derived using source apportionment techniques are mixtures of pollutants that are directly related to air pollution controls (Gehring et al., 2010; Kelly and Fussell, 2012; Maciejczyk and Chen, 2005; Sarnat et al., 2008). Traffic-related pollution is of particular interest due to the ubiquity of the source, particularly in highly populated areas, and observed associations with various health effects (Beelen et al., 2014; Brauer et al., 2008; Chen et al., 2013; Gehring et al., 2010; Kelly and Fussell, 2012; Nordling et al., 2008). Motor vehicles contribute to $PM_{2.5}$ emissions, such as elemental carbon (EC), organic carbon (OC) and trace metals, as well as to gas phase pollutants, such as carbon monoxide (CO), and nitrogen oxides (NOx, referring to the sum of nitric oxide (NO) and nitrogen dioxide (NO_2)). These motor vehicle related pollutants have been found to be associated with adverse health effects individually and in combinations (Delfino et al., 2006; Kelly and Fussell, 2012; Melen et al., 2008; Oakes et al., 2014b; Pachon et al., 2012).

Source impacts can be estimated using source apportionment receptor-based models, such as the chemical mass balance (CMB) model (EPA, 2004a) and the positive matrix factorization (PMF) method (Paatero and Tapper, 1994), and emission-based dispersion models and chemical transport models, such as the Research LINE-source dispersion model (R-LINE) (Snyder et al., 2013) and Community Multiscale Air Quality model with Decoupled Direct Method (CMAQ-DDM) (Napelenok et al., 2006). Receptor models for $PM_{2.5}$ are based on ambient measurements for $PM_{2.5}$ species, with or without predetermined source profiles (EPA, 2004a; Lee et al., 2008b). Their dependence on spatially sparse measurements limits the spatial and temporal coverage of the estimates. Studies have improved the temporal coverage using daily temporal interpolation method (Redman et al.,

2016). More spatially and temporally comprehensive source impact metrics can be developed using chemical transport models (Held et al., 2005; Ivey et al., 2015; Napelenok et al., 2006). Such models have biases due to limitations in inputs, such as emissions and meteorology, and simulation, such as transport and chemistry specifications. Efforts to combine the receptor models with dispersion models and regional scale chemical transport models (Hu et al., 2014; Ivey et al., 2015; Sturtz et al., 2014) reduce these biases but are expensive computationally.

Pachon et al. (2012) developed an emission-based Integrated Mobile Source Indicator (IMSI) using observed concentrations and estimated emissions of CO, NO_x, and EC to develop a unitless indicator of mobile source impacts. This method is easy to apply and the indicator was found to be significantly correlated with health outcomes at multiple locations (Oakes et al., 2014b; Pachon et al., 2012). This unitless local indicator does not, by itself, provide information on spatial variation in source impacts.

In this research, we extended the IMSI method to estimate daily mobile source impacts on $PM_{2.5}$ at 4km and 12km resolutions. The mobile source impacts were developed for use in studies of human health effects and exposures to multi-pollutant mixtures in Georgia.

3.2 Methods

The IMSI method is extended from providing single location unitless indicators to providing spatially resolved daily mobile source impacts on $PM_{2.5}$ using chemical transport model (CMAQ) fields fused with observational data, mobile source emission estimates, and receptor model (CMB) source impact estimates. The approach is applied for estimating

the total mobile, gasoline, and diesel source impacts on $PM_{2.5}$ in Georgia for 2002 to 2008 at 12 km resolution, and for 2008 to 2010 at 4 km resolution; these different resolutions are due to the availability of CMAQ results (Boothe et al., 2006).

The overall approach is depicted in Fig. 7 in four steps. First, daily 24-hr average concentration fields of EC, CO and NO_x are obtained using the CMAQ-observation data fusion method (Friberg et al., 2016a). Pachon et al. (2012) used central site measurements of 1hr maximum concentrations of CO and NO_x in developing the IMSI method. Here we used 24-hr averaged concentrations for CO and NO_x to obtain daily mobile source impact estimates that are temporally consistent over space. Second, spatially resolved weighting factors are generated from emission data for combining the indicator species. Third, daily integrated mobile source indicator fields are derived. Finally, the unitless indicators are calibrated and converted to mobile source impacts using CMB annual source impacts. The methods and the data used are described in detail below.

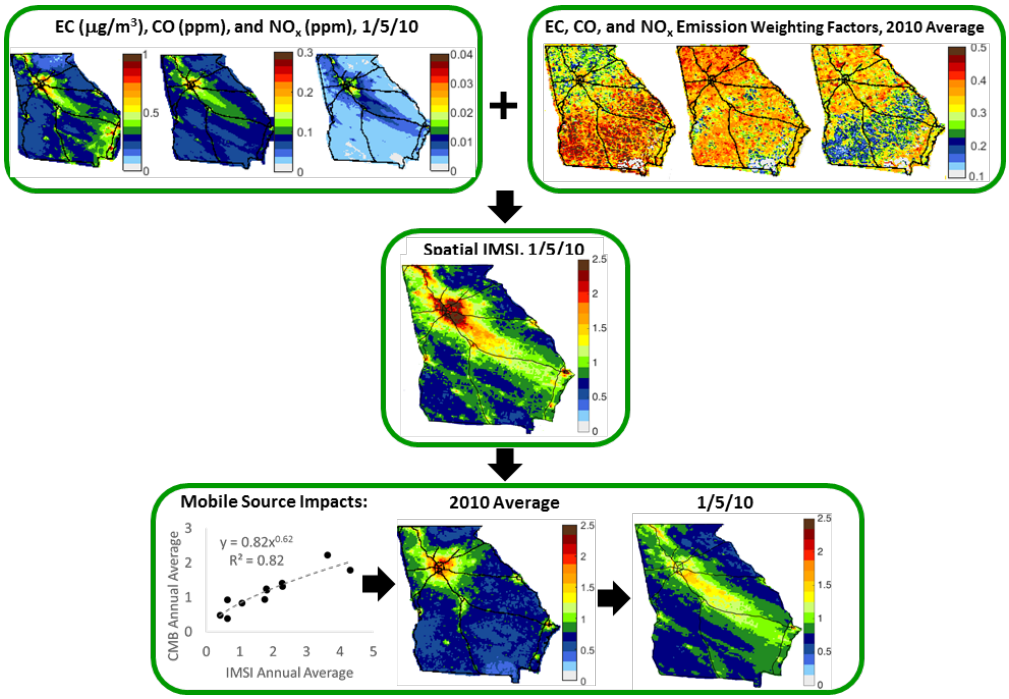

Figure 7. Procedure for estimating spatially and temporally resolved mobile indicators.

3.2.1 Integrated Mobile Source Indicator Method

As EC, CO, and NO_x are mainly emitted by mobile sources, Pachon et al. (2012) postulated that their variations could be representative of mobile source impact changes. The IMSI method uses EC, CO, and NO_x concentrations as indicator species of mobile sources and mobile emission fractions (of total emissions) as weighting factors to combine them into a unitless indicator (Equation 1). The IMSI method was also developed to estimate indicators of gasoline vehicle (GV) and diesel vehicle (DV) contributions separately (Equation 2 and Equation 3, respectively). As EC is mostly contributed by diesel vehicles and CO is mostly contributed by gasoline vehicles, the DV indicator combines EC and NO_x concentrations and the GV indicator combines CO and NO_x concentrations.

In the IMSI method, daily species concentrations (C) observed at central sites are first normalized by their standard deviations (σ) over one year. Then, these normalized values are averaged based on weighting factors (α) calculated from source emission estimates that vary in space but not in time (Equation 4 for the total mobile source indicator, and Equation 5 and 6 for the GV and DV indicators, respectively). The weighting factors, which are in essence emission coefficients, are defined as the ratios of mobile source (or GV/DV) emissions over total emissions for each species normalized by the sum of ratios over the three species. As such, these weighting factors do not vary over time and sum to 1 across the three species at each point in space for each source category (total mobile, GV and DV). The IMSI indicators are normally distributed with a mean of the weighted average of the normalized concentrations (C/σ).

$$IMSI_{mobile} = \alpha_{EC} \times \frac{C_{EC}}{\sigma_{EC}} + \alpha_{CO} \times \frac{C_{CO}}{\sigma_{CO}} + \alpha_{NOx} \times \frac{C_{NOx}}{\sigma_{NOx}} \quad \textit{Equation 1}$$

$$IMSI_{GV} = \alpha_{GV,CO} \times \frac{C_{CO}}{\sigma_{CO}} + \alpha_{GV,NOx} \times \frac{C_{NOx}}{\sigma_{NOx}} \quad \textit{Equation 2}$$

$$IMSI_{DV} = \alpha_{DV,EC} \times \frac{C_{EC}}{\sigma_{EC}} + \alpha_{DV,NOx} \times \frac{C_{NOx}}{\sigma_{NOx}} \quad \textit{Equation 3}$$

$$\alpha_s = \frac{\frac{E_{s,mobile}}{E_{s,total}}}{\frac{E_{EC,mobile}}{E_{EC,total}} + \frac{E_{CO,mobile}}{E_{CO,total}} + \frac{E_{NOx,mobile}}{E_{NOx,total}}} (s = EC, CO, and \cdot NO_x) \quad \textit{Equation 4}$$

$$\alpha_{GV,s} = \frac{\frac{E_{s,GV}}{E_{s,total}}}{\frac{E_{CO,GV}}{E_{CO,total}} + \frac{E_{NOx,GV}}{E_{NOx,total}}} (s = CO \cdot and \cdot NO_x) \quad \textit{Equation 5}$$

$$\alpha_{DV,s} = \frac{\frac{E_{s,DV}}{E_{s,total}}}{\frac{E_{EC,DV}}{E_{EC,total}} + \frac{E_{NOx,DV}}{E_{NOx,total}}} (s = EC \cdot and \cdot NO_x) \quad \text{Equation 6}$$

The CMAQ-observation data fusion method used to provide daily, spatially resolved concentration data is described in section 2.2, and the emission model used to provide weighting factors for indicator calculations is described in section 2.3.

3.2.2 CMAQ-Observation Data Fusion

Daily EC, CO, and NO_x concentration fields were generated by a CMAQ-observation data blending approach applied at 4 km and 12 km resolutions in Georgia; the approach is summarized briefly below, and is described in detail by Friberg et al. (2016c).

The applied data fusion approach blends ambient ground observations and modeled data from CMAQ to estimate daily spatial fields of pollutant metrics. Optimized spatiotemporal concentration fields are developed using weighted fields of daily-interpolated surface observations normalized to their annual means and daily-adjusted CMAQ fields that are rescaled to estimated annual mean fields. The estimated annual mean fields are developed from CMAQ-derived annual mean spatial fields adjusted to observed annual means using power regression models. The optimization is based on a spatiotemporal weighting factor that maximizes the degree to which the observation-based estimate predicts temporal variation relative to the CMAQ-based estimate, as a function of distance from an observation.

The CMAQ simulations were generated in the Public Health Air Surveillance Evaluation (PHASE) collaboration between the U.S. Environmental Protection Agency (EPA) and the Centers for Disease Control (Boothe et al., 2006) for 2002 through 2008 at 12 km resolution, and in the HiRes Air Quality Forecasting program by Georgia Institute of Technology for 2008 to 2010 at 4 km resolution (Hu, 2014; Hu et al., 2010). Observational data were collected from three available monitoring networks in Georgia: the Interagency Monitoring of Protected Visual Environments Network (IMPROVE), Chemical Speciation Network (CSN), and South Eastern Aerosol Research and Characterization (SEARCH) (Hansen et al., 2003; Solomon et al., 2014).

3.2.3 Emissions Data

The IMSI method of Pachon et al. (2012) uses county level National Emissions Inventory (NEI) data. Here we used simulated emissions at 4 km and 12 km resolutions averaged

over time from the HiRes Air Quality Forecasting program (Hu, 2014) to match the spatial resolution of the data fusion concentration estimates. These emission estimates were developed using the Sparse Matrix Operator Kernel Emissions Modelling System (SMOKE) (Houyoux et al., 2000) (Fig. 8). The emissions of diesel and gasoline vehicles separately were estimated at 36 km resolution and downscaled the ratios of gasoline/diesel to total emissions from 36 km to 4 km using the gasoline/diesel to total mobile emission ratio at 36 km resolution and mobile to total emission at 4 km resolution as described in supplemental material (Fig. A14). As traffic patterns changed very little over the study period, these weighting factors based on emissions were not varied over time. The temporal variation (e.g., by day-of-week, season, and year) in the weighting factors was found to be small compared to spatial variation. Mobile source emissions at protected natural resource areas, such as in the Okefenokee Swamp in the southeast corner of GA, are very low and highly uncertain. We excluded data in these areas in this study aimed at developing exposure metrics for health studies.

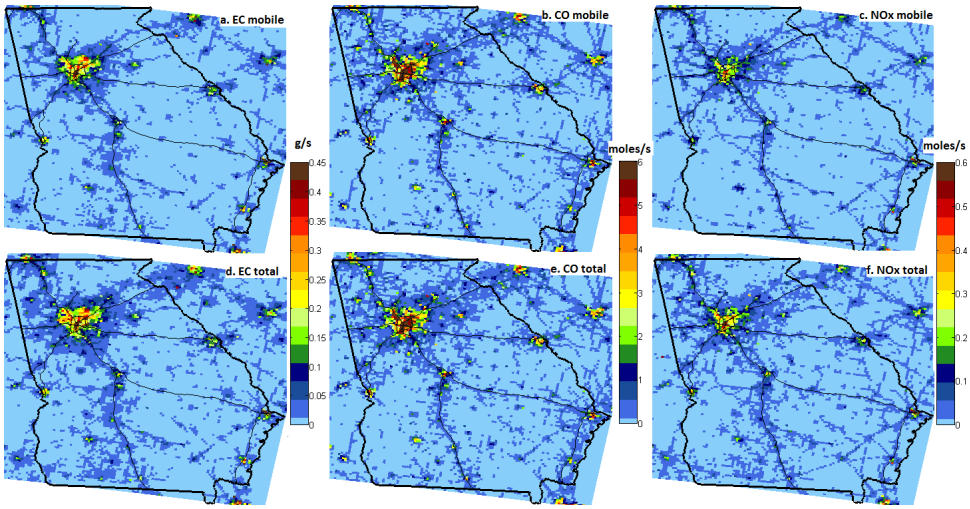

Figure 8. Spatial distributions of annual average emissions at 4 km resolution for mobile sources and total emissions.

3.2.4 CMB Source Apportionment

The source impacts cannot be measured directly. Mobile source impacts generated by the observation-based receptor model CMB are found to agree well with the long-term trends of NEI (Zhai et al., 2017). In this method, we used the CMB estimated mobile source impacts as representative of mobile source impacts. We calibrated the unitless indicators to CMB estimates and compared temporal variations of the generated source impacts with CMB estimates at each location.

CMB estimates the source impacts of $PM_{2.5}$ from different sources by solving mass conservation equations that fit species concentrations to different contributions of various source (Watson et al., 1984). To apportion the source impacts, tracer species concentrations are needed. In the Georgia domain, $PM_{2.5}$ species concentrations are monitored at 11 sites (Fig. A15) from the IMPROVE, SEARCH, and CSN networks from 2002 to 2011 (Hansen et al., 2003; Solomon et al., 2014). The species used in this study include five major species (sulfate, nitrate, ammonium, elemental carbon, and organic carbon) and 14 trace metals that are typically above detection limit (Al, Br, Ca, Cu, Fe, K, Mn, Pb, Sb, Se, Si, Sn, Ti, and Zn). The source profiles summarized by Marmur et al. (2005) for nine sources were used: light duty gasoline vehicle, heavy duty diesel vehicle, biomass burning, coal combustion, suspended dust, ammonium sulfate, ammonium bisulfate, ammonium nitrate, and unapportioned organic carbon. The profiles for light duty gasoline vehicle and heavy duty diesel vehicle were generated by Chow et al. (2004). More information about the CMB estimates can be found in Zhai et al. (2017).

3.2.5 Spatial PM2.5 Mobile Source Impact Modelling Approach

Daily IMSI fields are derived using a single standard deviation for all years and all locations to normalize the indicator species concentrations (see Equations 1-3). The unitless IMSI has the same spatial distribution as the weighted spatial distribution of the indicator species (e.g., see Fig. 7). To convert the unitless IMSI to a source impact concentration, we perform a power fit regression the annual average spatial IMSI with the annual average CMB results at monitor locations. We use these results to generate an annual average source impact field. Daily source impact ($SI_{x,y}$) fields are then generated using Equation 7. To evaluate the impact of the normalization method of the concentrations, we performed an alternative approach, which uses local standard deviation at each location, and uses $PM_{2.5}$ emissions to estimate the CMB annual averages. More details about the alternative local IMSI method can be found in supplemental material (Fig. A19 and A20).

$$SI_{x,y}(t) = \frac{IMSI_{x,y}(t)}{\overline{IMSI_{x,y}}} \times \overline{SI_{x,y}} \qquad \text{Equation 7}$$

3.2.6 Evaluation

We evaluated the performance of this global IMSI method to predict daily CMB estimates by comparing the IMSI-estimated daily source impacts with the daily CMB estimates at receptor locations using the Pearson correlation coefficient (R), normalized mean bias (NMB) (Equation 8), and normalized root mean squared error (NRMSE) (Equation 9). The bias is averaged using daily (d) bias for each year (y, *total D days,* $D \leq 366$), then normalized by annual averages of observation ($OBS_{m,y}$), and finally averaged across all years (N) and all sites (m). The root mean squared error is calculated using annual averages of daily squared errors, then normalized by the annual mean of observation, and finally averaged across N years and M monitors. Note that only annual average CMB estimates were used

in calibration. The temporal trends of CMB estimates and IMSI results are independent and can be used for evaluation.

$$NMB = \frac{1}{M}\sum_{m=1}^{M}\left(\frac{1}{N}\sum_{y=1}^{N}\frac{1}{D}\sum_{d=1}^{D}\left(\frac{(Estimate_{m,y,d}-OBS_{m,y,d})}{\overline{OBS_{m,y}}}\right)\right) \qquad Equation\ 8$$

$$NRMSE = \frac{1}{M}\sum_{m=1}^{M}\left(\frac{1}{N}\sum_{y=1}^{N}\frac{\sqrt{\frac{1}{D}\sum_{d=1}^{D}(Estimate_{m,y,d}-OBS_{m,y,d})^2}}{\overline{OBS_{m,y}}}\right) \qquad Equation\ 9$$

3.3 Results and Discussion

Results are presented below on the intermediate steps used to derive source impacts (i.e., emissions-based weighting factors (Equations 4-6) for averaging pollutant indicators and annual average CMB source impact fields for calibrating the IMSI), the spatial and temporal distributions of IMSI source impacts, an evaluation of IMSI source impact estimate performance, and a comparison with an alternative IMSI calibration methodology.

3.3.1 IMSI Weighting Factors

IMSI weighting factors (defined by Equations 4-6) are described in Tables A2 and Fig. A18. In this application of the IMSI method, the contributions of EC, CO and NO_x concentrations to the variation of the unitless indicators are substantially different at different locations (Fig. 9). The 2.5% to 97.5% quantile range of coefficients at 4 km resolution is 0.21 to 0.54 for EC, 0.19 to 0.43 for CO, and 0.15 to 0.42 for NO_x (Table A2). For example, there is a significant difference in the coefficients across three cities, where Atlanta and Denver have similar coefficients while EC coefficients at Houston (Oakes et al., 2014b) are smaller for mobile and DV indicators (Table A3). This is because Houston has other major sources of EC, such as the ships in its ports, which demonstrates the

importance of spatial variation caused by local sources. This demonstrates the importance of using more spatially resolved weighting factors than county- or city-level factors.

The weighting factors of CO distributions for mobile indicator are narrower (Fig. 9) than the other species. This is because at most locations CO emissions are largely from mobile sources whereas EC and NO_x have large contributions from other sources, such as power plants for NO_x and railyards and shipping ports for EC. For DV and GV, EC and CO respectively, are the major contributing species (Table A2).

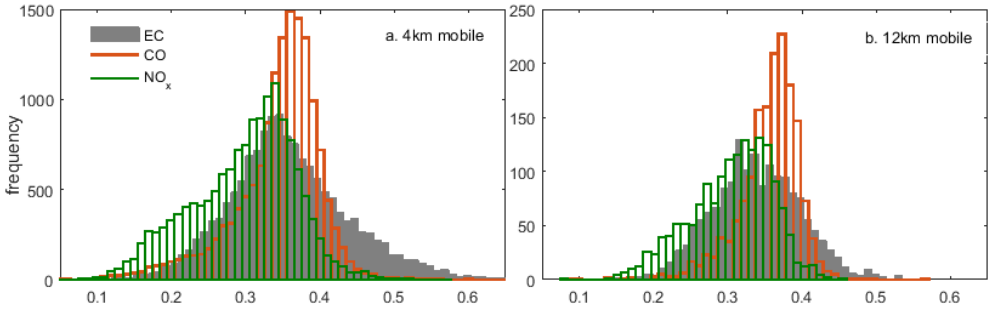

Figure 9. Distribution of weighting factors (Equations 4-6) at all grid cells in Georgia domain at 4km and 12km resolutions for mobile sources using annual average emissions.

3.3.2 Spatial CMB Annual Averages

The power fit regressions of annual averages of the IMSI indicators to CMB annual averages are shown in Table 1 for all years. The IMSI annual averages correlate well with CMB annual averages over space. The correlation is better for total mobile sources than for gasoline and diesel sources. As only annual averages of CMB source impacts are used in the calibration, the daily variations of the CMB results can be used for evaluation.

Table 1. Power fit regression ($y=ax^b$, where y=CMB and x=IMSI) coefficients for calibrating annual average indicators to annual average CMB source impacts. The

coefficients (a, b, and R^2) are calculated using the linear regression of log-transformed data.

Source		Total Mobile			GV			DV		
Resolution	Year	a	b	R^2	a	b	R^2	a	b	R^2
12 km	2002	0.44	0.83	0.90	0.25	0.89	0.67	0.13	1.28	0.79
	2003	0.56	0.73	0.90	0.39	0.58	0.37	0.28	0.98	0.78
	2004	0.60	0.79	0.82	0.44	0.62	0.45	0.28	0.98	0.62
	2005	0.61	0.79	0.86	0.39	0.72	0.43	0.28	1.12	0.72
	2006	0.67	0.79	0.89	0.45	0.62	0.45	0.32	1.02	0.72
	2007	0.57	0.76	0.81	0.41	0.51	0.42	0.25	1.11	0.44
	2008	0.72	0.59	0.81	0.36	0.80	0.45	0.28	0.89	0.45
4 km	2008	0.78	0.48	0.75	0.40	0.46	0.65	0.26	0.88	0.72
	2009	0.68	0.58	0.69	0.39	0.47	0.72	0.31	0.49	0.45
	2010	0.82	0.62	0.82	0.46	0.49	0.77	0.34	0.73	0.69

3.3.3 Spatial PM2.5 Mobile Source Impacts

Source impact fields are generated for 2557 days from 2002 to 2008 at 12 km resolution and 1096 days from 2008 to 2010 at 4 km resolution for total mobile sources, gasoline vehicles, and diesel vehicles. As an example, we present spatial distributions of the results on January 21, 2008 in Fig. 10 when data for both resolutions are available. The source impacts at the two resolutions are in similar spatial distributions with the same urban peaks and plume directions. However, the maxima of the 12 km resolution source impacts are substantially lower (maximum of 1.74 $\mu g/m^3$ for total mobile sources, 1.33 $\mu g/m^3$ for GV, and 1.75 $\mu g/m^3$ for DV on this date) compared to the 4 km fields (2.94 $\mu g/m^3$ for total mobile, 1.71 $\mu g/m^3$ for GV, and 3.96 $\mu g/m^3$ for DV). In the rural area, the 12km estimates higher impact than the 4km fields, likely due to the spatial smoothing at the 12km resolution. The GV source impacts are subject to less urban-to-rural difference compared to DV source impacts, which is consistent with the CMB estimates.

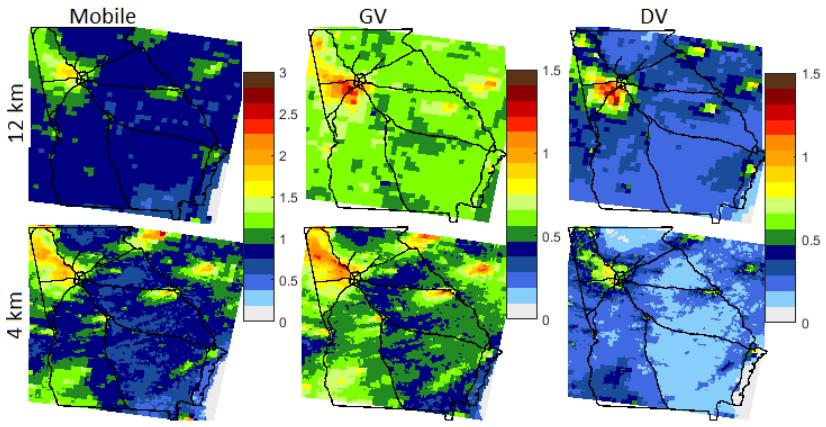

Figure 10. Daily source impact (μg/m^3) spatial distribution on 2008/1/21 at 12 km and 4 km resolutions for mobile source, GV, and DV.

3.3.4 Temporal Trends

Temporally, the estimated source impacts capture the expected day-of-week trends with higher impacts on weekdays than weekends because of more traffic on weekdays. Compared to the CMB trends, the estimated source impacts have similar day-of-week distributions. As an example, day-of-week trends are shown in Fig. 11 at the grid cells where the urban site in midtown Atlanta (JST site) and the rural site about 70 km west of midtown Atlanta (YRK site) are located. These two sites serve as representatives of urban and rural areas. The day-of-week trend is stronger at the urban site than at the rural site as expected due to the urban area's higher traffic density.

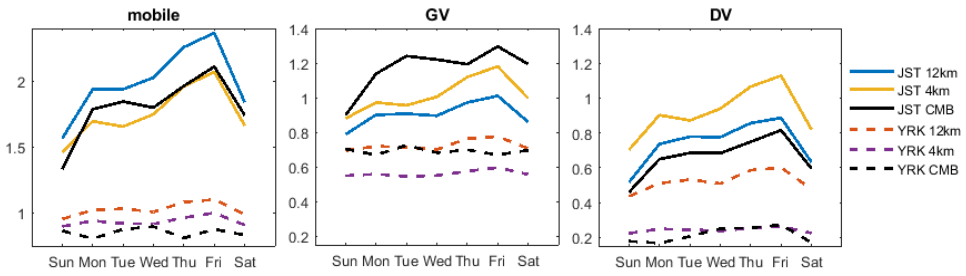

Figure 11. Weekly trends of estimated source impacts (μg/m^3) in 2008 at JST (solid lines) and YRK (dashed lines) sites for comparison of the source impacts by global IMSI

method and CMB estimates. JST is an urban site in Midtown Atlanta and YRK is a rural site about 70 km away from Midtown Atlanta.

3.3.5 Evaluation of the IMSI Source Impacts using Daily Observation-Based Estimates

We compared the global IMSI results with daily CMB source impacts at 11 sites to assess performance. Results are shown in Fig. 12 and bias, error and correlation results are listed in Table 2. The estimated total mobile source impacts are well correlated with the CMB estimates (R^2 = 0.74 and 0.70 for 12 km and 4 km results, respectively), with slope near one and intercept near zero. The average bias at both resolutions are small since calibration involves the use of the observation-based annual averages. NRMSE values are lower and correlations are higher for total mobile impacts than for DV or GV impacts. This can be caused by the uncertainties in CMB as well as in IMSI in separating GV and DV impacts. In CMB, EC and OC are both used as tracer species for GV and DV. For the days when other tracer species are not available, the impacts of the two sources are separated well. In IMSI, only two species are used as tracers for GV and DV with a common NO_x concentration while three tracers are used for mobile sources. This can lead to some bias in the separation of the two sources as well.

Table 2. Bias (NMB), error (NRMSE) and spatiotemporal correlation (RSQ) for mobile source, GV, and DV impacts, on $PM_{2.5}$ in comparison with CMB source impacts using the IMSI method.

		Total Mobile	GV	DV
NMB	12km	0.14	0.012	0.35
	4km	0.19	0.009	0.35
NRMSE	12km	0.53	0.71	1.32
	4km	0.60	0.64	1.05
RSQ	12km	0.74	0.24	0.42
	4km	0.70	0.41	0.47

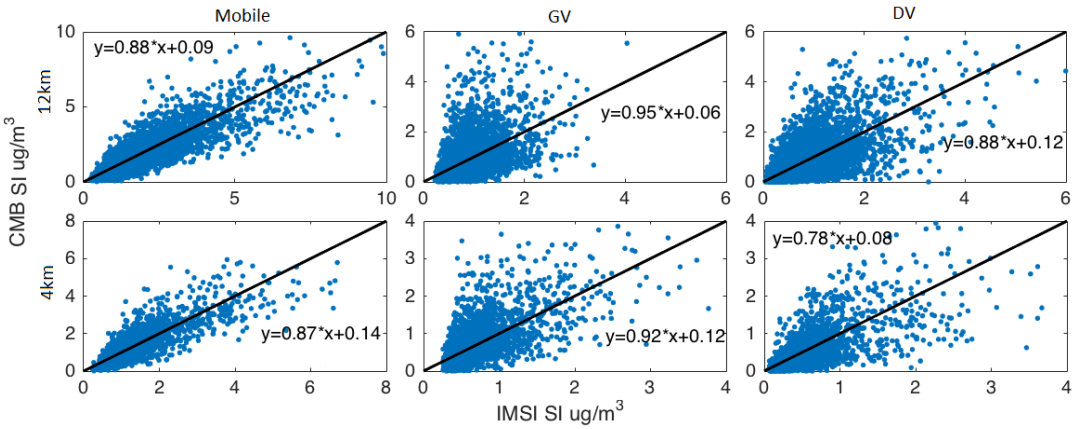

Figure 12. Daily mobile source impacts by CMB and by the global IMSI method (μg/m^3) at all sites and years for total mobile, GV, and DV in 12 km resolution (2002 to 2008) and 4 km resolution (2008 to 2010).

The overall spatiotemporal correlations (RSQ) are given in Table 2. In Table 3, temporal correlations (R) are given for each monitor site. These results show that the extended IMSI method agrees better with CMB estimates in locations with higher populations, likely due to the stronger mobile source indicators when traffic density is larger. This also reflect that the method works better at urban area where the major source of EC, CO, and NO_x are mobile sources. In suburban and rural area, the impact of other sources such as biomass burning on EC can impact the performance of the IMSI approach.

Table 3. Correlations (R) between temporal variations of the daily source impacts estimated by the IMSI method and CMB source impacts.

city	population	Total Mobile		GV		DV	
		4km	12km	4km	12km	4km	12km
Atlanta	420,003	0.88	0.91	0.57	0.51	0.84	0.68
Athens	115,452	0.64	0.62	0.39	0.25	0.53	0.45
Columbus	189,885	0.74	0.78	0.59	0.41	0.70	0.55
Macon	91,351	0.73	0.78	0.61	0.44	0.64	0.52
Augusta	195,844	0.76	0.81	0.63	0.60	0.64	0.64
Rome	36,303	0.63	0.42	0.37	0.33	0.47	0.35
Douglas	11,589	0.59	0.62	0.20	0.25	0.80	0.53
Charlton county	12,171	0.68	0.69	0.36	0.42	0.76	0.37
Yorkville	17,526	0.63	0.59	0.45	0.27	0.49	0.29

3.3.6 Comparison with an alternative IMSI method using local indicators

Instead of using a single standard deviation for all years and all locations to normalize the indicator species concentrations (which we here refer to as our global IMSI method), we investigated the use of location specific standard deviations (local IMSI method). Unlike the integrated indicator developed using the global method, the local IMSI does not provide spatial information. Therefore, to calibrate the indicator to source impacts, the annual average IMSI cannot be used in the local method to spatially resolve annual average CMB data. Instead, we develop the annual average source impact field used to calibrate the IMSI using spatially resolved annual average $PM_{2.5}$ emissions; these are shown in Fig. A16. The daily source impacts are then calculated, as before, using Equation 7. Results of the local IMSI method are summarized in Fig. A19-A21 and Tables A4 and A5 in Supplementary Material. These results are very similar to the global IMSI method in the application of Georgia, with the global method performing slightly better in terms of temporal correlation with the daily CMB source impacts. This method weights the three species differently and provides different spatial distributions with the global method. It provides an alternative method for locations where the spatial distribution of the three species are not representative of the spatial distribution of mobile sources.

3.4 Conclusion

We developed an approach to estimate the spatial and temporal source impacts of mobile sources on $PM_{2.5}$ using three indicator species: CO, NO_x and EC. The approach is computationally efficient to apply and has been applied for generating daily mobile source impacts in Georgia for total mobile sources and separated gasoline and diesel vehicles from

2002 to 2010. The generated source impacts can capture reasonable spatial distribution and temporal trends and show good spatial and temporal agreement with observational based source impacts estimated by CMB. The approach agrees well with CMB estimates for total mobile sources while show lower correlation and larger bias for gasoline and diesel vehicles likely due to the uncertainty in CMB estimates of separated GV/DV impacts. In addition, the approach shows better agreement with CMB estimate s in more populated areas because of less impact from other sources of EC, CO, and NOx in those area. In applying this extended IMSI method, we explored an alternative method with local normalization and found that two methods perform similarly in bias, error, and correlation when compared to daily CMB source impacts. We recommend using the global IMSI approach because it is simpler. Overall, the approach developed in this study can estimate spatially and temporally resolved source impacts on $PM_{2.5}$ of total mobile sources as well as separate gasoline and diesel vehicle sources. The results are currently being used to evaluate the long-term and statewide exposure to mobile sources of residents in Georgia.

3.5 Acknowledgement

This publication was developed under Assistance Agreement No. EPA834799 awarded by the U.S. Environmental Protection Agency to Emory University and Georgia Institute of Technology. It has not been formally reviewed by EPA. The views expressed in this document are solely those of the authors and do not necessarily reflect those of the Agency. EPA does not endorse any products or commercial services mentioned in this publication. We acknowledge the projects that provide the data, including the Georgia Tech HiRes2 Air Quality & Source Impacts Forecasting for Georgia, EPA and CDC PHASE Project, and the ambient air quality monitoring networks, IMPROVE, CSN, and SEARCH. We acknowledge Valerie Garcia and K. Wyat Appel for supplying PHASE CMAQ modeling results.

CHAPTER 4. CALIBRATING R-LINE MODEL RESULTS WITH OBSERVATIONAL DATA TO DEVELOP ANNUAL MOBILE SOURCE AIR POLLUTANT FIELDS AT FINE SPATIAL RESOLUTION: APPLICATION IN ATLANTA

As published in Atmospheric Environment 147 (2016): 446-457.

Abstract

The Research LINE-source (R-LINE) dispersion model for near-surface releases is a dispersion model developed to estimate the impacts of line sources, such as automobiles, on primary air pollutant levels. In a multiyear application in Atlanta, R-LINE simulations overestimated concentrations and spatial gradients compared to measurements. In this study we present a computationally efficient procedure for calculating annual average spatial fields and develop an approach for calibrating R-LINE concentrations with observational data. Simulated hourly concentrations of $PM_{2.5}$, CO and NO_x from mobile sources at 250m resolution in the 20-county Atlanta area based on average diurnal emission profiles and meteorological categories were used to estimate annual averages. Compared to mobile source $PM_{2.5}$ impacts estimated by chemical mass balance with gas constraints (CMB-GC), a source apportionment model based on $PM_{2.5}$ speciation measurements, R-LINE estimates of traffic-generated $PM_{2.5}$ impacts were found to be higher by a factor of 1.8 on average across all sites. Compared to observations of daily 1h maximum CO and NO_x, R-LINE estimates were higher by factors of 1.3 and 4.2 on average, respectively. Annual averages estimated by R-LINE were calibrated by regression with observations

from 2002 to 2011 at multiple sites for daily 1h maximum CO and NO_x and with measurement-based mobile source impacts estimated by CMB-GC for $PM_{2.5}$. The calibration reduced normalized mean bias (NMB) from 29% to 0.3% for $PM_{2.5}$, from 22% to -1% for CO, and from 303% to 49% for NO_x. Cross-validation analysis (withholding sites one at a time) leads to NMB of 13%, 1%, and 69% for $PM_{2.5}$, CO, and NO_x, respectively. The observation-calibrated R-LINE annual average spatial fields were compared with pollutant fields from observation-blended, 12km resolution Community Multi-scale Air Quality (CMAQ) model fields for CO and NO_x, with Pearson correlation R^2 values of 0.55 for CO and 0.54 for NO_x found. The calibrated fields of $PM_{2.5}$ were compared with 4 km resolution mobile source impact fields obtained from an indicator method using the observation-CMAQ fields, with an R^2 value of 0.53 found. The method developed provides high-resolution annual average spatial fields in a computationally efficient manner with low bias. The method is being applied in air quality planning efforts and the pollutant concentration fields are being used in long-term, fine spatial scale health studies.

4.1 Introduction

Traffic is a major source of ambient air pollution, including fine particulate matter ($PM_{2.5}$), carbon monoxide (CO), and nitrogen oxides (NO_x). Both long-term and short-term exposures to traffic-generated air pollutants are associated with adverse health effects such as cardiovascular disease, impaired lung development, and respiratory disease (Brook et al., 2010; Gauderman et al., 2007; Lim et al., 2012; Nordling et al., 2008). With 19% of the United States population living close to roads with heavy traffic, the health burden of

exposure to traffic-related pollutants is potentially significant (Rowangould, 2013). As a result, pollutant monitors have been located near roadways (Chen et al., 2013; EPA, 2009). Assessing exposure to traffic-related pollution is difficult, however, due to the steep, non-linear concentration gradients near roads. Distance to roadway is often used as a surrogate for traffic pollution exposure in health studies (Jerrett et al., 2005). New methods are warranted to provide improved traffic-concentration-exposure relationships for use in health studies.

Ambient measurements and model simulations have been used to assess exposures to traffic-related air pollutants, but both have their limitations. The major issue associated with using measurements is the sparse ambient air monitor network that severely limits the spatial representativeness of exposure estimates. While near-road monitoring does exist (EPA, 2009, 2011; Reche et al., 2011), the network is very limited with single monitors in a few urban areas. Spatial concentration gradients are difficult to capture and generalize to other areas. Further, it is not directly apparent what fraction of the pollutants measured at a monitoring site comes from mobile sources. Air quality models can be used to help address these limitations by simulating spatial and temporal distributions of traffic-related pollution. Air quality models use emissions from sources and meteorological conditions to simulate traffic impacts, typically at the hourly level, over a range of spatial scales. Over regional and global domains, chemical transport models (CTMs) are used to capture large-scale pollutant transport, transformation, and fate, including both primary pollutants emitted directly from sources and secondary species formed in the atmosphere such as ozone and secondary organic aerosol (Baldassarre et al., 2015; Ivey et al., 2015; Liu et al., 2010a). Due in part to the parameterizations used and computational requirements, CTM

approaches typically have spatial resolutions of 4 km or more and, therefore, miss the fine scale gradients of primary pollutants.

For city-level simulations, dispersion models can be used to simulate concentrations of primary pollutants at finer resolutions (Chang et al., 2015; Gulliver and Briggs, 2011; Jerrett et al., 2005; Venkatram et al., 2007). Such models are typically based on solving a simplified form of the pollutant transport equation (e.g., Gaussian models such as the Industrial Source Complex (ISC) model (Bowers et al., 1980)) and have limited descriptions of chemical transformation. Two of the more advanced and widely used dispersion models are the American Meteorological Society (AMS) and Environmental Protection agency (EPA) Regulatory Model (AERMOD) (Cimorelli et al., 2005) frequently used for stationary sources including industries, and the Research LINE-source dispersion model for near-surface releases (R-LINE) (Snyder et al., 2013). R-LINE is a steady-state plume model used in support of evaluating the exposures to near-traffic environments. It is specifically designed for line sources and is formulated with a new plume meandering algorithm for light wind conditions (Snyder et al., 2013; Venkatram et al., 2013). However, previous research found that dispersion models in general over-estimate the pollutant concentrations (Venkatram et al., 2004).

The biased results from emission-based models are being increasingly calibrated to receptor-based observations, as formulated in data blending and data assimilation methods (Crooks and Ozkaynak, 2014; Friberg et al., 2016b; Wilton et al., 2010). Such calibration procedures have long been used in more statistical approaches, such as satellite data models and land-use regression models (LUR) (Beckerman et al., 2013; Lv et al., 2016). Land-use

regression models are widely used for estimating fine-scale air pollution metrics (Arain et al., 2007; Hankey and Marshall, 2015; Wang et al., 2016). LUR models predict fine-scaled and area-specific air pollution fields utilizing predictor variables such as traffic information, population distribution, land use, and meteorology conditions (including, in some cases, wind speed and direction). Typically, LUR models capture the spatial distribution of annual average levels over urban areas. However, LUR model applications are limited to the area in which they are developed (Hoek et al., 2008).

In this study we use R-LINE model to develop 10 years of annual average fields for mobile source-derived $PM_{2.5}$, daily 1h maximum CO, and daily 1h maximum NO_x in the Atlanta metropolitan region. These metrics align with the National Ambient Air Quality Standards (NAAQS) (United States, 1990) and the 1h maximum values are commonly used as surrogate of NO_x and CO pollution in regional planning and health study applications (NAAQS is for NO_2 while we used NO_x). We use a regression approach to calibrate R-LINE model results to observations and to mobile source impacts estimated from observational data, and evaluate results using data withholding. Finally, the bias-corrected fine resolution R-LINE results are compared with regional scale fields derived using previously developed methods (Friberg et al., 2016b; Pachon et al., 2012).

4.2 Methods

Methods used in this work are described in three parts. First, R-LINE is applied to estimate annual concentrations of $PM_{2.5}$, CO, and NO_x from mobile sources in the Atlanta, GA, 20-county metropolitan area at 250 m resolution for 2002 to 2011. An approach was developed for calculating annual averages based on the application of STability ARray (STAR)

method to dispersion models (Chang et al., 2015; D'Onofrio et al., 2016; EPA, 1997) and adjusted with emission diurnal trends. Second, to reduce bias, these fields are calibrated using a regression model approach with ten years of observations for CO and NO_x at five and seven sites, respectively, and, in the case of mobile source $PM_{2.5}$, with ten years of estimates at three locations with speciated $PM_{2.5}$ measurements obtained via the receptor-based source apportionment Chemical Mass Balance Method with Gas Constraints (CMB-GC) (EPA, 2004a; Marmur et al., 2005). Cross validation by data withholding is performed to further evaluate the effectiveness of the calibration and the limitation of the number of monitors. Third, the resulting calibrated fields are then compared to fields at coarser resolution obtained from simulations with the Community Multi-Scale Air Quality (CMAQ) (Byun et al., 1997) blended with observations (Friberg et al., 2016b) by aggregating to the CMAQ grid (as described later).

4.2.1 R-LINE Dispersion Model

The R-LINE model is a steady-state dispersion model for line sources (Snyder et al., 2013). It simulates physical dispersion processes but not chemical processes, so is applicable for primary and chemically inert pollutants. It takes inputs such as wind speed, wind direction, Monin-Obukhov length for turbulence, surface friction velocity, and other meteorological parameters, but does not consider the impact of wet deposition (e.g., due to precipitation) or non-linear chemical transformation (Venkatram et al., 2013). In this research, we use annual average pollutant concentrations for evaluation, which are less impacted than hourly results by the lack of a wet deposition sink. The domain is the 20-county Atlanta metropolitan region. R-LINE simulates line-source emissions (described below) as point

sources along a line and calculates steady state concentrations by solving Gaussian dispersion equations. It provides two options: a numerical integration approach and an approximate analytical solution (Environmental Protection Agency, 2013b). Here we adopt the numerical approach and calculate annual average concentrations for ten years at multiple monitor locations (three for $PM_{2.5}$, five for CO, and seven for NO_x) for use in calibration, and at 250 m resolution (235,296 spatial locations) for use in spatial field development.

4.2.1.1 Meteorological Inputs.

Hourly meteorological data for 2002 to 2011 are generated using AERMET (Cimorelli et al., 2005; EPA, 2004b) and AERMINUTE (EPA, 2015), the meteorological processors of AERMOD. Surface meteorological data are from the National Weather Service (NWS) at the Hartsfield-Jackson International Airport. We use AERMINUTE (Version 15272) to process 1-min wind speed and wind direction data from the Automated Surface Observing Stations (ASOS) (http://www.nws.noaa.gov/ost/asostech.html) to reduce the number of calms and missing wind data in the hourly surface data. AERMET (Version 15181) processes hourly surface friction velocity, convective scale, Monin-Obukhov length, and surface roughness height within the surface layer. The missing hours (0.025% of the total for 2002 to 2011) are not included in the calculation, and meet the data completeness by requirements of EPA policy (more than 90% available) (EPA, 2000).

4.2.1.2 Emission Inputs

Emission inputs to R-LINE are 2010 link emissions based on Atlanta Regional Commission's (ARC) 20-county activity-based travel demand model and scaled to annual average levels for other years. Hourly emissions for 2010 at 43,712 links were generated for CO, NO_x and primary $PM_{2.5}$ over the 20-county regional area; 24h average emission data are shown in Figure 13 for $PM_{2.5}$, CO, and NO_x. Hourly emission rates for 24 hours (assumed to be an average weekday) were generated for the Atlanta Roadside Emissions Exposure Study (AREES) by ARC with the purpose of understanding traffic impacts on air quality in Atlanta. Local traffic emissions are based on the link-level information, including road type and location, traffic volume, and vehicle type and speed. Emission factors are developed using the Motor Vehicle Emission Simulator 2010b (MOVES2010b) (Environmental Protection Agency, 2012) using a 2010 base year with Atlanta traffic volume and speed and vehicle fleet composition information. Relative emissions for the three species differ spatially because of the patterns of diesel and gasoline vehicles. As more CO emissions are contributed by gasoline vehicles and more elemental carbon emissions in $PM_{2.5}$ are contributed by diesel vehicles (Lena et al., 2001; Parrish, 2006), relatively greater CO emissions are observed in the center of the city because pass-through truck traffic is limited on freeways inside the interstate highway (I-285) circling Atlanta .

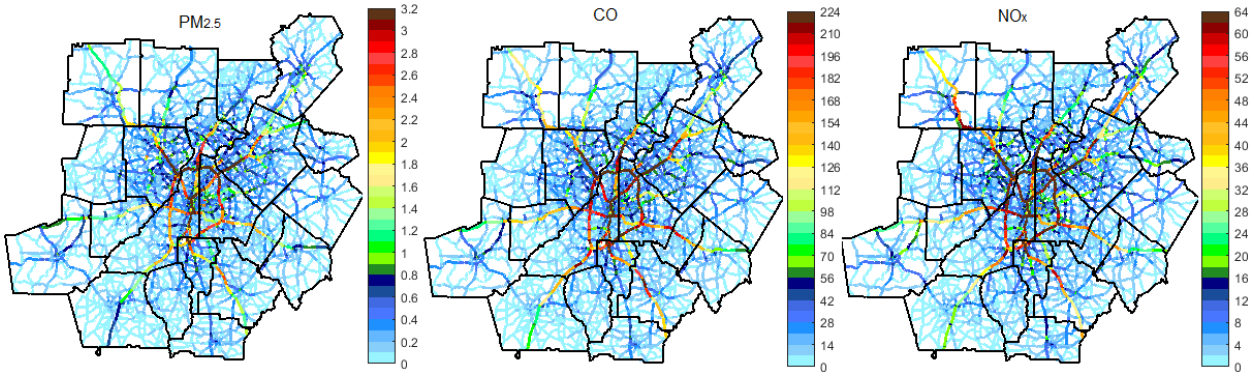

Figure 13. Emissions of $PM_{2.5}$, CO, and NOx by mobile sources for 2010 in 20-county area in Atlanta (24h average) (g/m/s).

4.2.1.3 Annual Average Approach

The STAR approach was developed for computational efficiency by grouping the frequency distribution of wind speed, wind direction, and stability (Environmental Protection Agency 1997), and has been applied to estimate annual mean fields (Chang et al., 2015; D'Onofrio et al., 2016). An annual averaging approach was developed here based on the application of STAR as well as diurnal emission profiles as described below (Fig. A22).

First, low wind speeds ("calm conditions", (EPA, 2000)) were treated by setting a minimum wind velocity of 1 m/s (see SI and Fig. A23 for discussion and analysis) to minimize unrealistically high simulated concentrations. Second, meteorological conditions are categorized for input to R-LINE. In this application, we chose Monin-Obukhov length, wind direction, and wind speed. We defined 80 categories based on these three parameters, with five levels of stability conditions defined by Monin-Obukhov length ranges, four wind directions, and four wind speed ranges (Table 4). Over the 10-year study period (2002-2011), 78 out of the 80 categories were observed.

Table 4. Stability categories for the meteorology conditions.

Parameter	Category	Range
Stability / Monin-Obukhov Length (m)	Unstable	-100 to 0
	Slightly Unstable	-500 to -100
	Neutral	<-500 or >500
	Slightly Stable	100 to 500
	Stable	0 to 100
Wind Direction (Degree)	N	0-45 & 315-360
	E	45-135
	S	135-225
	W	225-315
Wind Speed (m/s)	Bin 1	1≤n<2
	Bin 2	2≤n<4
	Bin 3	4≤n≤7
	Bin 4	>7

Third, we assume a consistent roadway link pattern and vehicle type distribution over time. Annual trends were based on total emissions of the 20-county region in Atlanta estimated by MOVES and are shown normalized to 2010 emissions in Figure 14a. We define an annual average emission ratio ($\overline{ER_j}$) as the ratio of year j emissions vs 2010 emissions in the 20-county area calculated using MOVES (Table A6). Link emissions for each year are the 2010 emissions multiplied by $\overline{ER_j}$ (Figure 14a). The annual emissions decrease over the ten-year period by a factor of 1.8, 1.5, and 2.0 for $PM_{2.5}$, CO, and NO_x, respectively (Figure 14a).

The 24h diurnal trend was scaled using emission ratios as well. With the diurnal emission pattern (24 hours) and 80 meteorological bins, there are 1,920 conditions for each year. Since R-LINE calculated concentrations are proportional to emissions (Venkatram et al., 2013), and the spatial distributions of emissions for each hour are highly correlated with the 24h average (R > 0.97 for CO and NO_x, R > 0.94 for $PM_{2.5}$), we further simplify the calculations by using 24h averaged emissions as input in R-LINE for all hours and retrieve

the emission trends using the ratios of the diurnal variation. Therefore, we define emission ratios for hour k (ER_k) as the total hourly emissions divided by the average of the 24 hourly emissions (Figure 14b). Seasonality and weekly trends are not included in this study.

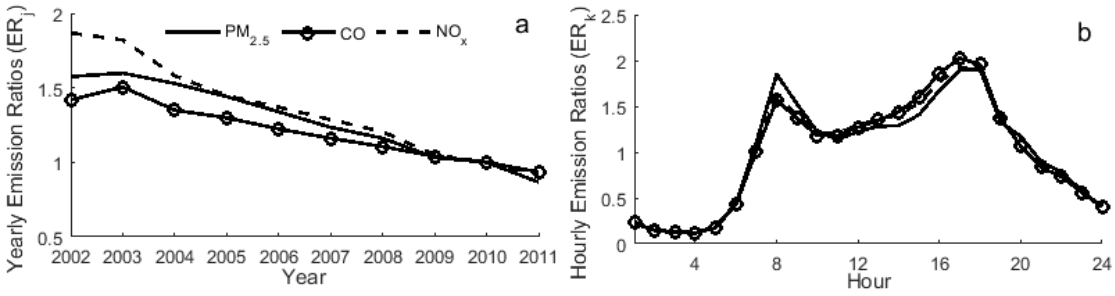

Figure 14. Yearly (a) and diurnal (b) ratios of emissions. ER_j: total emissions of year j over total emissions of 2010; ER_k: total emissions of hour k over 24h average total emissions.

Overall, the annual average is calculated from the concentrations at the same location, adjusted for hourly and annual emissions as Equation 10, where k and m are the diurnal hour and meteorological category hour i is in.

$$C_j = ER_j * \frac{\sum_{i=1}^{H} ER_k * C_m}{\sum_{i=1}^{H} ER_k} \quad \textit{Equation 10}$$

At each location, the annual average concentration for year j (C_j) is calculated from the annual average emission ratio ($\overline{ER_j}$) and an average over all hours (H) in each year with available meteorological data. The concentration of hour i out of H hours (H ≤8760 or 8784 for leap years) in year j is calculated using the STAR bin concentration for bin m (C_m) that matches the meteorological condition of hour i, and weighted by the emission ratio k ($1 \le k \le 24$) that hour i happens in a day. Using our annual average approach (Fig. A 22), we generated 10 years of annual average spatial fields of mobile source $PM_{2.5}$, CO, and NO_x in the Atlanta area. The method reduces the number of simulations by over 100 times,

making the approach efficient and effective for both air quality management and exposure quantification purposes.

4.2.2 R-LINE Model Calibration

Annual CO and NO_x concentrations estimated by R-LINE are calibrated to ten years of monitor data at five locations for CO and seven for NO_x. Annual $PM_{2.5}$ mobile source impacts estimated by R-LINE are calibrated to CMB-GC mobile source impact estimates that are derived from observational data at three monitor sites using pre-determined source profiles. Both linear and log-transformed regressions are explored to optimize calibration, with regression parameters and their confidence intervals estimated using the "jackknife" resampling method (Sahinler and Topuz, 2007). That is, regression parameters are estimated with each available observation data point withheld one-at-a-time, resulting in 40 sets of results for CO, 63 for NO_x, and 30 for $PM_{2.5}$. Regression parameters are obtained by averaging results.

4.2.2.1 Ambient Pollutant Monitor Data.

$PM_{2.5}$ species concentrations were obtained from three sites: Yorkville (YRK), Jefferson Street (JST) and South DeKalb (SDK) (Figure 15, Table A7). The YRK and JST sites are part of the Southeast Aerosol Research and Characterization network (SEARCH) (Hansen et al., 2003), and the SDK site is part of the Chemical Speciation Network (CSN) (Malm et al., 2011). These three sites also monitor CO and NO_x concentrations, along with additional two sites for CO and four additional sites for NO_x (Figure 15). Two of the CO sites and two of the NO_x sites do not have data for all years. There are two YRK monitors

for NO_x at the same location (within 10m). The gas concentrations are obtained from U.S. EPA's Air Quality System (AQS) and SEARCH Network (Environmental Protection Agency; Hansen et al., 2003). Annual averages of 2002 to 2011 for each site are shown in Appendix Table A9 and S10 for CO and NO_x. YRK and Conyers are located in rural areas.

Figure 15. Map of monitoring sites used in Atlanta with population density using 2010 census block data. White lines denote highways. There are two YRK sites: the SEARCH site monitors $PM_{2.5}$/CO/NO_x, and the AQS site monitors NO_x.

4.2.2.2 CMB-GC

The chemical mass balance model with gas constraints (CMB-GC) is a receptor model that modifies CMB with gas ratios (Marmur et al., 2005). CMB uses predetermined source profiles to identify the contribution from each source by using the species concentrations of $PM_{2.5}$. CMB-GC, previously referred as CMB-LGO (Marmur et al., 2005), requires

species concentrations of $PM_{2.5}$ to identify the sources and contributions, and gas concentrations (e.g. CO, NO_x, and SO_2) to help separate source impacts. In Atlanta, only three sites, YRK, JST and SDK, measure $PM_{2.5}$ species concentrations.

4.2.3 Evaluation Methods

Cross validation analysis is applied to evaluate the calibration models in two ways: leave-one-value-out and leave-one-site-out. The raw R-LINE estimates and the calibrated R-LINE estimates from cross validation analyses (referred as Estimate in the equations below) are compared with observations for CO and NO_x, and with CMB-GC estimates for $PM_{2.5}$ mobile source impacts, using normalized root mean square error (NRMSE) and normalized mean bias (NMB) metrics (Equation 8 and Equation 9). The leave-one-value-out approach provides 40 results for CO (available data in 10 years at 5 sites), 63 results for NO_x (available in 10 years at 7 sites), and 30 results for $PM_{2.5}$ (10 years and 3 sites). These results are used for estimating regression parameters for calibration, as already described, as well as for evaluating the calibration model performance. In the leave-one-site-out approach, one site is withheld (all ten years of data) and the sensitivity of calibration model results to the number of sites is assessed. For CO and NO_x, all monitors were withheld (one-at-a-time); for $PM_{2.5}$, only two of the three monitors were withheld, as accurate calibration requires at least one rural monitor.

4.2.4 Regional Scale Models

Calibrated R-LINE annual mean fields at 250m resolution are up-scaled to coarser resolutions for comparison with results from previous studies derived using regional scale models. The regional scale models used are described here.

4.2.4.1 CMAQ-Observation Fusion Method

The CMAQ model is a chemical transport model that simulates air quality, accounting for emissions, meteorology, chemical reactions, and physical transport (Byun et al., 1997). Friberg et al. (2016b) developed a method that fused CMAQ simulation results and observation data to minimize bias and to optimize simulations of temporal and spatial variation. We compare 2002-2011 annual mean concentration fields of 1h maximum CO and NO_x using the fused CMAQ-observation method at 12km resolution (97 grid locations in study area) with the calibrated R-LINE results up-scaled to this resolution (i.e., averaging 48x48 values at 250m resolution).

4.2.4.2 Integrated Mobile Source Indicator Method

The Integrated Mobile Source Indicator (IMSI) method is an approach that uses emission inventory information and concentrations of NO_x, CO, and EC to estimate the mobile source impacts on $PM_{2.5}$ (Pachon et al., 2012). The indicator is a weighted average of normalized concentrations of the three species, with the weighting determined by the ratios of mobile source emissions to total emissions for each species. The unitless indicator accounts for the temporal and spatial variation of NO_x, CO, and EC concentrations. This unitless indicator is scaled to the CMB-GC mobile $PM_{2.5}$ source impacts obtained at three

sites and multiple years by linear regression. The procedure is described in the Appendix (Equation A4).

We generated 2008-2010 annual mean mobile source impact fields at a 4 km resolution for spatial comparison with the R-LINE mobile source $PM_{2.5}$ results using concentrations fields from the fused CMAQ-observation approach (Hu et al., 2010) and emission weighting factors simulated by the Sparse Matrix Operator Kernel Emissions System (SMOKE) (Houyoux et al., 2000). The 4km CMAQ data are available from the Hu et al. (Hu et al., 2010) study (4km resolution data were not available for periods prior to 2008). Calibrated R-LINE results are up-scaled to 4km resolution (i.e., averaging 16x16, 250m resolution values).

4.3 Results and Discussion

4.3.1 R-LINE Model Estimates

Annual average concentration fields of 24h average $PM_{2.5}$, daily 1h maximum CO , and NO_x concentrations were developed by R-LINE in metropolitan Atlanta for 2002 through 2011 (Figure 16, a to c, for 2011, Fig. A24 for other years). Estimated annual average concentrations decreased over time substantially at urban locations, with little change at rural site locations (Fig. A25, a to c).

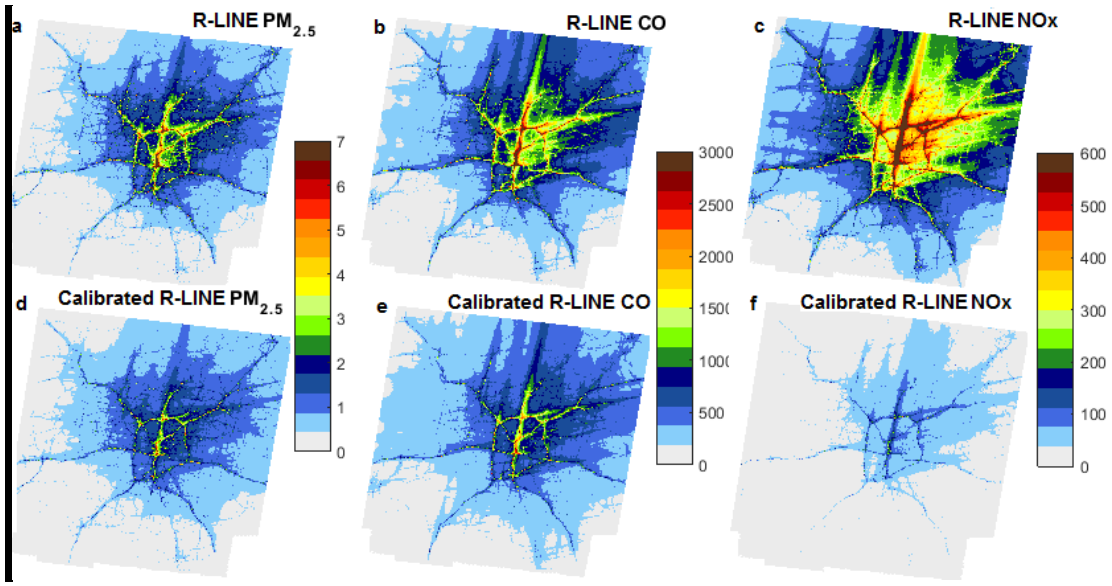

Figure 16. Annual averages of R-LINE estimates by mobile sources in 2011. Panels a and d for $PM_{2.5}$ ($\mu g/m^3$), panels b and e for daily 1h maximum CO (ppb), and panels c and f for daily 1h maximum NO_x (ppb). $PM_{2.5}$ R-LINE results in panel d were calibrated on a log basis, whereas CO in panel e and NO_x R-LINE results in panel f were calibrated on a linear basis.

The annual average approach is computationally efficient and reduces the impact of calm conditions. When calm conditions (wind speed < 1 m/s) are not reset, the calculated annual concentrations for all years increased by about 25% to 30% for $PM_{2.5}$, and 28% to 33% for CO and NO_x, averaged across the domain (Fig. A26). The largest relative impact of calm conditions occurs in rural areas, where $PM_{2.5}$ concentrations increases by about 4.5 times, and CO and NO_x concentrations increase by about 11 times (Fig. A27).

The adjustment of 24h diurnal emission ratios reduces the annual averages. As meteorological conditions and diurnal traffic patterns are correlated, using daily average emissions without diurnal emission profile increase the concentrations by 60% for $PM_{2.5}$, 33% for 1h maximum CO, and 30% for 1h maximum NO_x averaged across the domain (Fig. A28). The highest impact of the diurnal emission adjustment occurs in the lower concentrations regions (Fig. A29). The impact is lower for the daily 1h maximum

concentrations than 24h average concentrations. This is because the 24h average concentrations are highly overestimated when the lower nighttime emissions are not accounted for and the atmosphere tends to be stable.

While the spatial fields of annual means look similar across years due to the largely static distribution of traffic emissions, some differences in these spatial fields due to meteorological variations were observed and varied by region. In the urban core, where population densities are mostly above 200 people/km^2 (Figure 15) and the highest quartiles of concentrations are observed (Fig. A30), annual mean fields varied between years by up to 5%, 7%, and 7%, for $PM_{2.5}$, CO, and NO_x, respectively, based on the Pearson R^2 values for this quartile. The second and third quartiles of concentrations are in suburban areas with lower population density. Meteorological differences across years resulted in up to 81%, 67%, and 64% variations in the annual spatial patterns of the second quartile, and 63%, 71%, and 71% variations in the spatial patterns of the third quartile for $PM_{2.5}$, CO, and NO_x, respectively. For the lowest quartile concentrations which are in rural areas, up to 14%, 20, and 19% variations in the annual spatial patterns are attributed to meteorology for the three species. These results indicate that the change of spatial distribution in annual mean concentrations over years is greater in suburban areas than in urban and rural areas. This implies that the spatial distribution of pollutant concentrations in urban and rural areas is highly determined by traffic distribution; while in suburban area is highly influenced by meteorological impacts.

The maximum annual average concentrations from R-LINE model near roadways are very high. The maximum annual averages of mobile source $PM_{2.5}$, CO, and NO_x are observed

in the downtown and midtown areas of Atlanta where two interstate highways (I-75 and I-85) are merged and the 2013 annual average daily traffic is 289,740 (Georgia Department of Transportation, 2013). Over the 10-year period, the maximum mobile impacts simulated by R-LINE ranged from 27.5 (2011) to 52.5 (2002) $\mu g/m^3$ for $PM_{2.5}$, 8140 (2008) to 13141 (2002) ppb for CO, and 1683 (2011) to 3615 ppb (2002) for NO_x; within a 250m distance, these peak concentrations drop dramatically. Near-roadway studies suggest that the peak R-LINE concentrations and steep near-road gradients are too high. Based on data from a recent near-roadway measurement study in Atlanta (Environmental Protection Agency), measurements of CO and NO_x were lower than R-LINE estimates by a factor of 3.1 and 7.4, respectively; more details are provided in SI Fig. A33 and Table A11.

4.3.2 R-LINE Model Calibration and Evaluation

As 88% and 73% (averaged across the domain (Fig. A31)) of ground level CO and NO_x emissions, respectively, are estimated to be contributed by mobile sources, the annual spatial fields of mobile source contributed concentrations are directly compared with total ambient CO and NO_x observations. We compared the R-LINE derived mobile source $PM_{2.5}$ estimates, on the other hand, to CMB-GC estimated mobile source impacts of $PM_{2.5}$ based on observational data since a much smaller percentage of $PM_{2.5}$ is contributed directly by mobile sources.

We explore the relationships between R-LINE estimates at monitor locations and CO and NO_x measurements and CMB-GC estimates of $PM_{2.5}$ mobile source impacts using linear and log-transformed regressions (Figure 17). The comparison indicates that the R-LINE model captures the trends at monitor locations well, with Pearson R^2 values over multiple

years and locations for $PM_{2.5}$, CO, and NO_x of 0.72, 0.83, and 0.64, respectively, on a linear basis and 0.91, 0.91, and 0.89, respectively, on a log basis.

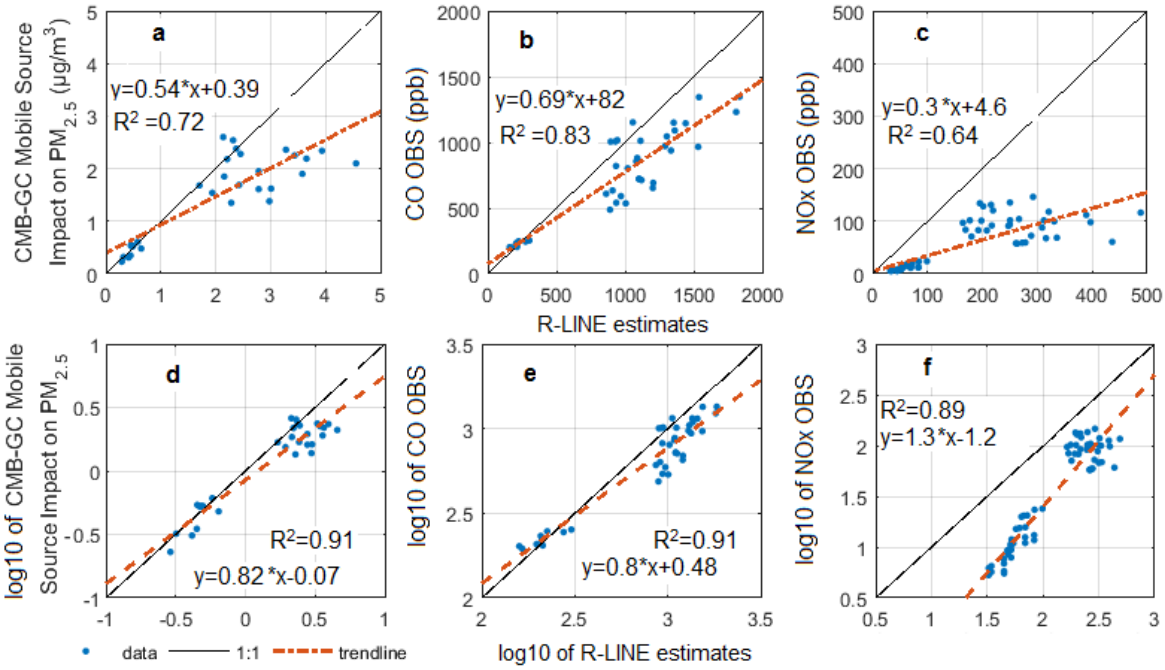

Figure 17. Regressions between R-LINE estimates and CMB-GC estimates of mobile source $PM_{2.5}$ and observations for CO and NO_x, performed on a linear basis in the top row and log basis in bottom row.

Simulated fields of all three species are biased high compared to observational data, indicating overestimation of the R-LINE model. Linear regression of R-LINE estimates and observational data (panels a - c) have slopes of 0.54, 0.69, and 0.30 for $PM_{2.5}$, CO, and NO_x, respectively, indicating higher simulated spatial gradients than observed. Several factors can lead to discrepancies between the R-LINE estimates at monitor locations and CO and NO_x measurements and CMB-GC estimates of $PM_{2.5}$ mobile source impacts. These include the formulation of the model, the properties of the pollutants, the impact from other sources, and the uncertainties in the models and data. The R-LINE model formulation does not include reaction and wet deposition. The R-LINE model generates least bias for CO as a primary pollutant gas with low reactivity and deposition loss. Wet deposition is a sink for

mobile source $PM_{2.5}$ (Zhang et al., 2015), and NO_x is lost by reaction in the atmosphere. At the rural sites (YRK and Conyers), R-LINE estimated NO_x concentrations are much higher than observations. This may be due to the lack of sinks in R-LINE resulting in larger impacts from urban core emissions, and due to an over-estimation of modeled emissions (Anderson et al., 2014; Fujita et al., 2012; Liu and Frey, 2015). Moreover, there is a mismatch between the R-LINE estimates and the data used for calibration from direct measurements and from CMB-GC estimates. For CO and, to a lesser extent, NO_x, the observations include impacts of other sources, such as CO derived from oxidation of organics in the atmosphere, whereas the R-LINE estimates are derived entirely from traffic emissions. For $PM_{2.5}$, the CMB-GC estimates, while observation based, are prone to modeling uncertainties of about 45% of mobile source impacts on average based on a study at JST conducted from 1999 to 2004 (Balachandran et al., 2013); this uncertainty is due to uncertainties in measurements and specified source profiles and limitations in the calculation methodology such as number of sources.

Calibrating R-LINE estimates based on observations and models that use observational data can substantially improve exposure assessment and more accurately reflect mobile source impacts on pollutant concentrations for planning purposes. Here we use linear and log-transformed regression analyses (Figure 17) to develop equations for calibrating R-LINE estimates to CO and NO_x measurements and CMB-GC $PM_{2.5}$ mobile source impacts using all available monitors from 2002 to 2011 in the domain. Error and bias for the raw R-LINE estimates and the calibrated R-LINE estimates are shown in Table 5. A discussion of results for each species follows.

Table 5. Error and bias from cross validation.

REGRESSION		NRMSE			NMB		
		Raw R-LINE	Leave-one-value-out	Leave-one-site-out	Raw R-LINE	Leave-one-value-	Leave-one-site-out
$PM_{2.5}$	linear	39%	35%	50%	29%	13%	12%
	log		24%	49%		0.3%	13%
CO	linear	33%	17%	20%	22%	2%	1%
	log		16%	16%		-1%	1%
NO_X	linear	326%	70%	101%	303%	49%	69%
	log		44%	63%		15%	20%

4.3.2.1 $PM_{2.5}$

For mobile source $PM_{2.5}$, the log-transformed regression of the R-LINE estimates and CMB-GC estimates performed better than the linear regression (Table 2) using leave-one-value-out cross validation, with lower NRMSE and NMB (Table 2), and higher R^2 (Figure 17 - 0.91 for log regression versus 0.72 for linear regression). The slope of log-transformed regression is less than one, and the NMB of R-LINE estimates at all three sites are positive compared to CMB-GC results, indicating that calibration reduces near-roadway gradients. Therefore, the log-transformed regression was used to calibrate the R-LINE mobile source impacts of $PM_{2.5}$.

The calibrated R-LINE estimates are spatially more homogeneous than the raw R-LINE results, with the lower values increased slightly and the higher values decreased (Figure 17d). The leave-one-value-out cross validation indicates that the calibration models are capable of estimating the mobile source impacts with lower NRMSE, 24% compared to 39% by R-LINE, and less NMB, 0.3% compared to 29% by R-LINE (Table 2).

However, with only three sites available for estimates of mobile source $PM_{2.5}$, one rural site and two urban sites, the impact of removing a site is substantial. In our leave-one-site-

out evaluation, we only considered withholding one of the two urban monitors as the regression results are very poor without the rural monitor. Calibration with an urban monitor withheld resulted in higher NRMSE than the raw R-LINE data (49% versus 39%) and lower NMB (13% versus 29%). The higher NRMSE in the calibrated R-LINE results suggests that at least three monitors, spatially distributed, are needed to provide reliable calibration.

4.3.2.2 CO

For 1h maximum CO, the log-transformed and linear regressions of the R-LINE estimates and observations performed similarly (Table 2). Linear regression yielded an intercept of 82 ppb (95% confidence interval as 81 to 83 ppb), which compares well with a U.S. background concentration estimated to as 40 to 200 ppb (Seinfeld and Pandis, 2012b) and with background levels found at rural locations in the southeastern U.S (Blanchard, 2013). When the background of 82 ppb is removed from observations and the log regression is rerun, a slope of 1.007 (±0.04) is found, indicating that, when the background is removed, the linear and log-transformed relationships are effectively the same. Therefore, we opted to use a linear calibration equation.

Compared to the raw R-LINE estimates, the calibrated R-LINE estimates using the linear calibration are slightly higher in rural areas due to the addition of a background concentration of 82 ppb (Figure 17e), and maximum concentrations decrease by about 30%. Linear calibration of the CO estimated NRMSE of 17%, compared to 33% by R-LINE, and NMB of 2%, compared to 22% by R-LINE.

Cross validation by withholding each monitor from the analysis yields smaller NRMSE and NMB, similar to the leave-one-value-out R-LINE results (Table 2). This suggests that the annual mean field estimated by R-LINE for 1h maximum CO, calibrated with five CO monitors in the metropolitan Atlanta area, is weakly sensitive to the number of monitors. With the CO monitors covers rural, urban, suburban, and near road locations, the calibration model is able to captures the spatial distribution using the sufficient inputs. As a result, the calibration model generates less errors and biases when monitors are more spatially distributed.

4.3.2.3 NO_x

For 1h maximum NO_x, comparison of R-LINE estimates with observations indicates that R-LINE overestimates NO_x at both urban and rural locations. The raw R-LINE NRMSE is 326% and NMB is 303%. NO_x is most biased at rural sites, with NRMSE 510% and NMB 490% at YRK site, compared to 250% for NRMSE and 230% for NMB averaged across all urban sites. Log-transformed regression yields a slope of 1.3, resulting in larger near-road concentrations than calibration by linear regression. The near-zero intercept of the linear regression is consistent with a traffic dominated impact on NO_x. Therefore, we chose the linear regression for calibrating NO_x.

Compared to the raw R-LINE estimates, the distribution of results using linear calibration (Figure 17f) shows a decrease of 59% at the lowest quartile, 64% at median, and 67% at top quartile. Linear calibration evaluated using the leave-one-value-out approach yields NRMSE of 70% compared to 326% by R-LINE, and NMB of 49% compared to 303% by R-LINE, substantially reducing the errors and biases.

Cross validation by withholding each of the six monitor locations one-by-one (two YRK sites withheld together) also shows lower NRMSE and NMB compared to R-LINE. This indicates the improvement by calibration over raw R-LINE results is only slightly sensitive to the number of monitor locations available for calibration in the case of NO_x with its six distinct monitor locations.

4.3.2.4 Model Selection

Based on the discussion above, the equations shown in Table 6 were selected for calibration. For $PM_{2.5}$, the log-transformed linear regression is selected with slope of 0.818 (95% confidence intervals as 0.817 to 0.819 using the jackknife regression method) and intercept of 0.072 (confidence interval as 0.069 to 0.075). For CO, linear regression selected with a background of 82 ppb (confidence interval of 81 to 83 ppb), and slope of 0.688 (confidence interval of 0.687 to 0.689) as scaling factor of the spatial gradients. For NO_x, linear approach is selected, with spatial scaling factor of 0.301 (confidence interval as 0.300 to 0.302) and intercept of 4.6 (confidence interval as 4.5 to 4.7). Calibrated fields for 2011 are shown in Figure 16, d to f; calibrated fields for years 2002-2010 are shown in Appendix (Fig. A32).

Table 6. Selected models for calibrating R-LINE.

Species	*Form*	*95% Confidence intervals of*		*Correlation Coefficient*
		Slope	Intercept	
$PM_{2.5}$	log10-transformed	0.818±0.001	0.072±0.003	0.95
1hr-max CO	linear	0.688±0.001	82±1	0.90
1hr-max NO_x	linear	0.301±0.001	4.6±0.1	0.80

4.3.3 Comparison with Regional Scale Model Results

To assess consistency between the fine resolution R-LINE modeling approach used here and regional scale approaches using coarser resolution chemical transport modeling, we compared calibrated R-LINE results aggregated to a 12 km resolution to correspond to CMAQ-observation fused estimates for CO and NO_x for 10 years (2002-2011), and aggregated to a 4 km resolution to correspond to IMSI mobile source impact fields for $PM_{2.5}$ for the three years 2008-2010, the time period for which data are available from other studies (Hu, 2014). The spatially averaged calibrated R-LINE estimates of CO and NO_x agree well with CMAQ-observation spatial distribution, with R^2 0.55 for CO, and 0.54 for NO_x, for $PM_{2.5}$ agree well with IMSI with R^2 0.53 (Figure 18).

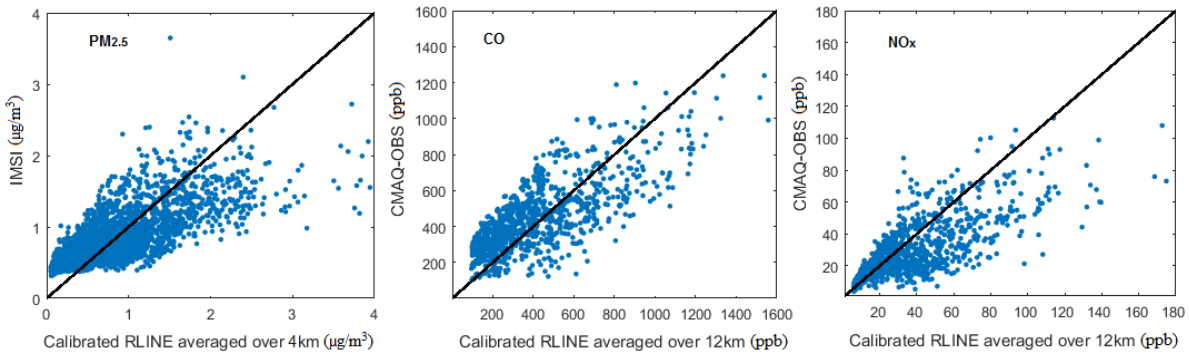

Figure 18. Calibrated R-LINE results versus IMSI mobile source $PM_{2.5}$ estimates at 4 km resolution for 2008-2010 and versus CMAQ-observation fused CO and NO_x at 12 km resolution for 2002-2011.

The comparisons in Figure 18 are spatiotemporal, with 3 years and 873 locations for $PM_{2.5}$ and 10 years and 97 locations for CO and NO_x. The calibrated R-LINE $PM_{2.5}$ results

approach zero at low concentrations whereas the IMSI results have a non-zero minimum. The IMSI minimum concentration is due to the inclusion of background CO and EC levels in the IMSI estimation; the R-LINE results include no background and no intercept was used in the $PM_{2.5}$ calibrations.

4.3.4 Population-Weighted Concentration

To assess the impact of the fine resolution modeling on exposure estimates, we use 2010 census block data (Census Bureau, 2012), distributed to 250 m grid cells by weighting the population in each cell by area in the block, to estimate population-weighted concentration. Population at 250m, 4km and 12km resolution are estimated and population-weighted spatial averages are obtained by equation 11.

$$\text{population weighted concentration} = \frac{\sum_i^N conc_i \times population_i}{\sum_i^N population_i} \qquad \textit{Equation 11}$$

Here, N is the number of 250m grid cells (235,296). Population-weighted annual mean concentration estimates using raw R-LINE, calibrated R-LINE, and regional scale model fields were calculated for the three pollutants (Table 7 for 2010 and Table A9 for all years). The mobile contributed concentrations based on calibrated R-LINE and IMSI are 11% and 9% of the concentrations based on total $PM_{2.5}$ concentrations using a CMAQ-OBS data fusion approach at 4km resolution in 2010 (12.8 $\mu g/m^3$). Over the 10-year period (2002-2011), calibration reduced the R-LINE-based population-weighted concentration by 28% to 36% for mobile contributed $PM_{2.5}$, by 24% to 30% for CO, and by 202% to 216% for NO_x (Table A9). Even after calibration, the population-weighted concentration based on R-LINE is greater than the population-weighted concentration based on regional scale

modeling, possibly due to the coarse resolution of the regional scale modeling underestimating urban exposures. On the other hand, exposure estimates based on central site data alone, such as the CMB-GC mobile source impact estimates and observations of CO and NO_x at the Atlanta central monitor JST, are higher than the population-weighted concentrations based on calibrated R-LINE, on average by 12% for $PM_{2.5}$, by 60% for NO_x, and by 21% for CO. This suggests that the fine scale spatial distributions of traffic-related pollution and population are correlated and likely results in higher exposures than predicted by regional scale models and lower exposures than predicted by central site monitors.

Table 7. Population-weighted concentration in 2010 by the raw R-LINE, calibrated R-LINE, and regional scale models.

	R-LINE	*calibrated R-LINE*	*IMSI/ CMAQ-OBS*
$PM_{2.5}$ mobile source impact ($\mu g/m^3$)	1.88	1.37	1.11
CO (ppb)	733	588	295
NO_x (ppb)	148	49	31

4.3.5 Limitations

The calibrated R-LINE approach developed here for estimating annual average mobile source pollutant concentration fields at fine resolution is computationally efficient and consistent with available observational data. However, there are several limitations to the approach.

One limitation of our approach is use of the STAR method for categorizing meteorological parameters in the development of R-LINE annual average fields. For example, in this study we divided the wind direction into four bins, which can lead to substantial spatial

discrepancies. Finer categorization can help reduce these errors, but at the cost of computational efficiency. Evaluation of the STAR method, coupled with the treatment of calm conditions and the use of average diurnal emission trends described in this work, could be improved with better spatial coverage of observations to better characterize the tradeoffs between computational efficiency and accurate simulations.

A second limitation of the calibrated R-LINE approach is its dependence on available monitor data in developing the calibration models. Although there may be a sufficient number of years available, a study area may not have a sufficient number of monitors to provide adequate spatial coverage. In this study of metropolitan Atlanta, the three monitors with speciated $PM_{2.5}$ were marginally sufficient to calibrate mobile source $PM_{2.5}$ R-LINE estimates, reducing bias but increasing error. For CO and NO_x, the numbers of monitors available (five and seven, respectively) were sufficient to reduce bias and error in the R-LINE annual estimates based on cross-validation results. The spatial distribution of monitors used for calibration is also an important factor in calibration of R-LINE estimates.

The use of CMB-GC to estimate mobile source $PM_{2.5}$ is another limitation of the calibrated R-LINE approach. As there is no direct measurement of mobile source impacts and mobile sources contribute only a small portion of total $PM_{2.5}$, R-LINE $PM_{2.5}$ calibration is based on CMB-GC source apportionment modeling that uses speciated $PM_{2.5}$ data. Uncertainties in source apportionment modeling are large, as evidenced by the range of results obtained by applying different methods (Balachandran et al., 2013). Moreover, the availability of speciated $PM_{2.5}$ measurements is limited over time and space. One solution is to compare the mobile source impacts to the more commonly measured total $PM_{2.5}$ concentrations

assuming a spatial homogeneous contribution from all other sources in the domain, as applied in D'Onofrio et al. (2016).

While R-LINE can be used to estimate mobile source pollutant concentrations at very fine resolution, the accuracy of results will be limited by the use of the STAR approach developed for computational efficiency as well as the emission data used for road links. Calibration can reduce biases in near-road gradients in the R-LINE estimates, but long-term (i.e. five or more years) monitoring at multiple sites that are spatially distributed (e.g. at least one urban, suburban and rural monitor) are needed to develop the regression models. Finally, attention must be paid to the potential mismatch of R-LINE estimates of pollutant concentrations, which are from mobile sources only, and pollutant measurements used for calibration, which are from all sources.

4.4 Conclusion

Calibrated R-LINE modeling provides high-resolution annual mean concentration fields useful for air quality planning and long-term exposure studies. In particular, we extended the STAR approach for the treatment of calm meteorological conditions, diurnal emission adjustment, and calibration to observational data. In the application of R-LINE with a ten-year period in the metropolitan Atlanta region, the annual average approach reduces computation time, and the treatment of calm conditions and application of diurnal emission ratios in calculating that annual averages reduce the estimates substantially. The calibration method reduces bias and NRMSE. The calibration model requires at least three spatially distributed sites; otherwise it becomes sensitive to the change of sites used. The calibrated R-LINE results at the fine resolution present higher population exposures than estimated

by calibrated regional scale models. This study for the spatial information help improve and understand the infrastructure project planning. The approach has been applied to scale simulated concentrations for air quality analyses by the ARC (D'Onofrio et al., 2016). The results are also being used for fine scaled health analysis.

4.5 Acknowledgement

This study was conducted as part of the Southeastern Center for Air Pollution and Epidemiology (SCAPE) supported by U.S. EPA under Grant Number R834799. Its contents are solely the responsibility of the grantee and do not necessarily represent the official views of the U.S. EPA. Further, U.S. EPA does not endorse the purchase of any commercial products or services mentioned in the publication. We would like to acknowledge the measurement networks IMPROVE, CSN, and SEARCH. We acknowledge Yongtao Hu for providing the data for comparison in our modeling process.

CHAPTER 5. CHARACTERIZATION OF TRAFFIC RELATED POLLUTANT CONCENTRATION GRADIENTS USING AIR DISPERSION MODEL R-LINE, PASSIVE SAMPLER DETECTORS, A MOBILE PLATFORM, AND FIXED-SITE MONITORS

Abstract

Spatial gradients of ambient air pollutant concentrations can affect human exposure to pollution. In the assessment of human exposure to traffic related pollutants, both measurements and simulations can be used to capture the local pollutant concentration gradients. Though the line-source dispersion model Research-Line (R-LINE) is able to generate near-road spatial gradients, it needs to be calibrated to correct for biases. In this study, we characterized the spatial gradients of two-week averaged near-road pollution, comparing measurements and simulations in a larger region over the Atlanta metropolitan area. We compared measurements of concentration gradients of multiple air pollutants, NO_x, NO_2, $PM_{2.5}$, black carbon, and eight volatile organic compounds, from four methods, passive sampler detectors, mobile platform sampler, fixed monitors, and R-LINE simulations. We found that concentrations decrease by a factor of up to 3.1 from highway adjacent areas (<100m away from highway) to remote areas (>1500m away from highway) for all pollutants in measurements, and by a factor of up to 4.2 in R-LINE estimates. The R-LINE simulations yield larger spatial gradients and higher concentration levels due partially to the overestimation of the emissions and insufficient dispersion near roadways.

The comparison of a mobile platform measurement system with fixed monitors suggests a good agreement of concentrations. The comparison of near-road spatial gradients by passive sampler detectors and R-LINE indicates that the calibrated R-LINE estimation well captures the near-road gradients of both concentration levels and spatial variations. R-LINE better simulates averaged concentrations than hourly ones because of the uncertainties in meteorology and emissions inputs.

5.1 Introduction

The traffic-related air pollutants (TRAPs) have been the major source of human exposure in urban areas (Colvile et al., 2001; Rowangould, 2013). Typical TRAPs include black carbon (BC), carbon monoxide (CO), nitrogen oxides (NO_x), fine particulate matters ($PM_{2.5}$), and volatile organic compounds (VOCs). Exposure to those pollutants is found to result in adverse health effects such as cardiovascular diseases and asthma (e.g., Chen et al., 2015; Chen et al., 2013; Gehring et al., 2010; Pennington et al., 2017a; Strickland et al., 2010). However, the accuracy of the exposure measurements still needs evaluation and improvement as many factors can affect the measurements, such as the exposure time and mobility during exposure (Dons et al., 2013; Ganguly et al., 2015; Jerrett et al., 2005; Kingham et al., 2013; Pennington et al., 2017b).

One important aspect of the exposure measurements is the fine-scale spatial gradients of the TRAPs. The estimates of spatial gradients of on-road and near-road concentrations largely affect the accuracy of the exposure assessment at fine scales. For example, Riley et al. (2014) observed that the BC concentration increased three-folds within 10m of the roadway edge as compared to far-road measurements in a study conducted in New Mexico.

As such, in exposure projections, estimates in coarse resolutions cannot capture the high near-road exposure, while a fine resolution estimate might not be accurate. Spatial gradients are necessary for the accuracy of exposure assessment. Attention has been given to the evaluation of the spatial gradients of the TRAPs using different measurement techniques and modeling techniques (Batterman et al., 2014; Dons et al., 2013; Moutinho et al., 2016; Patton et al., 2017; Riley et al., 2014).

The mobile monitoring platform is a widely used measurement method for assessing spatial and temporal gradients (Hagler et al., 2010; Hu et al., 2012; Riley et al., 2014). In addition to measuring real-time on-road and near-road concentrations, the mobile platform can also be used to estimate the concentrations in a small area (e.g., radius in 600m), referred to as a 'fuzzy point' (FP) (Riley et al., 2016a). FPs can provide more robust averages as well as spatial distributions of concentrations by including concentrations from all directions (Larson et al., 2009; Riley et al., 2016a) and, therefore, is a good measurement for evaluation of spatial representativeness of fixed monitors.

Passive sampler detectors (PSDs) are often used in spatial gradients measurements of air pollutant concentrations (Knibbs et al., 2016; Lai et al., 2004; Riley et al., 2016b). The PSDs are set at a fixed location to collect air pollutants over a time period. They can detect a large number of VOCs but are limited by temporal resolution as they typically need several days for sample collection (Riley et al., 2016b). The PSD measurements over the sampling period are less affected by meteorology conditions and more representative of the average spatial gradients than measurements with high temporal resolutions (e.g.,

hourly measurements) when used in the characterization of spatial gradients because of the relatively long collection time.

The dispersion model R-LINE is designed to estimate impacts of line source emissions (Snyder et al., 2013), such as traffic emissions. It has been used to capture spatial gradients of air pollution concentrations at fine resolutions (e.g., 10m resolution and 250m resolution) (Batterman et al., 2015; Chang et al., 2015; Moutinho et al., 2016; Patton et al., 2017; Zhai et al., 2016). However, it was found that R-LINE overestimated the annual average concentrations of CO, NO_x, and $PM_{2.5}$ in a study conducted in Atlanta (Zhai et al., 2016) and elsewhere (Venkatram et al., 2013). Given the overestimation issue in R-LINE, the model needs to be calibrated to simulate spatial gradients.

To characterize the spatial gradients of near-road concentrations, we compared the concentrations of traffic related pollutants such as NO_x, CO, and VOCs using dispersion model R-LINE and measurements of passive sampler detectors and mobile platform in Atlanta. We used the PSD measurements set close to roadways and R-LINE to characterize the spatial gradients of near-road concentrations, and the FP measurements to evaluate the representativeness of the regulatory fixed monitors for the surrounding areas.

5.2 Methods

5.2.1 Mobile Platform at Fuzzy Points

The mobile platform used in this study was developed in the Center for Clean Air Research (CCAR) project and described in Riley et al. (2014) for instrument and methodology, and in Riley et al. (2016a) for measurement conditions in Atlanta. The FPs are locations that

the mobile measurement platform drove around in radius smaller than 600m between 13:00 to 19:30 local time on September 7th to September 17th, 2013. The vehicle with the mobile platform drove around FPs for ~6 to ~10 minutes and collects a measurement every 10 seconds. The medians of the measurements during collection period were considered as a representative of the ambient pollutant concentrations. The measurements of NO_x, NO_2, black carbon (BC), and particles by nephelometer are reported.

The locations of the FP locations are located in areas with different traffic emissions as reflected by NOx hourly emissions (Figure 19). The red circle line on the map denotes the perimeter I-285 which is one of the most trafficked highways in Atlanta. The light blue lines are the roads with light traffic. There were 29 FPs set in Atlanta near roads with different traffic volumes. The FPs includes the areas of fixed monitor sites, i.e., Jefferson St site (JST) and South DeKalb site (SDK), the I-75/I-85 connector where I-75 and I-85 merge, the large highway intersection in northeastern Atlanta, remote locations stet up to ~60 km west where the rural SEARCH monitor at Yorkville is located, and locations close to railyards.

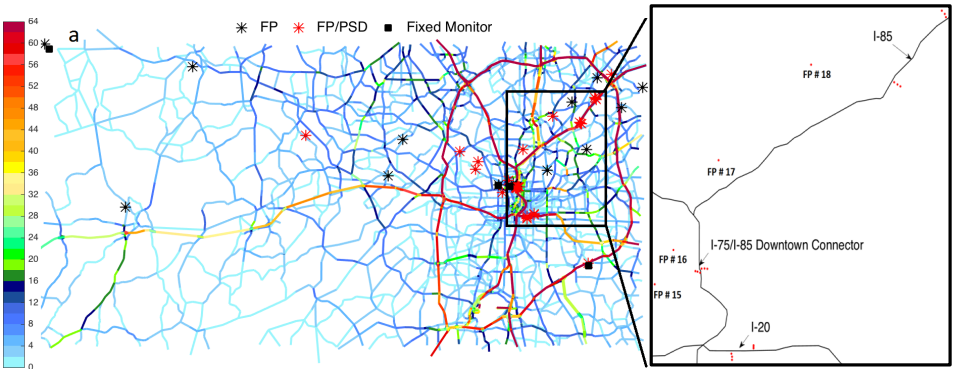

Figure 19. Map of FP, PSD, and fixed monitor locations. The color lines in the background of the map are the hourly link-level mobile source emissions(g/m/s) for all roads in the areas. The box on the right zooms in the squared area in the left map to show

the PSD spatial gradients sampling design. On the zoomed map, the black lines are the major highways as marked, and the red spots are locations of near-road PSD samplers. Four FP set for background impact of highways are marked for FP # 15 to # 18.

5.2.2 Passive Sampler Detectors

The passive sampler detectors measured NO_x and the 8 VOC pollutants to assess mobile source impacts near road. The VOCs measured are short-chain alkane, pentane, three long-chain alkanes (*n*-nonane, *n*-decane, and *n*-undecane), and aromatic hydrocarbons (benzene, toluene, *m*-xylene, and *o*-xylene).

The samplers passively collected air pollutants from ambient environment starting from 11 am on September 5th to 9 pm on September 18th, 2013 (local time). In total, 28 passive sampler detectors were placed near major highways of Atlanta as well as railyard and rural areas at the same locations with FP (Table 8, Figure 19). Their distances to major highways are used to reflect the spatial resolutions of the gradients. The distances were measured using Google Map Measure function using the latitude and longitude of the PSD location to location of the edge of roads.

We grouped the 28 PSDs into 7 groups (Table 8). The first three groups monitored fine scale near-road gradients on both sides of the highways between ~100m to ~2000m away from highway edges. The highways monitored are I-75/I-85 downtown connector, I-20 downtown section, and I-85 in northeast area of Atlanta. Four locations (FP # 15 to # 18 in Figure 19) that are 1km to 2km away from the I-85 and I-75/I-85 connector are included to reflect the background impact of the highways to relatively far areas. The background impact of I-20 can be reflected by FP # 15 and #16 as they are all in the Midtown to Downtown area of central Atlanta. Group 4 measured the impact of railyard to nearby

neighborhood with the detectors ~100m away from the edge of railyards. Group 5 measured the rural area which reflects the background impact of the traffic from central Atlanta area. Group 6 and 7 are located near to the interstate I-285 and the Spaghetti Junction at the cross of I-285 and I-85, reflecting the near-road impact from heavy traffic.

Table 8. PSD locations and their distance to major highways in Atlanta. The distances are from monitoring location to the edge of closest highways. For I-75/I-85 connector, I-20, and I-85, three detectors are located on both sides of the roadways.

Group	Highway	Distance (m)
1	I-75/I-85 Downtown Connector	30
		135
		218
		18
		130
		253
		1900
		1060
2	I-20 Downtown (SE) section	89
		153
		222
		102
		232
		366
3	I-85 NE	100
		260
		408
		55
		195
		380
		971
		2340
4	Railyard	150
		95
5	Rural area	5090
		7650
6	I-285 SE	340
7	Junction of I-85 & I-285	700

5.2.3 Fixed Monitors

The hourly measurements at regulatory monitors in the studied areas are used for comparison with the FP and R-LINE data (Figure 19). There are four monitors used in this study for NO_x, NO_2, BC, and particles by nephelometer. All four measure hourly NO_x and NO_2 and two of them measure BC and particles by nephelometer. The Jefferson Street (JST) in midtown Atlanta area provides a comprehensive set of air quality measurements as part of the Southeast Aerosol Research and Characterization network (SEARCH) (Hansen et al., 2003). The South DeKalb (SDK) site is a U.S. EPA Air Quality System (AQS) (Environmental Protection Agency) monitor located near Interstate I-285 (~600m away). The Yorkville site is a SEARCH network monitor located ~70km away from center of Atlanta in a rural environment. The site at Georgia Institute of Technology campus close to the I-75/I85 connector (GaTech site) is an U.S. EPA site that measures NO_x and NO_2 hourly concentrations. The YRK and JST sites have nephelometer measurements which can be used to estimate $PM_{2.5}$.

5.2.4 Dispersion Model R-LINE

The Research-Line model (R-LINE) is a steady-state dispersion model that is designed for line sources (Snyder et al., 2013). It estimates concentrations using line emissions and meteorology inputs and generates concentration estimates based on dispersions without processing of wet deposition and chemical reactions. In this study, we used hourly link-level emissions of NO_x, CO, and $PM_{2.5}$ that were generated by Atlanta Regional Commission's (ARC) 20-county activity-based travel demand models for a typical weekday in 2010 for 43,712 links in the Atlanta area. We used the same emission distributions for the period from 2010 to 2013 with total emissions scaled year to year.

Therefore, we obtained hourly emissions for 2013 scaled from 2010 link-emissions using the total emissions developed by the Motor Vehicle Emission Simulator 2010b (MOVES2010b) (Environmental Protection Agency, 2012). The meteorological inputs were estimated using AERMET and AERMINUTE (EPA, 2004b, 2015) for each hour. More information about the emissions and meteorology information can be found in Zhai et al. (2016). The concentrations were simulated at the locations of the FPs and PSDs using for the same time period.

5.3 Results and Discussion

We compare the R-LINE estimates with field measurements in two ways: near-road concentrations at two-week average levels for R-LINE and PSD; the cross method comparison at hourly levels for R-LINE, FP by mobile platform, and fixed monitors. For the near-road gradients, we first present the gradients for each highway by the two methods, and then compare the spatial variation of the two. For the hourly comparison, we first compare the two measurements by mobile platform and by fixed monitors, and then compare the R-LINE estimates versus the two measurements. Overall, R-LINE estimates the spatial variation in relatively good agreement with PSD measurements but overestimates the spatial gradients. FP and fixed monitors agree well in the spatio-temporal comparison. However, R-LINE does not have good agreement with the two measurements in the spatio-temporal variations on hourly level (Appendix D.1 and D.2).

5.3.1 Near-road Spatial Gradients by PSD and R-LINE

The I-75/I-85 downtown connector is located in the highly populated midtown to downtown areas of Atlanta and merges the two major highway, I-75 and I-85. Therefore, it has the highest near-road concentrations of most pollutants and sharpest decrease of the three highways for R-LINE and PSD (Figure 20, brown lines). The I-20 highway is located near downtown area of Atlanta and has relatively heavy traffic. It shows the second highest concentration for most pollutants (Figure 20, yellow lines). The highway I-85 in the northeast area of Atlanta carries mostly light-duty vehicle traffic and limited heavy-duty vehicle traffic because all heavy-duty vehicle traffic going through Atlanta without a destination inside the perimeter I-285 are required to use I-285 for detour (State of Georgia, 2013). Therefore, it has relatively lighter concentrations of pollutants compared to the other two highways (Figure 20, green lines).

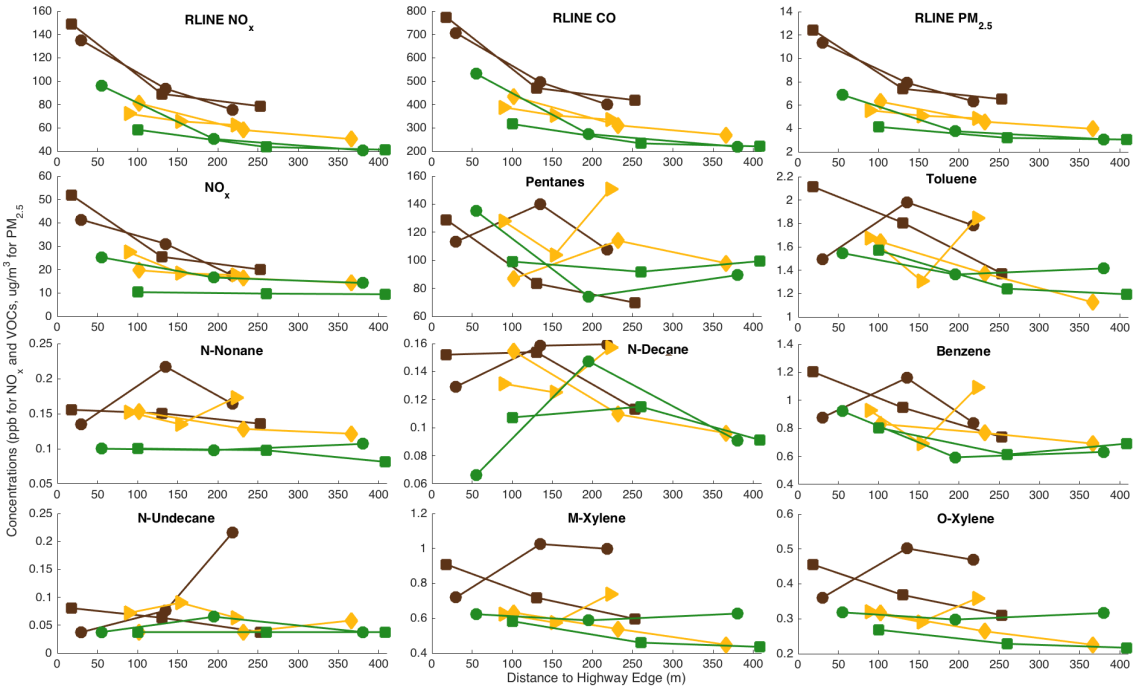

Figure 20. Near-road spatial gradients of R-LINE and PSD with distance (m) to the edge of highways. The concentrations of $PM_{2.5}$ by R-LINE are in $\mu g/m^3$ and for all other pollutants are in ppb. The colors denote the highways and shapes denotes direction to the

highways. Brown denotes for the locations close to I-75/I85 Downtown Connector; yellow for I-20 Downtown (SE) section; green for I-85 in NE Atlanta. The square points are for locations on the east of highway; dots for west; triangles for north; and diamonds for south.

5.3.1.1 Spatial Gradients by R-LINE

The spatial gradients estimated by R-LINE align well with the inverse of distance to road edge, with concentration dropping from near-road (<100m away) to far-road (>1000m). The concentrations decreased by factors of 3.65, 3.55, and 4.16, for NO_x, CO, and $PM_{2.5}$, respectively, from near-road sampler near I-75/I-85 connector (FP #5) to the downtown background sampler (FP #15). For the gradients near the I-20 downtown sector, the concentrations at the near-road sampler are factors of 2.00, 2.01, and 2.05 higher for NO_x, CO, and $PM_{2.5}$, respectively, compared to the downtown background sampler (FP #15). The concentrations near I-85 dropped by factors of 2.57, 2.65, and 2.55, for NO_x, CO, and $PM_{2.5}$, respectively, compared to the background sampler near I-85 (FP #17). Overall, the I-75/I-85 connector with the heaviest traffic shows the sharpest spatial gradients by R-LINE, with similar decreasing folds for the three pollutants.

5.3.1.2 Spatial Gradients by PSD

The PSD measurements show the largest NO_x decrease of a factor of 3.1 near the I-75/I-85 connector to the far-road site about 2km away from highway. The decrease for I-20 and I-85 are factors of 1.6 and 2.1, respectively, to the far-road site. Benzene, toluene, *m*-xylene, and *o*-xylene also display decreasing trends going away from roadway except for the sets of samplers on north side of I-20 and west side of I-75/I-85 connector. The spatial gradients on the east side of I-85 are smaller than the gradients on the west side for NO_x, *m*-xylene,

and *o*-xylene by PSD, likely caused by the traffic of the two monitored areas. The aromatic hydrocarbons show stronger near-road concentration pattern than the long-chain alkanes. This may be caused by the more stable chemical properties of the aromatic hydrocarbons than alkanes.

The two rural samplers, located most far away from highways, show the lowest concentrations among all PSD locations. The SDK and spaghetti junction of I-285 and I-85 show relatively high concentrations, which reflects the impact of the heavy traffic of I-285. The concentrations near the railyard are lower than the urban backgrounds (FP # 15 to 18) but higher than the rural background (FP # 34 and 35), indicating moderate impact from railyard on air quality.

5.3.1.3 R-LINE and PSD Spatial Gradients Comparison

R-LINE estimates slightly higher near-road gradients of NO_x concentrations than PSD measurements (Figure 20). The regression in Figure 21 shows good agreement in the spatial variations of NOx by R-LINE and PSD with correlation coefficient R^2 of 0.55, but the concentrations by PSD is about 0.25 times of that by R-LINE, indicating overestimation by R-LINE. This is consistent with the observation from Figure 20. To reduce the bias of R-LINE in overestimating both concentrations and the spatial gradients, we calibrated the NO_x concentrations of R-LINE using the regression in Figure 21. The calibration reduced the normalized mean bias from 2.0 to -0.0001, and normalized mean squared errors from 2.3 to 0.3, greatly improves the estimation of R-LINE.

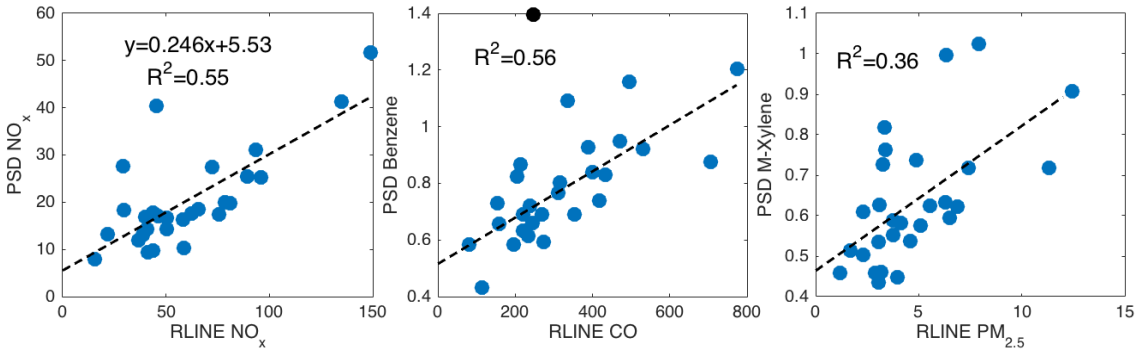

Figure 21. Regression of PSD vs R-LINE at all locations. NO_x is direct comparison; R-LINE CO compared with benzene; R-LINE $PM_{2.5}$ compared with m-xylene. There is one outlier removed from the regression for comparison of benzene and CO.

CO simulated by R-LINE is most correlated with benzene measured by PSD, which corresponds well with the fact that both CO and benzene are enriched in gasoline emissions (Dearth et al., 1992). $PM_{2.5}$ by R-LINE is most correlated with NO_x by PSD, and also highly correlated with *m*-xylene by PSD. As the R-LINE estimated $PM_{2.5}$ is impacted by mobile source only, it reflects the variation of overall mobile emission contributions. Similarly, NO_x and *m*-xylene are also found in both gasoline and diesel vehicles.

We compared the gasoline derived CO concentrations and total mobile source derived $PM_{2.5}$ concentrations by R-LINE (Figure 21) for common sources by using benzene as tracer of gasoline and *m*-xylene as tracer of total mobile sources. Benzene and *m*-xylene are tightly scattered around the regression trend lines, showing good agreement in the spatial variations. However, due to the limited availability of the measurements by PSD, we cannot evaluate the overestimation of R-LINE in CO and $PM_{2.5}$.

5.3.2 FP and Fixed Monitors Comparison

The mobile platform concentrations are collected every 10 seconds and the medians of the fuzzing trip were used for comparison with other methods. For fixed monitors, we used

hourly measurements, which is less affected by the meteorology condition. In Figure 22, fixed monitors and FP are compared to evaluate whether the fixed monitors can represent the pollution conditions for the ~600 m radius areas.

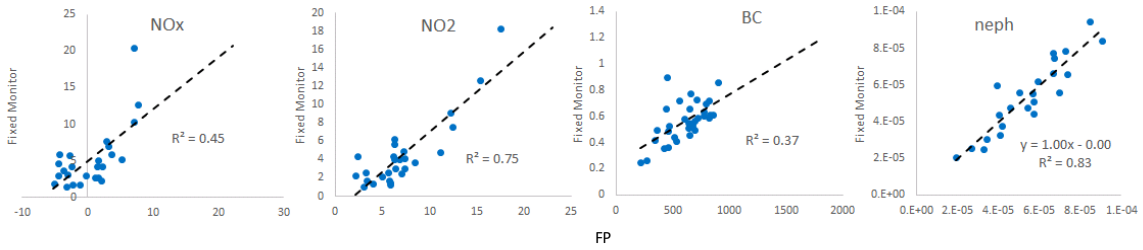

Figure 22. Comparison for mobile platform FP with fixed monitors for NO_x, NO_2, BC and nephelometer.

The medians of the mobile platform measurements at FPs are chosen as representative of the 6 to 10 min driving trip fuzzing around the fixed monitor locations. The 10s measurements by FP reflects the variation only. The four pollutants, NO_x, NO_2, BC, and particles measured by nephelometer, are in good agreement with those measured by the mobile platform and fixed monitors, showing Pearson R^2 of 0.45, 0.75, 0.37, and 0.83, respectively (Figure 22). These correlations suggest that the mobile platform can capture the spatio-temporal gradients similar to the fixed monitors. The fixed monitors can represent the surrounding areas.

5.4 Conclusions

In this study, large near-road spatial gradients are found in both PSD measurements and R-LINE simulations. The concentrations of <100m near major highways are up to 3 to 4 times of the concentrations ~2km away from the same area. The R-LINE simulations capture the spatial gradients slightly higher than PSD and generate the average concentrations ~7 times

higher than PSD. Overall, R-LINE overestimated near-road average concentrations but estimated similar spatial variations compared with PSD measurements.

For the hourly level concentrations, the medians of mobile platform measurements agree well with the fixed monitors, suggesting that the mobile platform can capture the concentrations similar to the fixed monitor sites. The mobile platform measurements can also be used to provide finer spatial resolution concentrations. The good agreement in the variations of the two methods also shows good spatial representativeness of the fixed monitors to the surrounding areas. The R-LINE comparison with fixed monitor and FP shows some correlation with the mobile source driven pollutants, but largely overestimate the concentrations.

In general, R-LINE captures the spatial variations on two-week average, hourly, and annual averages (Zhai et al., 2016) for traffic related air pollutants. For all three time-resolution estimates, R-LINE overestimates the concentrations, with the largest overestimation in hourly level and lowest overestimation in annual average level.

5.5 Acknowledgement

This publication was developed under Assistance Agreement No. EPA834799 awarded by the U.S. Environmental Protection Agency to Emory University and Georgia Institute of Technology. Additional support was provided by the U.S. Environmental Protection Agency (RD-83479601) for the UW CCAR project. It has not been formally reviewed by EPA. The views expressed in this document are solely those of the authors and do not necessarily reflect those of the Agency. EPA does not endorse any products or commercial services mentioned in this publication.

CHAPTER 6. CONCLUSION AND FUTURE WORK

6.1 Conclusions

The multiple spatial and temporal modeling approaches presented in this dissertation help us better understand the mobile source impact distribution at different spatial resolutions. The approaches with calibration of modeling simulations to field measurements at different spatial scales improve the accuracy of the modeling results and increase the spatial and temporal resolutions of the measurement fields. The applications of the approaches in 2002 to 2013 for CMB, 2002 to 2010 for IMSI, and 2002 to 2011 for R-LINE provide long-term exposure information to traffic related air pollution for health studies and air quality planning efforts. The conclusions of this work are summarized below.

Daily impacts of 9 sources are estimated at 13 sites in Georgia for the years 2002 to 2013. Temporally, the long-term analysis shows that annual $PM_{2.5}$ averaged across sites decreased from 13.8 $\mu g/m^3$ to 9.2 $\mu g/m^3$; seven sources decreased significant with more than 80% decrease of the total $PM_{2.5}$ concentration attributed to decreases in ammonium sulfate and ammonium bisulfate. The trends of the estimated source impacts agree well with NEI annual averages, reflecting the outcome of the emission control policies to ambient concentration levels. Spatial patterns of the distribution of source impacts help understand spatial representativeness of the fixed monitors. The data for secondary pollutants based on each monitor are representative for larger areas, regional sources such as biomass burning and dust are representative within smaller areas, and mobile vehicle sources and coal combustion are only representative in local areas. The spatial and

temporal distributions generated in this study can benefit policy makers in reducing air pollution emissions and provide insights for pollutant exposure studies and health impact assessment.

To further evaluate mobile source impacts, we developed an extended IMSI approach that could estimate spatial and temporal mobile source impacts on $PM_{2.5}$ concentrations at finer scales than CMB with similar source impact levels. This approach is easy to apply with inputs of three pollutant concentrations, CO, NOx, and EC, and with relatively small biases compared to the CMB estimated daily mobile source impacts. In the employment of the IMSI method, we explored and evaluated two different ways of calibrating the indicators to source impacts, the global and local normalizations. The results suggest that the two ways generate similar performance in comparison with daily CMB results but the global method is easier to apply with less input in the procedure. The approach was applied for estimating daily total mobile source impacts as well as separated gasoline and diesel vehicle impacts for 2002 to 2008 in 12km resolution and 2008 to 2010 in 4km resolution in Georgia. Such long-term and statewide fine resolution mobile source impact information provides reference to evaluate the human exposure to traffic-related air pollution for population living in areas with traffic conditions.

In the effort to develop high-resolution fields for traffic related air pollutants, a calibrated R-LINE modeling approach was developed and evaluated for annual average concentrations of CO, NOx, and $PM_{2.5}$ impacts by mobile sources. This approach can generate annual average fields with significantly reduced computation time with the extension of the STAR approach. The overestimated R-LINE fields were calibrated to

observational data with significantly reduced biases. The application of the approach is limited by its dependency on the spatial distribution of the monitor sites since at least three sites are required for robustness of the performance. In this study, the 250m resolution annual concentrations of the three pollutants are estimated for Atlanta from 2002 to 2011. Compared to the 4km IMSI mobile source impacts, the calibrated R-LINE fields can capture the high concentrations that are smoothed in the 4km grids and provide improved exposure information for the highly populated Atlanta area. The high-resolution concentration fields have been used in several health analyses to evaluate health impacts of traffic on pregnant women (Pennington et al., 2017b) and childhood asthma incidence (Pennington et al., 2017a). In addition, the spatial information helps improve the infrastructure project planning and has been used for air quality analysis by ARC (D'Onofrio et al., 2016).

Other than the resolution of the concentration fields, the distance to sources is also critical factors for evaluating the human exposure to traffic. In the study of the characterization of near-road spatial gradients, we found the concentrations of CO, NOx, and $PM_{2.5}$ show sharp decreasing gradients and the concentrations within <100m near major highway regions are up to 3 to 4 times of the concentrations ~2km away from the same area using both PSD measurements and R-LINE simulations. The measurements using PSD are at high expenses and it's hardly possible to use the measurements for the city-level near-road spatial gradients. The R-LINE estimated spatial gradients are highly correlated with PSD measurements for NOx (R^2=0.55) but the spatial gradients and concentration levels are overestimated in R-LINE. We calibrated the R-LINE to the PSD levels and the new fields show low biases compared to PSD measurements. The same calibration can be used for

more locations and enables the possibility of near-road exposure estimation for near-road residence health impact studies.

In general, R-LINE captures the spatial variations well compared to observational data on both two-week average concentrations and annual average concentrations for traffic related air pollutants but overestimates the hourly concentrations with larger overestimation hourly simulations than the two-week average and annual average concentrations. Using the observational data, R-LINE estimates can be calibrated with smaller biases but higher resolution and more accurate exposure information for health impact analysis. These findings are important for understanding the impact of air pollutants to human health.

6.2 Future work

This dissertation has developed and applied multiple useful modeling tools to estimate mobile source impacts and concentrations at different spatial scales and temporal resolutions. The generated high-resolution traffic related pollutant concentrations fields have supported relevant research in evaluating mobile source impacts on human health. More health analysis is being conducted using the readily generated data from this study. The tools can also be applied for different locations and years to generate high-resolution exposure fields for longer time periods at finer resolutions such as 50m resolution.

The IMSI method can be further evaluated for the impact of other sources such as non-anthropogenic sources. In locations where gas phase pollutants are measured, CMB-GC can be used for calibration of the estimated GV and DV source impacts for better separation of the two sources. The annual average R-LINE method can be improved by extending to

capture finer meteorology categories such as 8 or 16 wind directions. Further, the calibration of R-LINE to measurements can be applied for hourly, daily, and monthly concentrations for better temporal resolutions. The calibrated near-road R-LINE concentrations are imperative to capture the near-road exposure variation. This can be of great interest for the health impact assessment in highly trafficked and populated urban areas. The near-road gradients of all road conditions such as local roads other than highways can be assessed using sensors monitors.

In summary, the fine-resolution modeling techniques developed in this dissertation combine the advantages of observations and models. The methods are helpful to generate high-resolution concentration fields, especially for mobile sources. The generated concentration fields lay the foundation of the human exposure study and benefit urban infrastructure planning.

APPENDIX A. CHAPTER 2 SUPPLEMENTAL INFORMATION

More details on $PM_{2.5}$ species measurement methods and CMB model description for Chapter 2 are presented here. Additional descriptive analyses of $PM_{2.5}$ species concentrations and source apportionment results are presented and discussed here.

A.1 Methods

A.1.1 $PM_{2.5}$ Species Data

To evaluate potential artifacts due to the TOT to TOR conversion, we compared measured TOR OC/EC data and those converted from TOT data at SDK over April 2009 to April 2010, when the concentrations were measured with both TOT and TOR. The converted TOR OC and EC are highly correlated with the measured TOR (R^2 =0.76 and 0.69, respectively, with p values <0.001) with relative bias of 7% and 29%.

When converted TOR and measured TOR data are used in CMB separately, the estimated source impacts of OTHROC and HDDV are the most impacted. The converted TOR OC concentrations are highly correlated with the measured TOR OC with slope near 1 (0.90±0.06), intercept near 0 (0.11±0.15), and R about 0.86. But the daily variations in the source impacts are different, which contributed to the difference in the estimated source impacts.

The OC/EC concentrations by CSN using TOR method were not field blank adjusted which can result in biases (Chow et al., 2010). EC field blanks were less than 0.7% of the total concentrations and no correction was used. OC field blanks were assumed to be 0.11 $\mu g/m^3$ based on averages of measurements from April 2009 to March 2010 at three sites (0.11 $\mu g/m^3$ at SDK, 0.11 $\mu g/m^3$ at Columbus, and 0.12 $\mu g/m^3$ at Athens). The IMPROVE site

measurements were blank adjusted (Chow et al., 2007). Conversion of TOT to TOR levels included the blank correction.

A.1.2 CMB Model

CMB uses species concentrations (C_j, j for species) of $PM_{2.5}$ and source profiles to solve mass conservation equations (Equation 1) (EPA, 2004a).

$$C_j = \sum_{k=1}^{N} f_{jk} S_k + e_j \qquad (j = 1, \dots, n;\ k = 1, \dots, N)$$

Equation A 1

The source profiles are the fractions (f_{jk}, k for sources) of each species j in each source k. The estimated species concentration is the sum of all the contributions from all the sources (Equation A1). By minimizing the square of the error (e_j) between estimated and observed concentrations, source impacts (S_k) are estimated. CMB version 8.2 developed by the EPA was used here, which incorporates an effective variance weighted least-squares fitting and minimizes the uncertainty-weighted square error χ^2 (Equation A2, where i is sample i, j and k are the same with Equation A1) (Watson et al., 1984).

$$\chi^2 = \sum_{j=1}^{n} \left[\frac{(C_{ij} - \sum_{k=1}^{N} f_{jk} S_k)^2}{(\sigma_{C_{ij}}^2 + \sum_{k=1}^{N} \sigma_{f_{jk}}^2 S_k^2)^2} \right] \qquad (j = 1, \dots, n;\ k = 1, \dots, N) \qquad \text{Equation A 2}$$

A.2 Results and Discussion

A.2.1 $PM_{2.5}$ Species Concentration Trends

Significant decreasing trends were found for all sites for sulfate, nitrate and ammonium ($p < 0.001$) (Fig. A2). Sulfate decreased from 4.7 μg/m^3 to 1.6 μg/m^3 (66%), ammonium from 1.48 μg/m^3 to 0.44 μg/m^3 (70%), and nitrate from 0.72 μg/m^3 to 0.42 μg/m^3 (42%).

NH_4^+ has a similar trend as SO_4^{2-} (Fig. A2). EC and OC increased slightly before 2007 and started to decrease after 2007. High rainfall in 2009 resulted in lower average concentrations of $PM_{2.5}$ and its components in that year (Fig. A2).

The different measurements and treatments of possible artifacts are explored here to explain the difference in the R_{SO4} ranges at the CSN and SEARCH sites. There are potential artifacts in the measurements associated with the shipping, storage, and analysis of the samples. At the CSN and IMPROVE sites, positive artifacts of nitrate, sulfate, and ammonium, were estimated and removed from the reported data (Environmental Protection Agency, 2011). At the SEARCH sites, filter-based 24-hr concentrations correlate well with continuous measurements (Fig. A4 for 2011, with slope of 0.93 ± 0.03 and intercept of -0.03 ± 0.04), which are not subject to shipping and storage artifacts. This result is consistent with the estimated artifacts of ammonium measurement, i.e., between 6 and 14% of the total concentration (Edgerton et al., 2005). As average residual artifacts of the three species are expected to be similar over time and space, we assume the long-term and regional trends of R_{SO4} ratio are not likely to be substantially impacted.

The comparison of the concentrations of ammonium, sulfate, and nitrate at a SEARCH site in Atlanta (JST) and a CSN site in Atlanta (SDK), shows that the concentrations are generally lower at CSN sites (Fig. A4), with even lower ammonium than sulfate and nitrate. The measurements at SEARCH and CSN sites in the same region suggests that the difference is caused by the treatment of artifacts. At CSN sites, the artifacts are removed from the total concentration, similar to the treatment of ammonium concentrations, while at SEARCH sites the artifacts are not removed. The larger difference in ammonium

measurements than sulfate and nitrate measurements is caused by the larger bias in the ammonium measurements due to its semi-volatility property.

A.3 **Figures and Tables:**

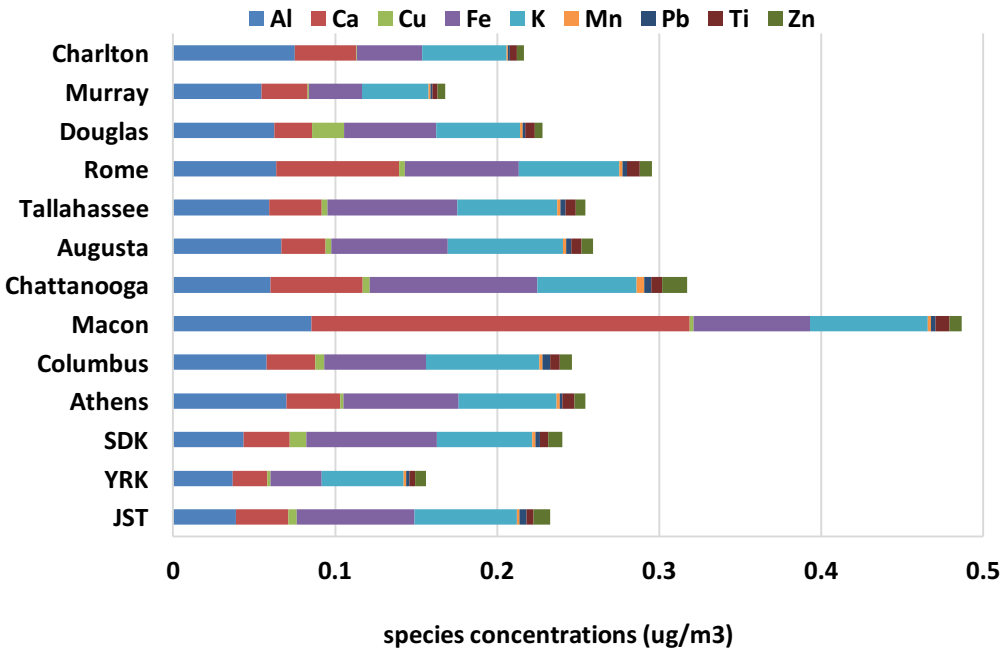

Figure A 1. Concentrations of Metals: averages cross 12 years for each site.

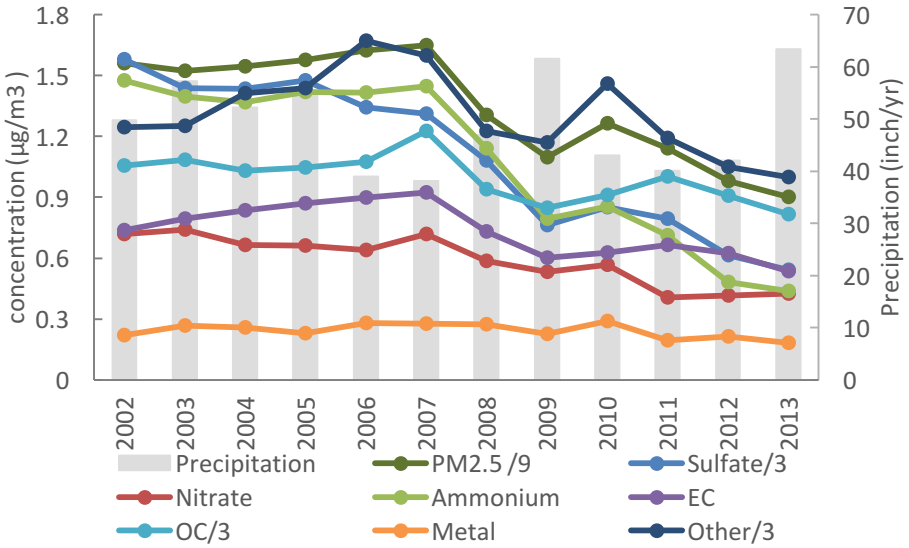

Figure A 2. Annual average trends of $PM_{2.5}$ and its species concentrations averaged across sites. Axis on the right represents the annual precipitation of Georgia.

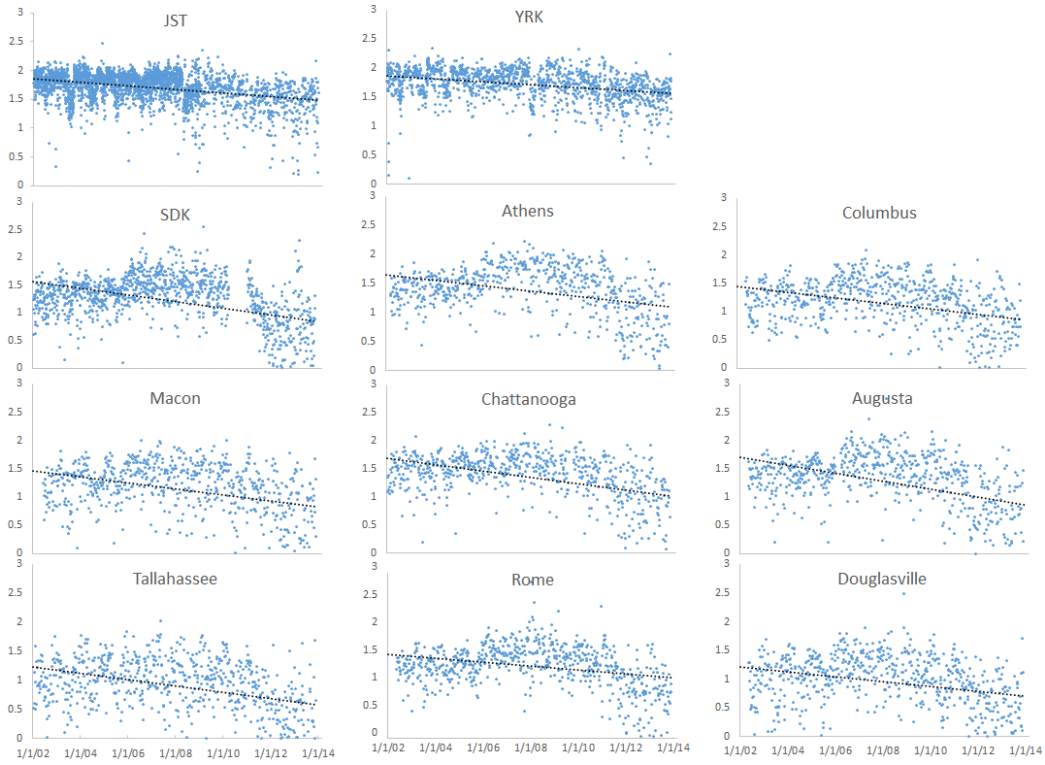

Figure A 3. Daily variations and long-term trends of R_{SO4} ratios at SEARCH and CSN sites.

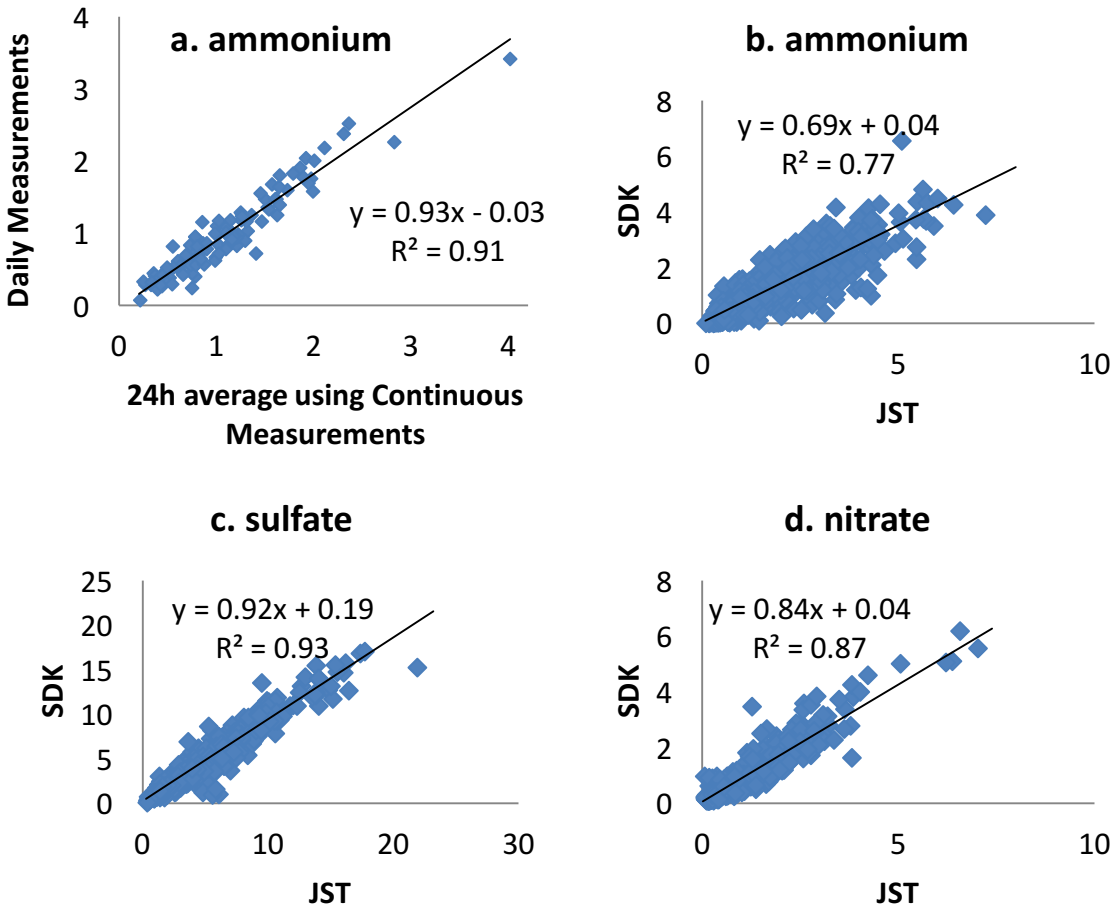

Figure A 4. a. Comparison of continuous and daily measurements of ammonium concentrations for 2011 at JST site; b, c, d. Comparison of SEARCH JST site (x) and CSN SDK site (y) for ammonium, sulfate, nitrate.

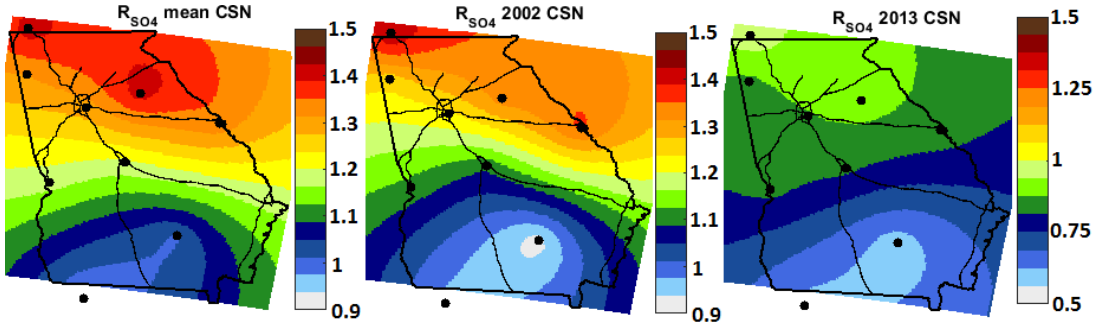

Figure A 5. Spatial variation of R_{SO4} ratios CSN sites using ordinary kriging method. Lines denote state border and major highways, and black circles denote site locations.

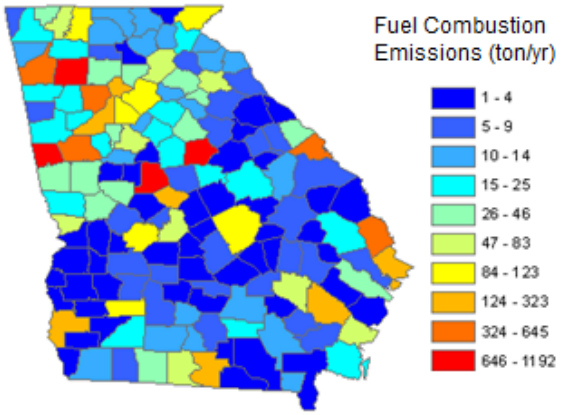

Figure A 6. $PM_{2.5}$ emissions of fuel combustions by 2011 NEI for counties in Georgia.

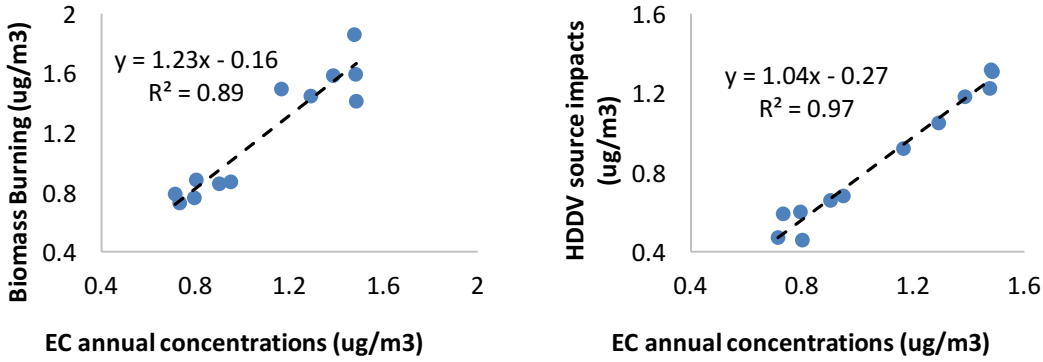

Figure A 7. EC vs source impacts of BURN and HDDV.

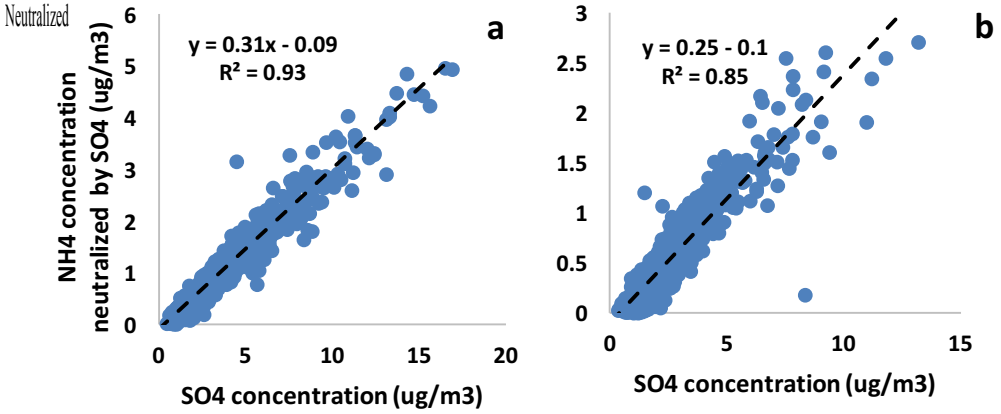

Figure A 8. Regressions of SO_4^{2-} vs NH_4^+ neutralized by SO_4^{2-}, (a) for Chattanooga and (b) for Douglas. We assume the neutralization status of the ammonium to sulfate and nitrate is similar at the nearest sites. Therefore, we estimated ammonium concentrations at Murray and Charlton using the regressions of SO_4^{2-} vs remaining NH_4^+ after removing

the part of NH_4^+ that is associated with NO_3^- at Chattanooga (closest to Murray) and Douglas (nearest to Charlton).

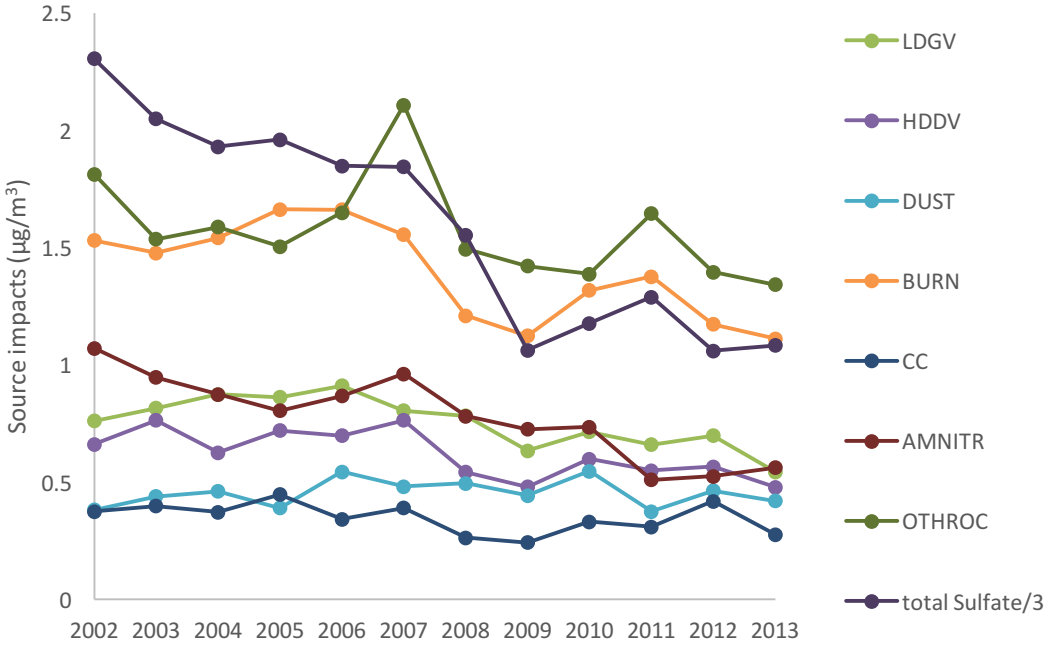

Figure A 9. Temporal trends of annual averages for source impacts. Total sulfate represents for the sum of ammonium sulfate and ammonium bisulfate, and the values shown are 1/3 of the actual value.

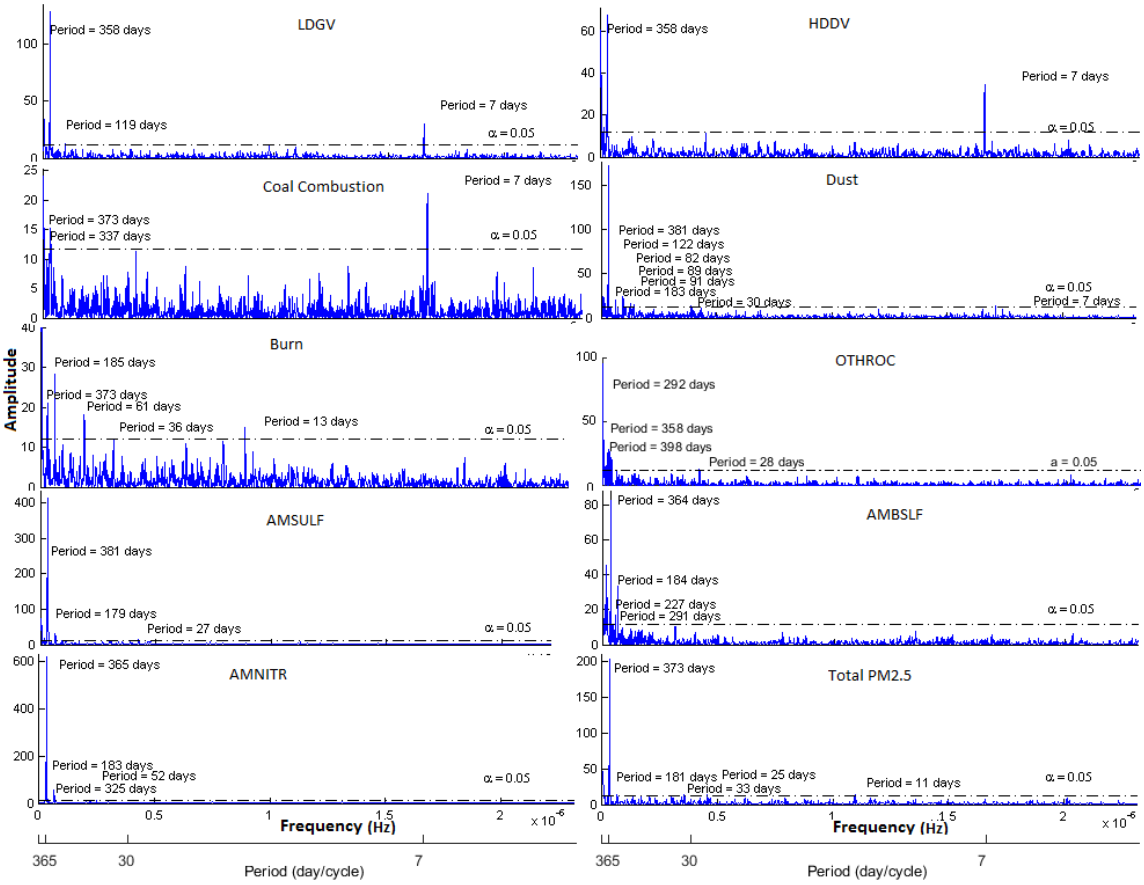

Figure A 10. Spectrum plots of frequencies vs amplitude at JST with significant level 0.05: significant periods marked on plots. The axis on the bottom shows the periods at a year, a month, and a week at corresponding frequencies.

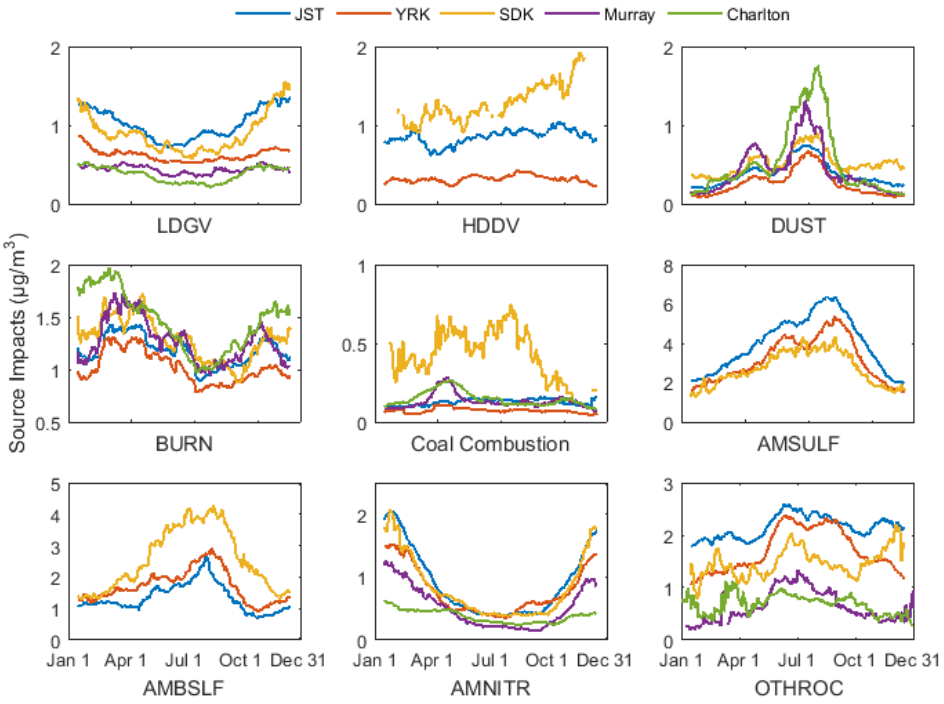

Figure A 11. Seasonality by running average at five sites with more sufficient data (every-three-day or daily). HDDV source impacts at Murry and Charlton were not continuous so not shown in the figure. The estimated AMSULF and AMBSLF source impacts at Murray and Charlton are not shown in the figure.

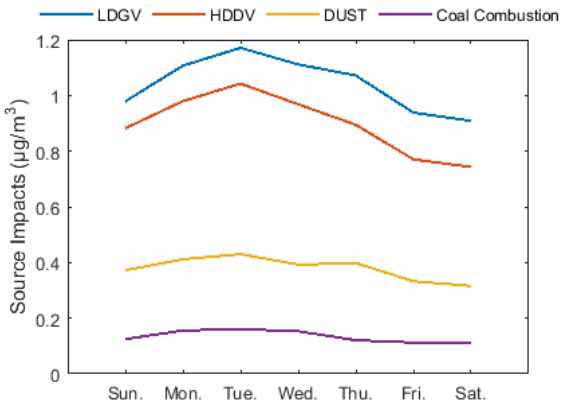

Figure A 12. Weekly trends of source impacts at JST site for LDGV, HDDV, dust, and coal combustion. Data are averaged across all one-week periods.

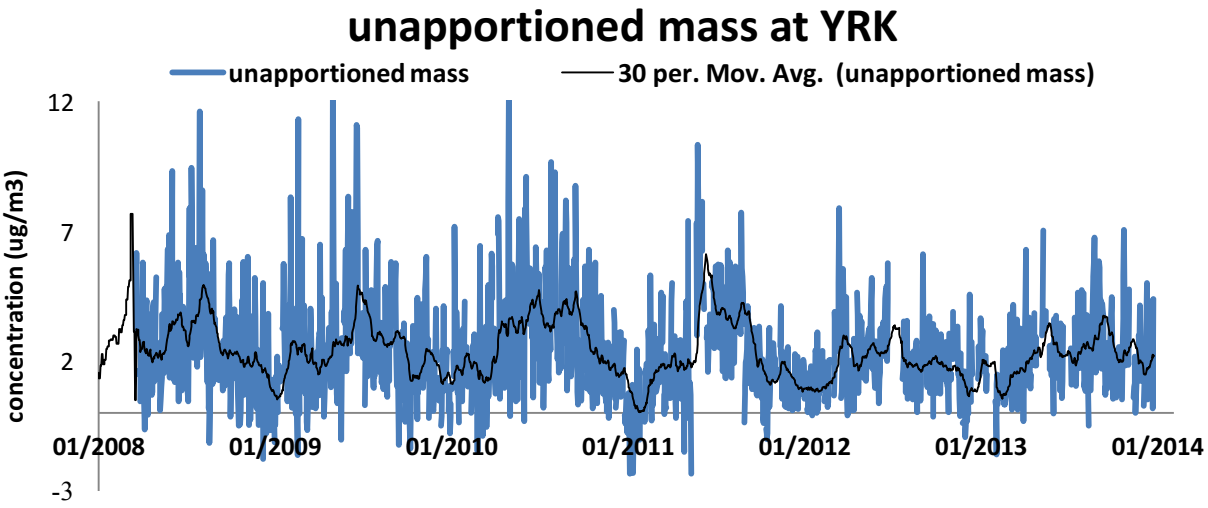

Figure A 13. Unapportioned $PM_{2.5}$ mass at YRK.

Table A 1. Significant periods (in days) by spectral analysis for all sites and sources. The dust and CC did not converge significant periods around one year. The not available (N.A.) data indicated no significant period around one year converged for that source and site.

Period	BURN	LDGV	HDDV	AMSULF	AMBSLF	AMNITR	OTHROC
JST	375	364	364	375	354	354	358
YRK	365	365	398	355	355	365	376
SDK	363	363	362	363	353	384	N.A.
Athens	358	N.A.	N.A.	358	368	358	N.A.
Columbus	371	361	379	351	361	371	N.A.
Macon	378	367	367	357	357	378	N.A.
Chattanooga	N.A.	364	N.A.	374	364	354	N.A.
Augusta	N.A.	371	359	360	360	371	1800
Tallahassee	364	364	363	N.A.	364	374	N.A.
Rome	2520	371	N.A.	360	359	350	1793
Douglas	375	N.A.	N.A.	N.A.	364	364	N.A.
Murray	361	3253	N.A.	N.A.	N.A.	N.A.	N.A.
Charlton	353	363	369	N.A.	N.A.	N.A.	N.A.

APPENDIX B. CHAPTER 3 SUPPLEMENTAL INFORMATION

B.1 Estimation of diesel and gasoline weighting factors

We use the spatial distribution of ratios of diesel/gasoline to mobile emissions in 36km resolution and ratios of mobile sources to total emissions in 4km resolution to downscale the weighting factors to 4km resolution based on Equation A3. We assume homogenies ratios of diesel to mobile emissions and gasoline to mobile emissions across the 81 4km-by-4km grids within each 36km-by-36km grid. As mobile emissions and total emissions in 36km resolution are found to be the same with the 4km resolution aggregated emissions for mobile sources and total in the same areas (slopes about 1 and R^2=0.99, Fig. A14), we assume that if the 36km emissions are downscaled to 4km resolution, the spatial distributions of ratios of mobile to total emissions are the same with the 4km resolution. Therefore, we use the spatial distribution of ratios of mobile to total emissions in 4km resolution to downscale the diesel to total emission ratios. The 36km resolution emissions are for 2006, which is readily prepared in the Southeastern Center for Air Pollution & Epidemiology (SCAPE) study. We use emission ratios instead of directly using ratios of diesel/gasoline to total emissions so the results depend on relative fractions from the same platform of emission profiles.

$$\frac{E_{i,DV}}{E_{i,total}}(4km) = \frac{E_{i,DV}}{E_{i,mobile}}(36km) \times \frac{E_{i,mobile}}{E_{i,total}}(4km)$$

Equation A 3

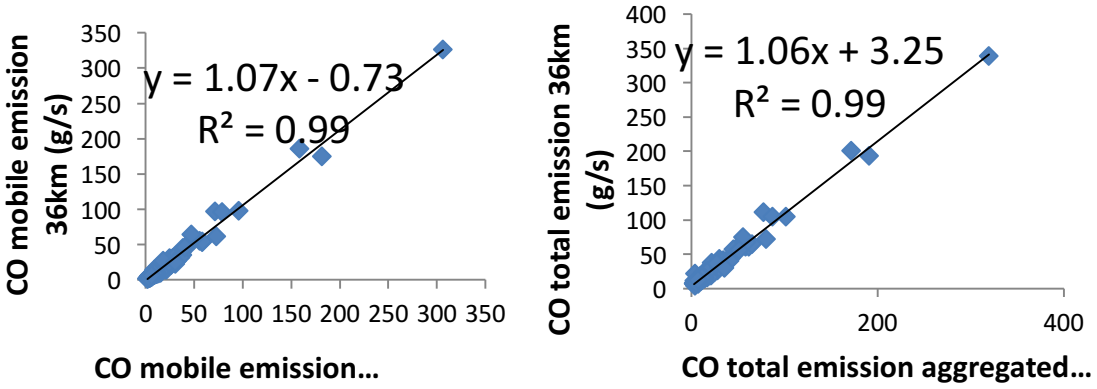

Figure A 14. Comparison of the 36km emissions with 4km emissions.

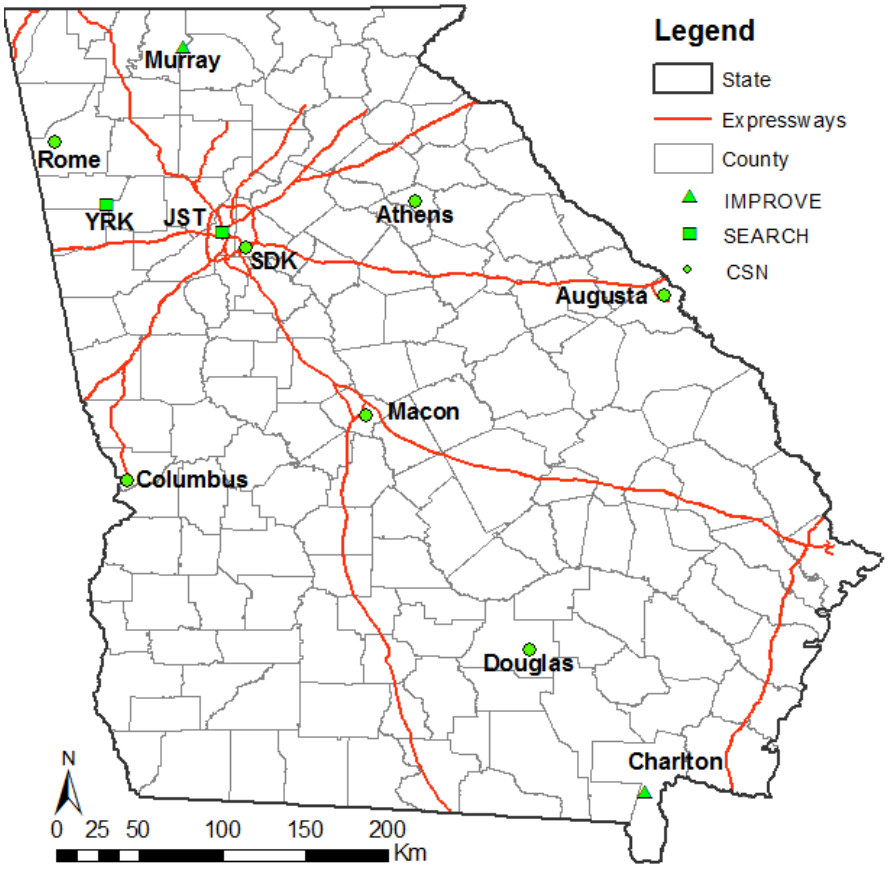

Figure A 15. $PM_{2.5}$ sites with species measurements in GA.

B.2 Local IMSI method

The normalization method of the concentrations can impact the variation of the estimated IMSI indicators. Therefore, we performed the local IMSI method that uses a local standard deviation for each location in the step of normalizing the concentrations. This way the concentrations are normalized to their local levels and the variations of the generated indicators are representative of the local source impact variations over time. These indicators do not provide any spatial information.

In the local IMSI method, estimated CMB annual averages are obtained using the regression of the scaled spatial distribution of the $PM_{2.5}$ mobile emissions to annual averages of CMB mobile source impacts. We estimated the spatial distribution of mobile source impact calibration for each year using power regressions. Annual CMB mobile source impacts at 11 available monitoring sites in Georgia (Fig. A15) are used with $PM_{2.5}$ mobile emissions at the corresponding locations. We used one set of $PM_{2.5}$ mobile emissions for spatial distributions to avoid the impact of changes in emission model platforms over time. $PM_{2.5}$ annual average emissions for GV and DV are calibrated similarly with the weighting factors described above with Equation A3 and S4.

CMB annual averages for total, gasoline and diesel impacts at 4 km or 12 km resolutions were spatially resolved using regressions between CMB annual averages and the $PM_{2.5}$ annual average emissions for total, gasoline and diesel sources (Fig. A16). When using the emission distributions for the spatial distribution of the source impacts, we include the impact from surrounding grids. The impacts are weighted using the inverse of area weighted distance as calculated by Equation A4. We include impacts from all surrounding grids in a 36km by 36km area. The distances for each surrounding grid to central grid are

shown in Fig. A17. Table A2 provides regression results of the local IMSI annual averages with CMB annual averages for all years.

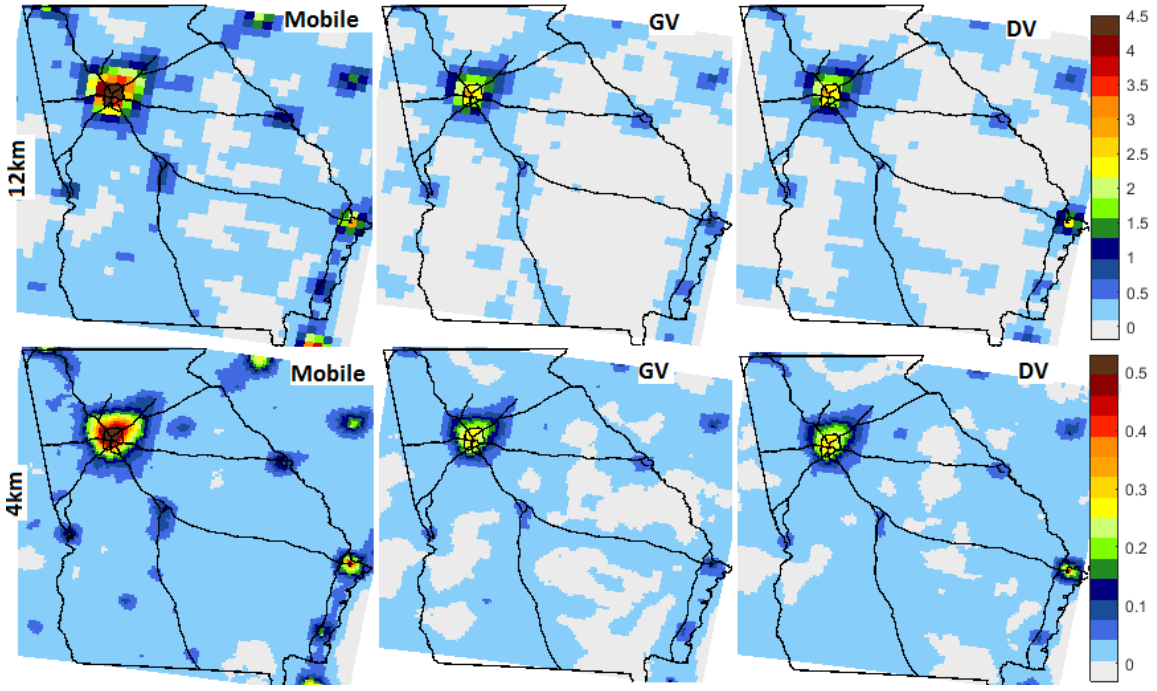

Figure A 16. Spatially weighted $PM_{2.5}$ emissions (g/s) from mobile sources and GV/DV sources at 4 km and 12 km resolutions.

$$r^2 = \frac{1}{\Delta x \Delta y} \int_{x1}^{x2} \int_{y1}^{y2} (x^2 + y^2) dx dy$$

Equation A 4

22.7	20.0	17.9	16.5	16.0	16.5	17.9	20.0	22.7
20.0	17.0	14.5	12.7	12.1	12.7	14.5	17.0	20.0
17.9	14.5	11.4	9.0	8.1	9.0	11.4	14.5	17.9
16.5	12.7	9.0	5.8	4.2	5.8	9.0	12.7	16.5
16.0	12.1	8.1	4.2	**1.5**	4.2	8.1	12.1	16.0
16.5	12.7	9.0	5.8	4.2	5.8	9.0	12.7	16.5
17.9	14.5	11.4	9.0	8.1	9.0	11.4	14.5	17.9
20.0	17.0	14.5	12.7	12.1	12.7	14.5	17.0	20.0
22.7	20.0	17.9	16.5	16.0	16.5	17.9	20.0	22.7

Figure A 17. Distances of surrounding grids to central grid (km). The weighting factor is the inverse of distance to the sum of all inverse distances.

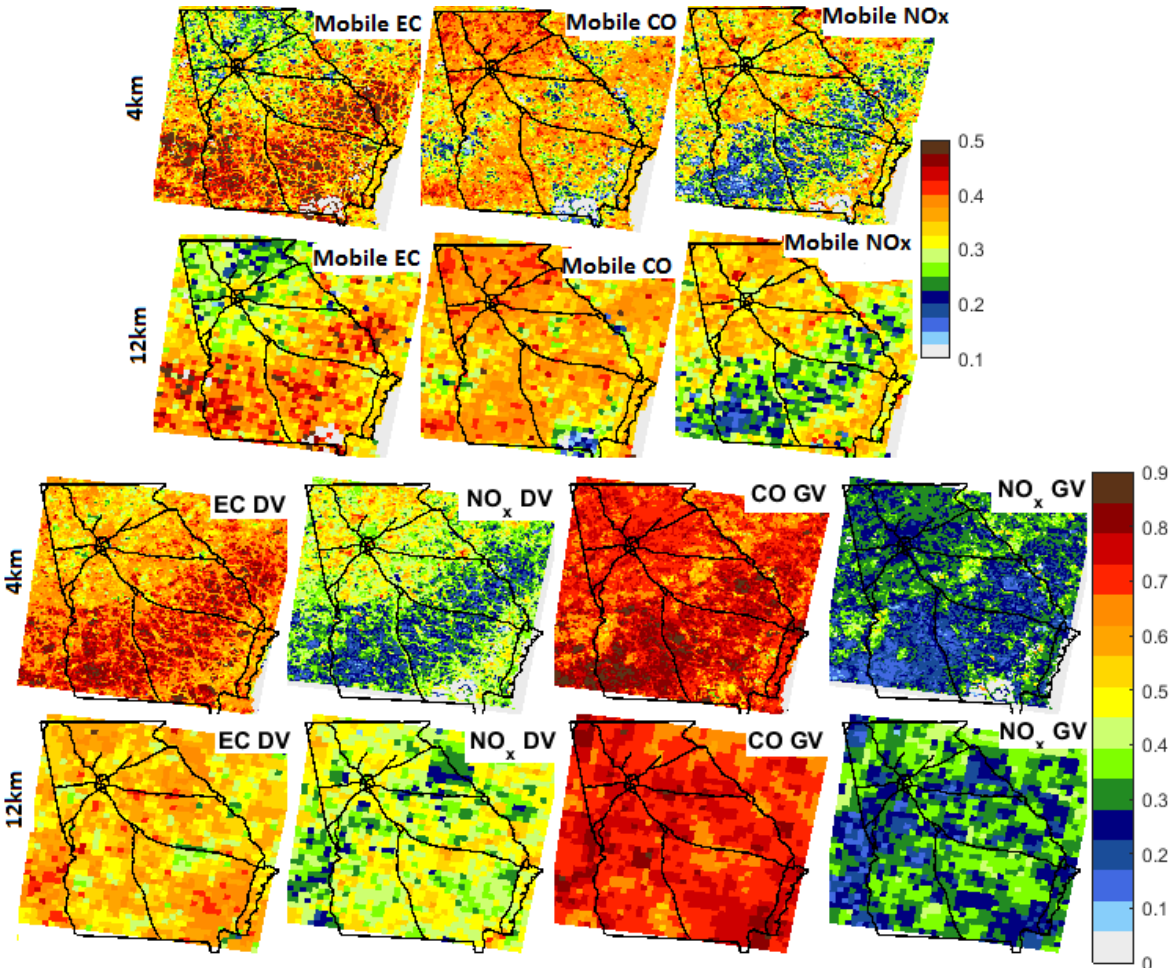

Figure A 18. Weighting factors for 4km and 12km total Mobile sources, GV, and DV.

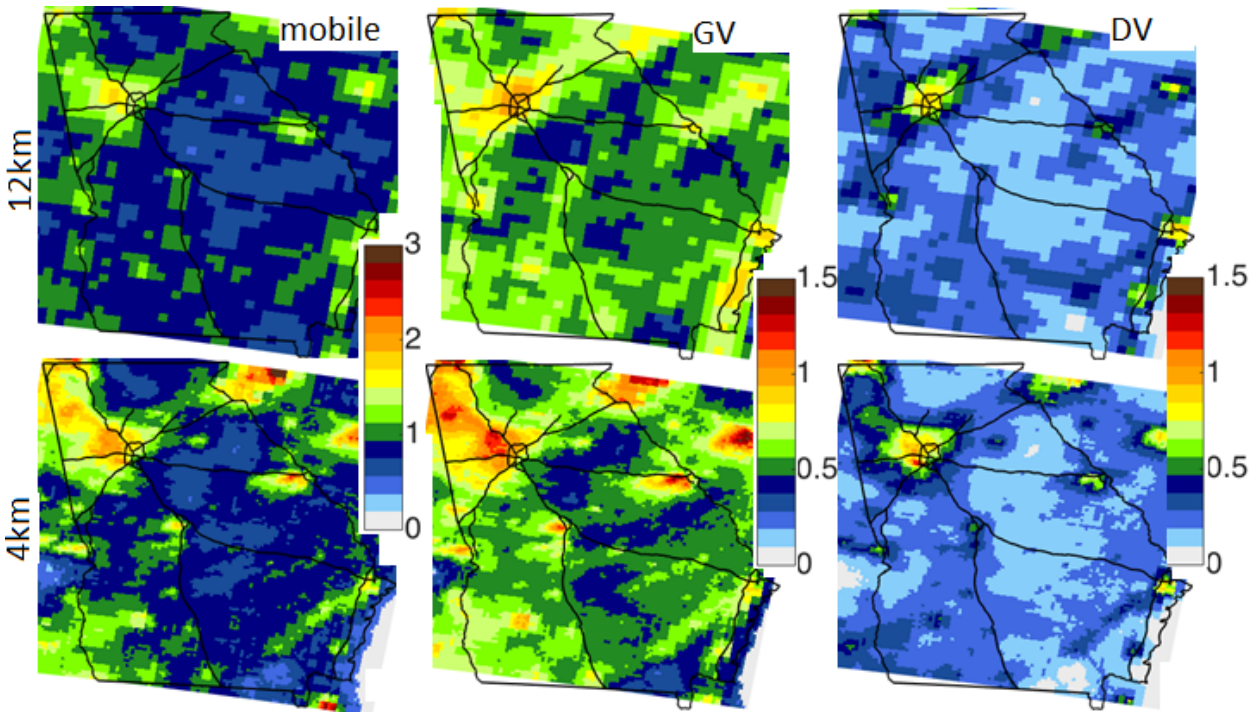

Figure A 19. Daily source impact (µg/m3) spatial distribution on 2008/1/21 at 12 km and 4 km resolutions for mobile source, GV, and DV using the local IMSI method.

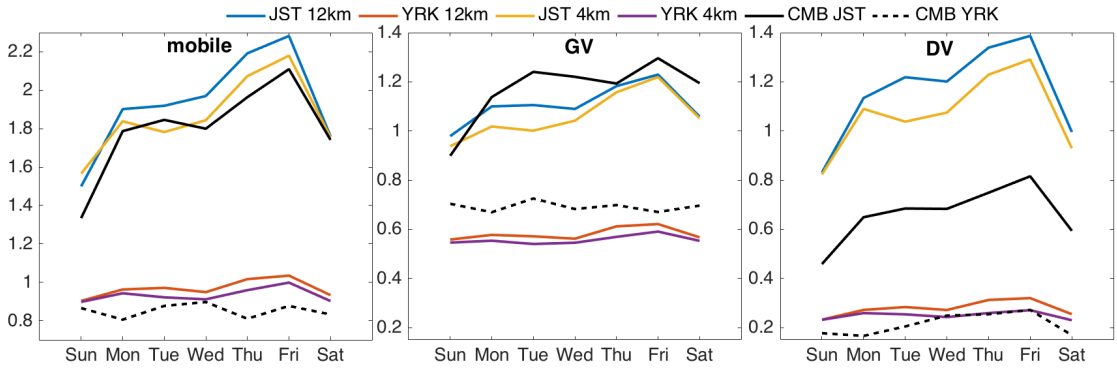

Figure A 20. Weekly trends of estimated source impacts (µg/m^3) using the local IMSI method in 2008 at JST and YRK sites for comparison with CMB estimates. JST is an urban site in Midtown Atlanta and YRK is a rural site about 70 km away from Midtown Atlanta.

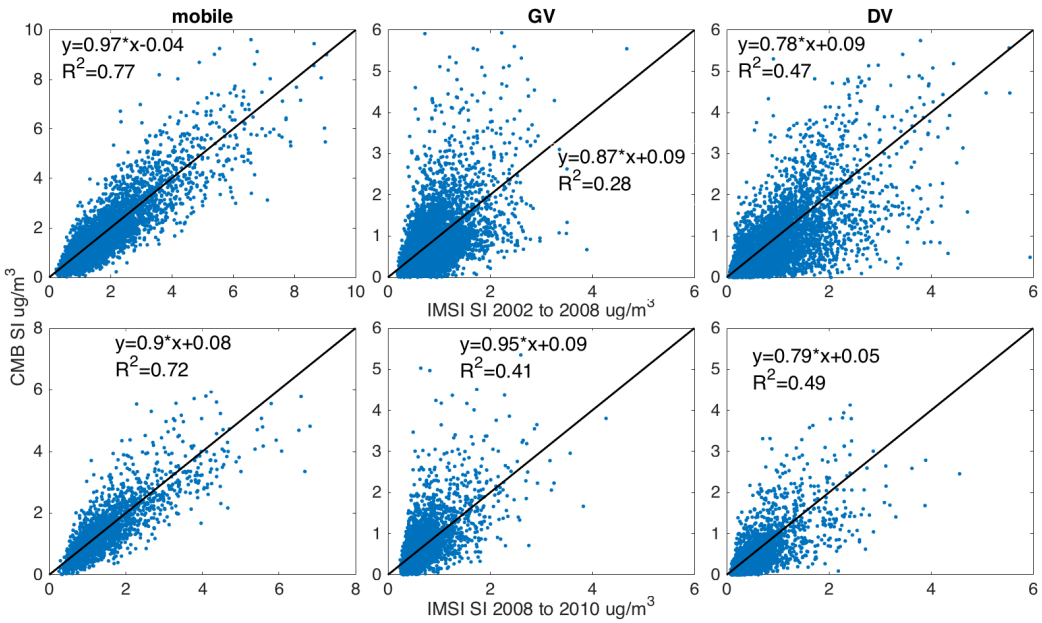

Figure A 21. Daily mobile source impacts by CMB and by the local IMSI method (µg/m3) at all sites and years for total mobile, GV, and DV in 12 km resolution (2002 to 2008) and 4 km resolution (2008 to 2010).

$$PM_{2.5\_GV}(12km) = \frac{PM_{2.5\_GV}}{PM_{2.5\_mobile}}(36km) \times PM_{2.5\_mobile}(12km) \quad \text{Equation A 5}$$

$$PM_{2.5\_DV}(4km) = \frac{PM_{2.5\_DV}}{PM_{2.5\_mobile}}(36km) \times PM_{2.5\_mobile}(4km) \quad \text{Equation A 6}$$

Table A 2. Distribution of the weighting factors.

		4 km resolution in GA			12 km resolution in GA		
		median	2.5%	97.5%	median	2.5%	97.5%
mobile	EC	0.35	0.21	0.54	0.34	0.23	0.46
	CO	0.35	0.19	0.43	0.36	0.25	0.42
	NO_x	0.31	0.15	0.42	0.31	0.19	0.39
DV	EC	0.63	0.44	0.84	0.56	0.39	0.69
	NO_x	0.37	0.14	0.53	0.44	0.26	0.56
GV	CO	0.72	0.56	0.86	0.71	0.61	0.81
	NO_x	0.28	0.09	0.39	0.31	0.17	0.41

Table A 3. Weighting factors in Atlanta by Pachon et al. (2012) and in Denver and Huston by Oakes et al. (2014b).

		County level		
		Atlanta	Denver	Houston
mobile	EC	0.33	0.33	0.22
	CO	0.36	0.37	0.40
	NO_x	0.31	0.29	0.38
DV	EC	0.69	0.70	0.55
	NO_x	0.31	0.30	0.44
GV	CO	0.63	0.68	0.65
	NO_x	0.37	0.32	0.35

Table A 4. Power fit regression ($y=ax^b$, where y=CMB) coefficients for calibrating the indicators to CMB source impacts. The Local IMSI method uses power fit regressions of CMB annual averages and fused $PM_{2.5}$ emissions (x) of total mobile sources, GV, and DV. The coefficients (a, b, and R^2) are calculated using the linear regression of log-transformed data.

Source		Mobile			GV			DV		
Resolution	Year	a	b	R^2	a	b	R^2	a	b	R^2
12 km	2002	0.33	1.18	0.94	0.22	0.91	0.89	0.53	0.63	0.82
	2003	0.30	1.31	0.90	0.20	0.90	0.80	0.45	0.87	0.85
	2004	0.33	1.50	0.91	0.19	1.03	0.84	0.47	0.81	0.79
	2005	0.31	1.48	0.89	0.20	0.98	0.85	0.47	0.88	0.81
	2006	0.30	1.58	0.94	0.18	0.99	0.86	0.46	0.89	0.84
	2007	0.28	1.41	0.88	0.15	0.83	0.82	0.57	0.98	0.73
	2008	0.23	1.30	0.83	0.20	0.90	0.79	0.50	0.69	0.72
4 km	2008	0.22	2.08	0.77	0.19	1.32	0.76	0.48	1.85	0.71
	2009	0.25	1.83	0.70	0.17	1.04	0.77	0.24	0.83	0.42
	2010	0.32	2.54	0.79	0.20	1.28	0.80	0.43	1.72	0.57

Table A 5. NMB and NRMSE for mobile source, GV, and DV impacts, on PM2.5 in comparison with CMB source impacts using Local IMSI method.

		mobile	GV	DV
NMB	12km	0.132	0.010	0.280
	4km	0.193	-0.002	0.426
NRMSE	12km	0.514	0.675	1.146
	4km	0.581	0.628	1.098

APPENDIX C. CHAPTER 4 SUPPLEMENTAL INFORMATION

Descriptions of Treatment of Calm Conditions, the IMSI method, and Comparison of Near-road Measurements with R-LINE Estimates are in the last section for Chapter 4.

C.1 Tables and Figures

Table A 6. Annual emissions of 20 counties from mobile sources.

Atlanta mobile emissions (ton/day)	*$PM_{2.5}$*	*CO*	*NO_x*
2002	21.8	2123.4	406.6
2003	22.1	2254.1	396.2
2004	21.1	2021.3	344.1
2005	19.9	1944.1	314.8
2006	18.5	1831.9	298.0
2007	17.1	1738.5	280.0
2008	16.1	1654.9	262.2
2009	14.3	1556.9	228.6
2010	13.8	1497.1	217.6
2011	12.0	1399.7	200.1

Table A 7. Site Information.

Species	*Site Name*	*Longitude*	*Latitude*
$PM_{2.5}$ species/NO_x/CO	JST	-84.4170	33.7770
	YRK	-85.0453	33.9283
	SDK	-84.2903	33.6875
NO_X	Tucker	-84.2136	33.8478
	GA Tech	-84.4008	33.7758
	YRK	-85.0453	33.9283
	Conyers	-84.0667	33.5856
CO	DeKalb Tech	-84.2358	33.7892
	Roswell Rd	-84.3803	33.8764

Table A 8.CMB-GC annual averages at three sites.

CMB ($(\mu g/m^3)$	*JST*	*YRK*	*SDK*
2002	2.10	0.48	1.95
2003	2.34	0.61	1.69
2004	2.19	0.53	2.28
2005	2.25	0.53	2.38
2006	2.36	0.54	2.60
2007	1.90	0.52	2.54
2008	1.62	0.31	2.18
2009	1.38	0.35	1.54
2010	1.61	0.32	1.85
2011	1.35	0.23	1.68

Table A 9.CO observation annual averages at five sites.

CO (ppb)	*JST*	*YRK*	*SDK*	*DeKalb Tech*	*Roswell Rd*
2002	1145.0	253.3	N.A	1231.3	1347.6
2003	971.7	244.8	1152.4	965.5	1343.9
2004	1011.7	224.1	1016.8	N.A	1150.0
2005	856.1	232.1	1006.5	N.A	1090.1
2006	881.0	219.4	1005.4	N.A	1045.5
2007	723.3	247.3	802.6	N.A	937.9
2008	591.1	207.7	819.9	N.A	713.1
2009	535.8	204.0	N.A	N.A	692.1
2010	540.4	195.4	633.9	N.A	653.1
2011	487.4	202.1	608.7	N.A	719.9

Table A 10. NOx observation annual averages at seven sites.

NO_x (ppb)	*JST*	*YRK*	*SDK*	*Tucker*	*GA Tech*	*YRK*	*Conyers*
2002	111.9	13.1	146.3	60.7	116.3	11.7	23.9
2003	118.1	12.5	135.5	68.6	98.1	11.0	23.3
2004	104.2	10.7	131.3	72.3	99.7	10.2	20.5
2005	91.1	9.3	128.3	59.4	101.5	8.5	20.4
2006	93.6	9.3	134.1	57.3	87.9	8.9	19.9
2007	101.9	9.4	120.5	N.A	67.6	7.9	15.7
2008	91.9	7.6	100.9	N.A	58.9	6.9	15.4
2009	82.4	5.8	83.7	N.A	58.0	5.5	10.9
2010	82.9	5.7	101.6	N.A	N.A	6.5	15.1
2011	70.8	5.3	97.0	N.A	N.A	6.2	11.9

Table A 11. $PM_{2.5}$ annual averages at sites by R-LINE µg/m^3.

$PM_{2.5}$ ($\mu g/m^3$)	*JST*	*YRK*	*SDK*
2002	4.4	0.7	2.7
2003	4.3	0.7	2.8
2004	3.9	0.5	2.8
2005	3.8	0.6	2.5
2006	3.6	0.6	2.3
2007	3.8	0.6	2.4
2008	3.3	0.5	2.4
2009	3.3	0.6	2.0
2010	3.0	0.4	2.4
2011	2.3	0.3	1.7

Table A 12.1hr max CO annual averages at sites by R-LINE.

CO (ppb)	*JST*	*YRK*	*SDK*	*DeKalb Tech*	*Roswell Rd*
2002	1394.9	336.5	1099.5	1570.7	1574.6
2003	1423.2	325.3	1200.4	1638.9	1609.1

2004	1211.6	246.7	1081.5	1509.7	1492.7
2005	1206.3	283.9	1027.3	1409.1	1393.4
2006	1113.2	251.6	921.7	1258.4	1263.9
2007	1176.1	269.0	966.1	1383.5	1409.9
2008	1100.1	227.1	1022.5	1363.0	1292.0
2009	1073.1	267.7	853.2	1226.8	1247.0
2010	1067.0	224.3	1103.5	1413.8	1226.9
2011	890.5	159.0	862.3	1204.6	1101.8

Table A 13. RLNE NOx 1hr max ppb.

NO_x (ppb)	*JST*	*YRK*	*SDK*	*Tucker*	*GA Tech*	*YRK*	*Conyers*
2002	353.5	86.1	263.6	352.5	432.4	86.2	86.1
2003	329.7	76.1	265.3	331.3	400.0	76.2	87.9
2004	271.8	55.7	231.0	299.4	336.2	55.7	77.2
2005	257.7	61.0	208.4	267.9	318.1	61.1	68.1
2006	238.5	54.3	188.4	235.4	287.5	54.4	62.6
2007	250.1	57.6	194.7	263.3	306.6	57.7	63.4
2008	229.8	47.8	202.9	252.9	284.4	47.9	65.6
2009	207.8	52.1	156.9	210.7	251.7	52.2	52.3
2010	204.9	43.4	200.2	245.3	262.1	43.5	62.2
2011	166.5	30.1	151.9	203.9	215.4	30.1	48.3

Table A 14. Population weighted exposure for R-LINE, CALIBRATED R-LINE, IMSI, and CMAQ-OBS.

	$PM_{2.5}$ ($\mu g/m^3$)			*CO (ppb)*			*NO_x (ppb)*		
	R-LINE	Calibrated R-LINE	IMSI	R-LINE	Calibrated R-LINE	CMAQ-OBS	R-LINE	Calibrated R-LINE	CMAQ-OBS
2002	2.90	1.96	N.A.	1058	812	671	281	89	45
2003	2.36	1.66	N.A.	911	710	665	224	72	41
2004	2.30	1.62	N.A.	797	632	553	189	61	39
2005	2.19	1.55	N.A.	795	631	551	179	58	37
2006	2.02	1.45	N.A.	765	610	572	173	57	35
2007	2.24	1.59	N.A.	816	645	464	183	60	35
2008	1.93	1.40	N.A.	712	573	414	157	52	27
2009	1.85	1.35	0.96	727	583	381	148	49	29
2010	1.88	1.37	1.11	733	588	295	148	49	31
2011	1.50	1.14	1.44	682	552	356	136	45	27

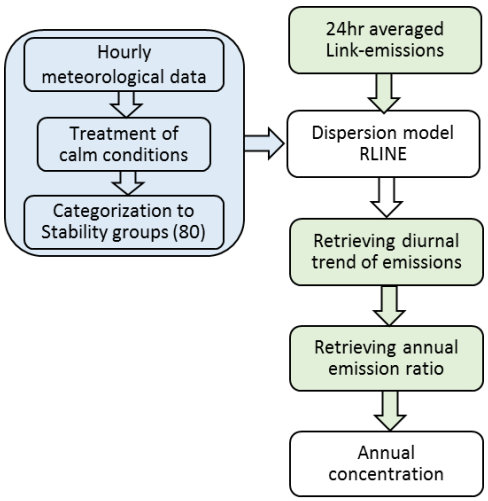

Figure A 22. Flow chart of the annual average approach.

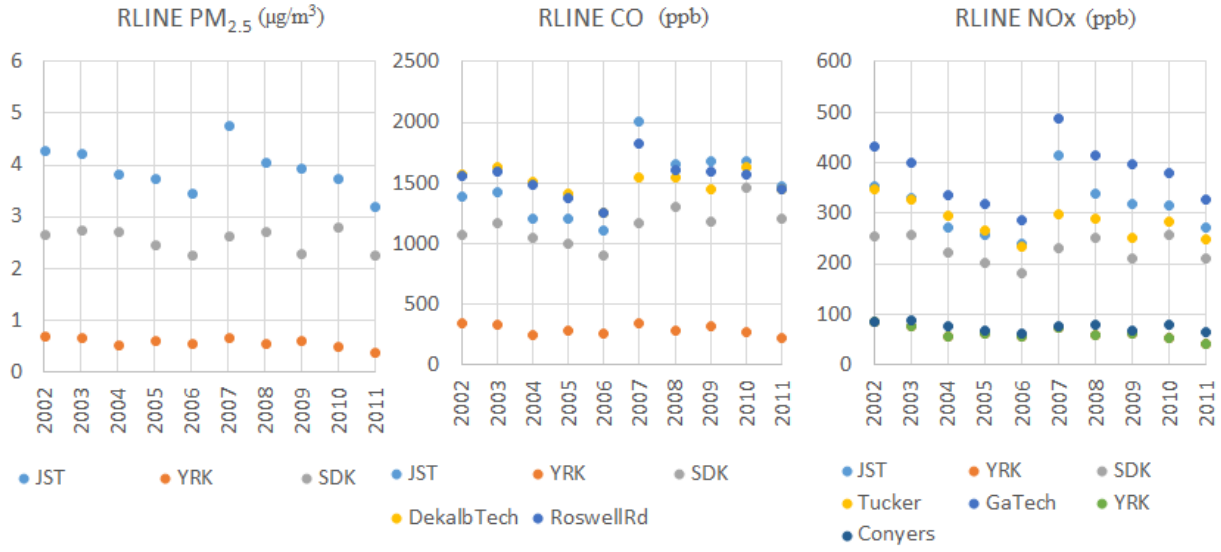

Figure A 23. Temporal trends of R-LINE estimates at sites with calm condition threshold as 0.5m/s for 2007 to 2011.

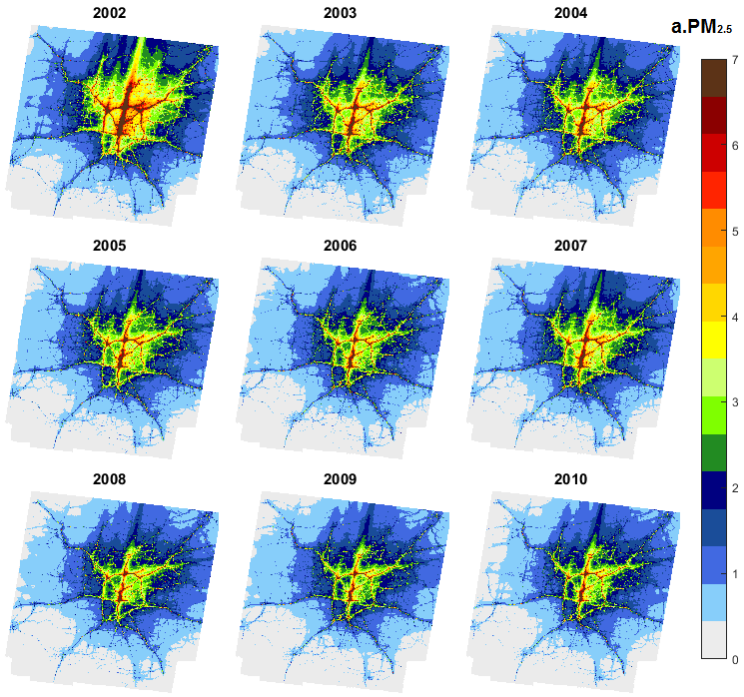
2002
2003
2004
a.PM2.5
2005
2006
2007
2008
2009
2010
7
6
5
4
3
2
1
0

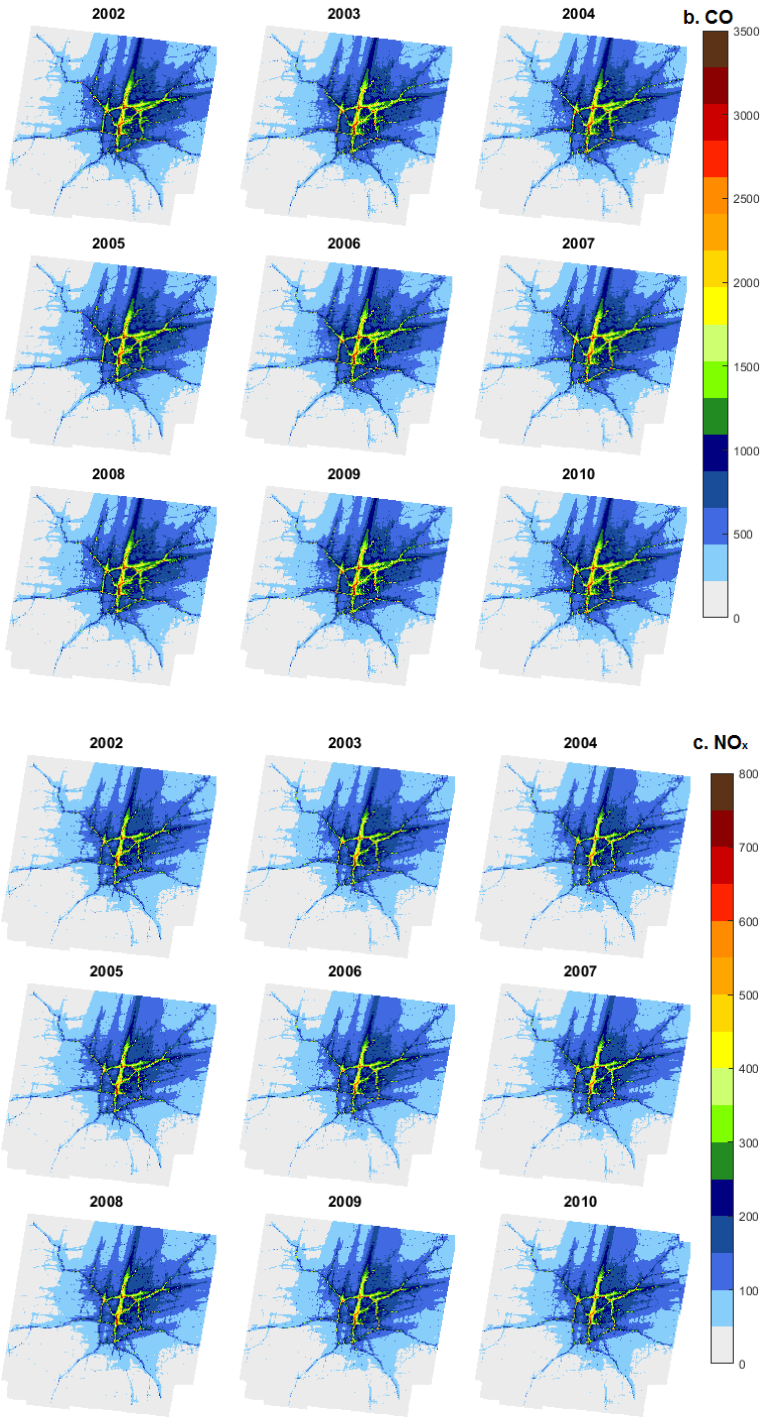

Figure A 24. Annual averages of R-LINE estimated $PM_{2.5}$ in $\mu g/m^3$ (a), daily 1h maximum CO in ppb (b), and daily 1h maximum NOx in ppb (c) by mobile source in 2002 to 2010.

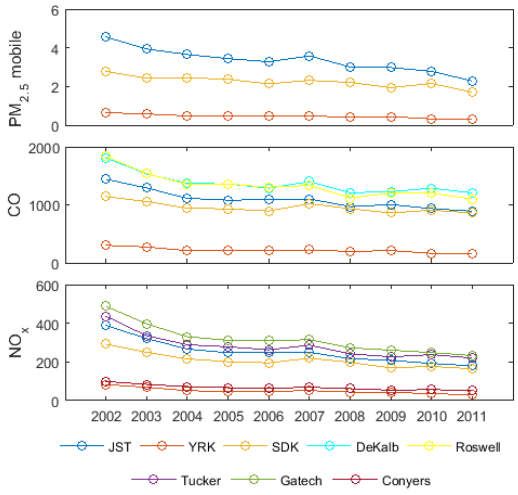

Figure A 25. R-LINE estimated annual averages at sites for three species.

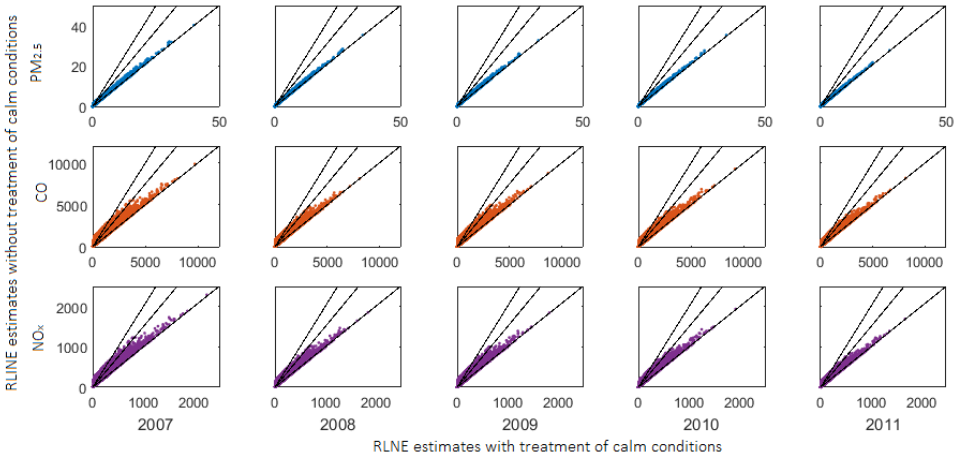

Figure A 26. Comparison of concentrations with (x) vs without (y) treatment of calm conditions (resetting 1m/s wind speed) for 2007 to 2011.

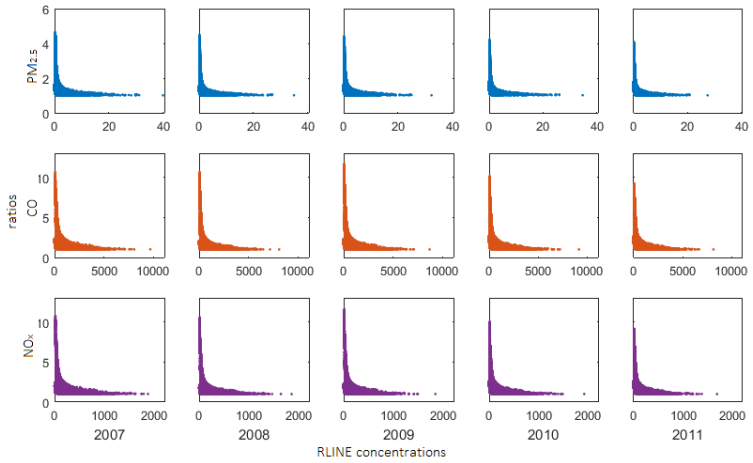

Figure A 27. Relationship of concentrations (x) and ratios (y) of without calm-treatment concentrations to with calm-treatment concentrations. This figure shows that the lower

concentrations levels are more impacted than the higher concentration levels by the calm treatment.

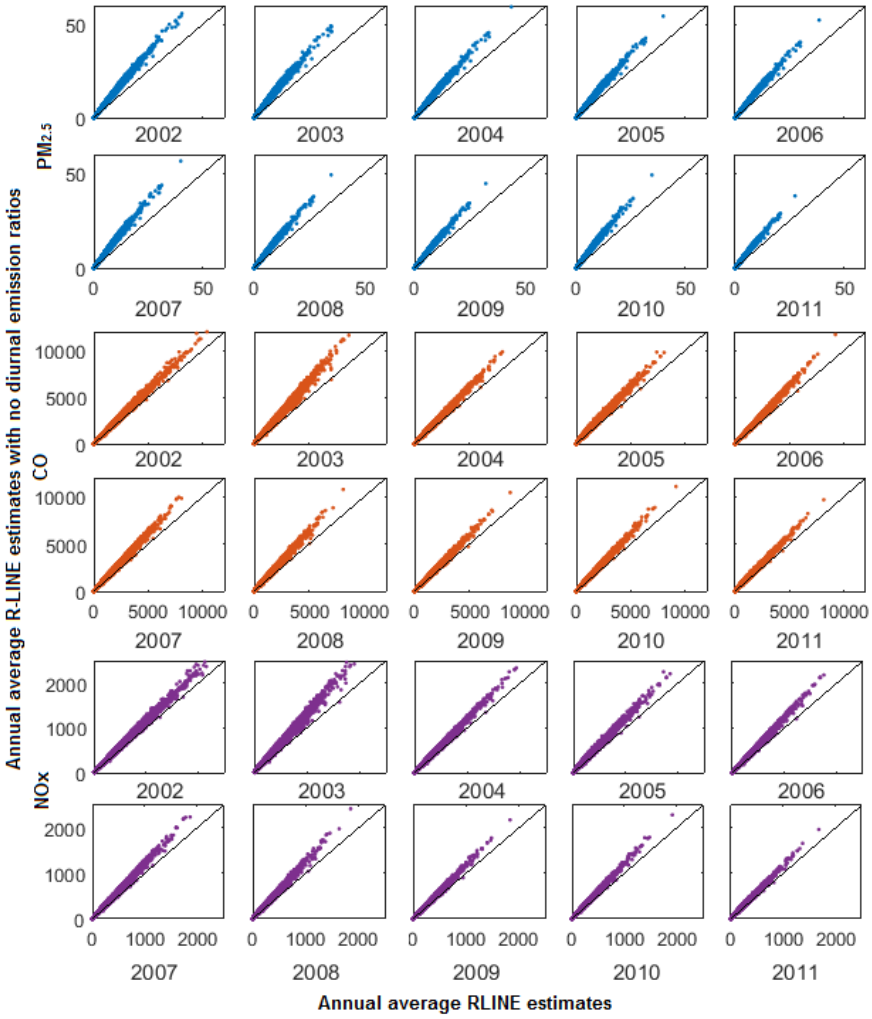

Figure A 28. Comparison of concentrations with (x) vs without (y) application of diurnal emission ratios.

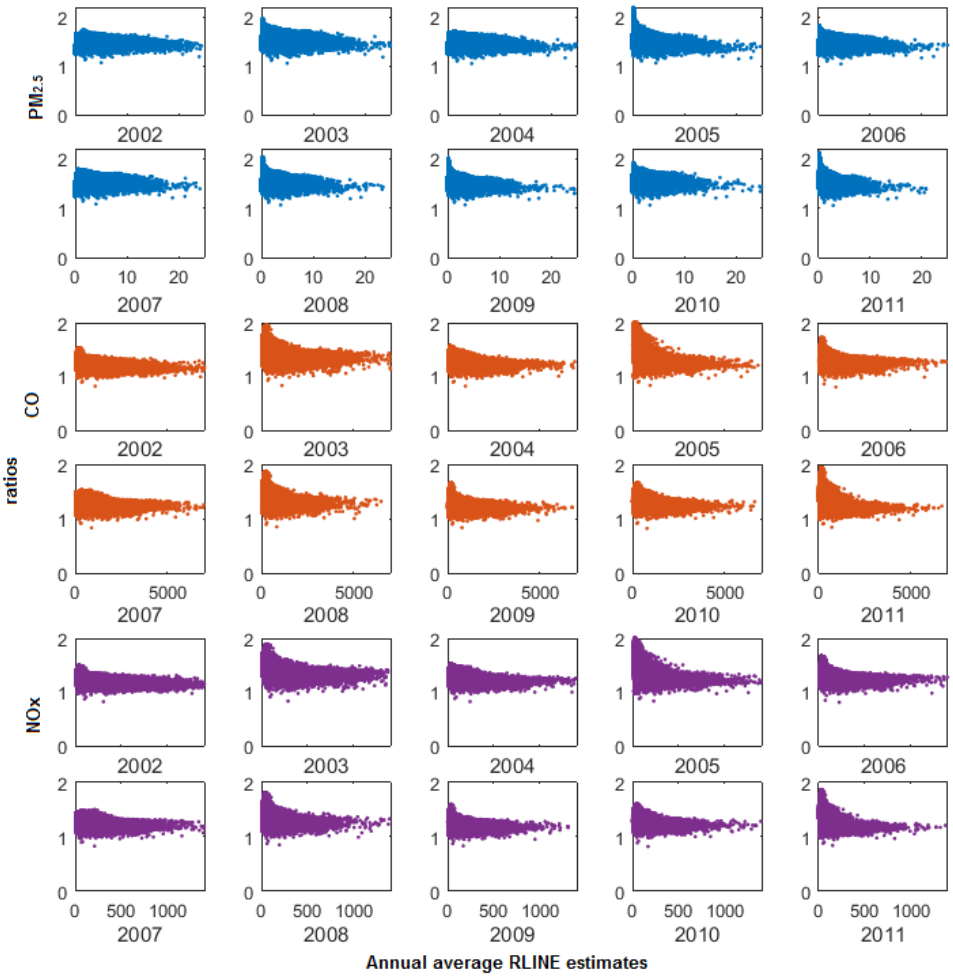

Figure A 29. Relationship of concentrations (x) vs ratios (y) of no diurnal emission ratio concentrations to with emission ratio concentrations. This figure shows a higher impact of the emission ratios at lower concentrations.

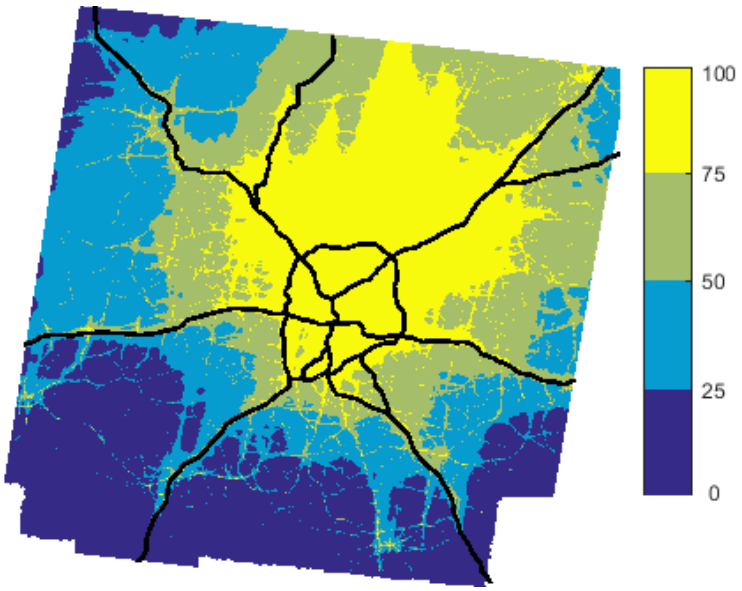

Figure A 30. Spatial distribution of quantiles of $PM_{2.5}$ in 2011 (in percentage). Similar spatial distributions are found in the quartiles of all three species and all years.

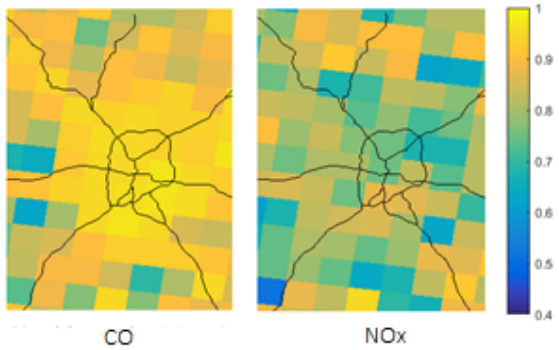

Figure A 31. Ratios of mobile emissions to total emissions for CO and NO_x estimated by SMOKE in 12km resolution.

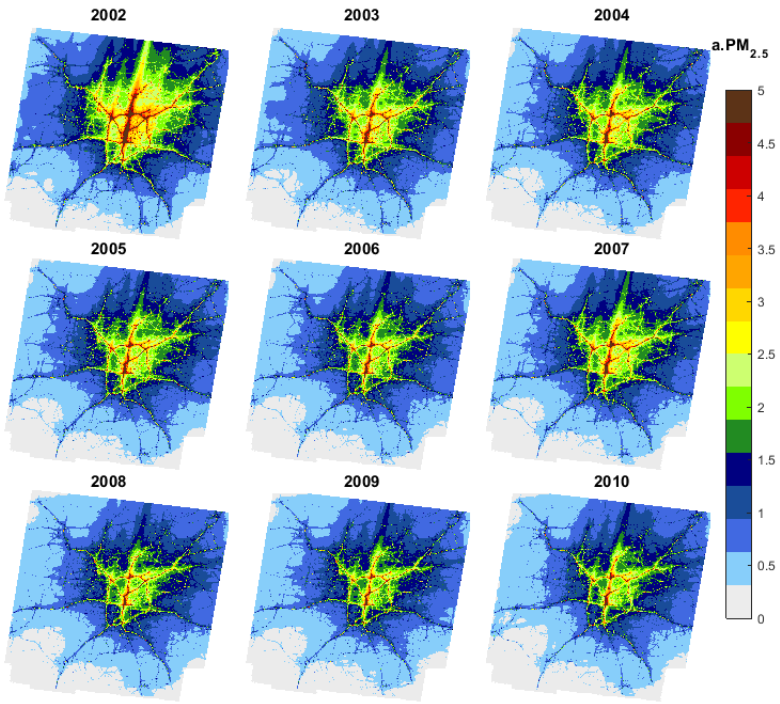

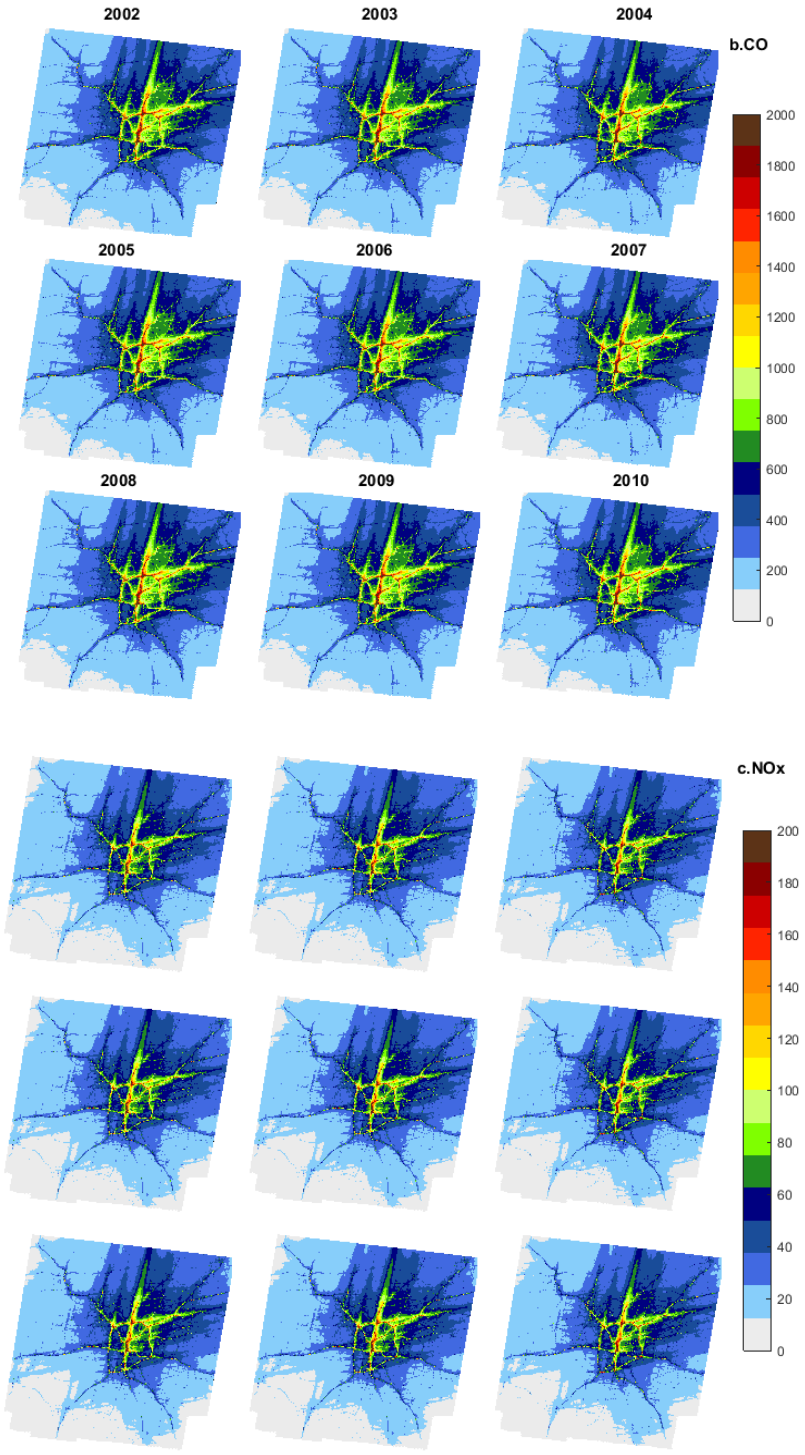

Figure A 32. Annual averages of calibrated $PM_{2.5}$ in $\mu g/m^3$ (a), daily 1h maximum CO in ppb (b), and daily 1h maximum NO_x in ppb (c) by mobile source in 2002 to 2010.

C.2 Treatment of Calm conditions.

The treatment of calm conditions is to limit the unrealistically high concentrations under those conditions in steady-state dispersion models. EPA recommended a calm condition threshold of 0.5m/s in 2013 (Environmental Protection Agency, 2013a) and 1m/s in 2000 (EPA, 2000). We found no wind speeds below 1m/s were reported for 2002 to 2006 but for 2007 to 2011, wind speeds between 0.5m/s to 1 m/s occurred 126-156 hours/year. For consistence in the meteorological input across years, we suggest resetting the hours with wind speeds below 1 m/s to 1 m/s (677 hours in 2007 to 2011). Otherwise, the temporal trends are biased (Fig. A15).

C.3 Comparison of Near-road Measurements with R-LINE Estimates

While there is no direct comparison at peak near-roadway locations in the studied years, we can compare the R-LINE model results with data obtained from a near-road measurement study by the Georgia Environmental Protection Division in 2015. A near-road site located next to a major highway (I-85/I-75 connector) in Midtown Atlanta and next to the peak location, as shown in Fig. A25 below, measured $PM_{2.5}$, CO and NO_x for 2015. For comparison, we estimated the averaged R-LINE concentrations during this period using the annual average approach. Results are shown in Table A15.

The R-LINE estimates of $PM_{2.5}$, CO and NO_x are 1.3, 3.1 and 7.4 times the measurements. Since R-LINE estimates are only for mobile source impacts, these estimates are expected to be lower than actual measurements, particularly in the case of $PM_{2.5}$ for which the direct

mobile source impacts are expected to be only a small part of the total $PM_{2.5}$ mass. These results suggest large near-road biases in R-LINE model results.

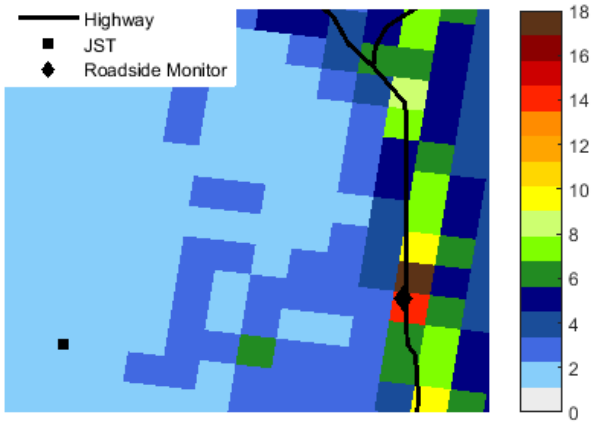

Figure A 33. Near-road measurement location. The concentration field shown is raw R-LINE $PM_{2.5}$ mobile concentrations of 2015 (A 3km by 3.5 km area in central Atlanta in 250-m resolution, $\mu g/m^3$). The square denotes JST site location. The diamond denotes the near-road site by GA EPD, located next to the maximum concertation.

Table A 15. Near-road comparison of measured and R-LINE estimated $PM_{2.5}$, CO and NOx for 2015. Near-road measurements are total, whereas R-LINE estimates are from mobile source only.

Concentrations	**$PM_{2.5}$ ($\mu g/m^3$)**	**CO**	**NOx**
Near-road measurement	10.4	1268	99
R-LINE estimates	13.8	3909	735

APPENDIX D. CHAPTER 5 SUPPLEMENTAL INFORMATION

D.1 Tables and Figures

Table A 16. Concentrations by R-LINE and PSD at the railyard area, rural area, near SDK site, and near the Spaghetti Junction. Units for $PM_{2.5}$ is $\mu g/m^3$ and for other pollutants ppb.

site	D (m)	R-LINE $PM_{2.5}$	R-LINE CO	R-LINE NOx	NOx	pentane	N-nonane	N-decane	N-undecane	benzene	toluene	m-xylene	O-xylene
Railyard	150	2.7	227.0	74.0	18.3	120.0	0.12	0.17	0.05985	0.66	1.36	0.50	0.25
	95	2.7	222.2	72.7	27.6	108.9	0.11	0.08	0.03758	0.73	1.56	0.61	0.32
Rural	5090	1.8	165.2	54.1	13.2	89.5	0.07	0.07	0.03756	0.43	1.08	0.51	0.27
	7650	1.1	114.2	37.9	7.95	70.1	0.08	0.10	0.03757	0.58	1.10	0.46	0.24
SDK	340	4.2	352.6	112.0	40.4	233.5	0.11	0.11	0.03773	1.39	2.33	0.82	0.42
Spaghetti	700	4.3	343.7	109.4	17.8	185.0	0.15	0.15	0.03772	0.72	1.95	0.76	0.38

D.2 R-LINE and Fixed Monitors Comparison.

The R-LINE estimates are compared with fixed monitors for evaluation. The concentrations of NO_x monitored and by R-LINE have medium correlation (R^2=0.13, Fig. A34), but the gradients in monitor measurements is only 0.07 times of R-LINE. NO_2 and CO are both heavily enriched in mobile emissions and therefore, the comparison of the two shows that R-LINE simulates relatively good variations of mobile source impacts on air pollution (Fig. A34). However, the estimates of $PM_{2.5}$ by R-LINE are found to be negatively correlated with the variations of BC and nephelometer. The nephelometer represents total $PM_{2.5}$ variations while the R-LINE $PM_{2.5}$ is only the impact of mobile sources. The negative correlation can be caused by other leading sources for total $PM_{2.5}$ in the areas such as secondary pollutants ammonium sulfate pollutants (Zhai et al., 2017). The

negative correlation of BC with $PM_{2.5}$ is also likely to be caused by other sources of BC than mobile sources in the areas. As this is a combined spatial and temporal comparison, the inconsistent major sources for BC in the 43 FP can lead to such negative correlations with R-LINE $PM_{2.5}$ by mobile sources.

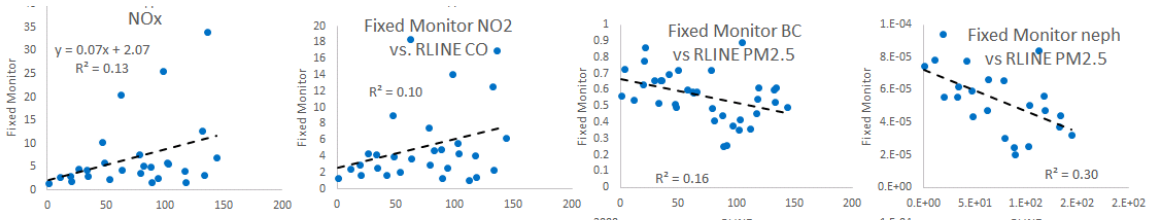

Figure A 34. Comparison for R-LINE estimates (x) with fixed monitors (y) for NO_x, NO_2, BC and nephelometer with paired pollutants with common sources.

D.3 R-LINE and Mobile Platform Comparison.

We compared all pollutants by R-LINE with all pollutants by mobile platforms at FP (Table 5 for Pearson R). As the R-LINE estimates are all by mobile source emissions, the concentrations of NO_x, CO, and $PM_{2.5}$ are all correlated with the measurements of the mobile driven pollutants NO_x and NO_2. The BC have little correlation with R-LINE estimates while nephelometer have negative correlations, which can be caused by similar reasons, existing other leading sources of the pollutants than mobile sources.

Table A 17. Pearson correlation coefficient R for R-LINE vs mobile platform FP for all pollutants.

Pearson R		*FP*			
		NO_x	NO_2	BC	Nephelometer
R-LINE	NO_x	0.516	0.583	0.268	-0.317
	CO	0.518	0.582	0.268	-0.324
	$PM_{2.5}$	0.532	0.591	0.285	-0.317

REFERENCES

Anderson, D.C., Loughner, C.P., Diskin, G., Weinheimer, A., Canty, T.P., Salawitch, R.J., Worden, H.M., Fried, A., Mikoviny, T., Wisthaler, A., Dickerson, R.R., 2014. Measured and modeled CO and NOy in DISCOVER-AQ: An evaluation of emissions and chemistry over the eastern US. Atmos Environ 96, 78-87.

Andersson, A., Deng, J.J., Du, K., Zheng, M., Yan, C.Q., Skold, M., Gustafsson, O., 2015. Regionally-Varying Combustion Sources of the January 2013 Severe Haze Events over Eastern China. Environ Sci Technol 49, 2038-2043.

Arain, M.A., Blair, R., Finkelstein, N., Brook, J.R., Sahsuvaroglu, T., Beckerman, B., Zhang, L., Jerrett, M., 2007. The use of wind fields in a land use regression model to predict air pollution concentrations for health exposure studies. Atmos Environ 41, 3453-3464.

Balachandran, S., 2013. The development, application and evaluation of advanced source apportionment methods. (Doctoral dissertation).

Balachandran, S., Chang, H.H., Pachon, J.E., Holmes, H.A., Mulholland, J.A., Russell, A.G., 2013. Bayesian-Based Ensemble Source Apportionment of PM2.5. Environ Sci Technol 47, 13511-13518.

Balachandran, S., Pachon, J.E., Hu, Y.T., Lee, D., Mulholland, J.A., Russell, A.G., 2012. Ensemble-trained source apportionment of fine particulate matter and method uncertainty analysis. Atmos Environ 61, 387-394.

Baldassarre, G., Pozzoli, L., Schmidt, C.C., Unal, A., Kindap, T., Menzel, W.P., Whitburn, S., Coheur, P.F., Kavgaci, A., Kaiser, J.W., 2015. Using SEVIRI fire observations to drive smoke plumes in the CMAQ air quality model: a case study over Antalya in 2008. Atmos Chem Phys 15, 8539-8558.

Bateson, T.F., Schwartz, J., 2008. Children's response to air pollutants. Journal of toxicology and environmental health. Part A 71, 238-243.

Batterman, S., Burke, J., Isakov, V., Lewis, T., Mukherjee, B., Robins, T., 2014. A Comparison of Exposure Metrics for Traffic-Related Air Pollutants: Application to Epidemiology Studies in Detroit, Michigan. Int J Env Res Pub He 11, 9553-9577.

Batterman, S., Ganguly, R., Harbin, P., 2015. High resolution spatial and temporal mapping of traffic-related air pollutants. Int J Environ Res Public Health 12, 3646-3666.

Beckerman, B.S., Jerrett, M., Serre, M., Martin, R.V., Lee, S.J., van Donkelaar, A., Ross, Z., Su, J., Burnett, R.T., 2013. A Hybrid Approach to Estimating National Scale

Spatiotemporal Variability of PM2.5 in the Contiguous United States. Environ Sci Technol 47, 7233-7241.

Beelen, R., Raaschou-Nielsen, O., Stafoggia, M., Andersen, Z.J., Weinmayr, G., Hoffmann, B., Wolf, K., Samoli, E., Fischer, P., Nieuwenhuijsen, M., Vineis, P., Xun, W.W., Katsouyanni, K., Dimakopoulou, K., Oudin, A., Forsberg, B., Modig, L., Havulinna, A.S., Lanki, T., Turunen, A., Oftedal, B., Nystad, W., Nafstad, P., De Faire, U., Pedersen, N.L., Ostenson, C.G., Fratiglioni, L., Penell, J., Korek, M., Pershagen, G., Eriksen, K.T., Overvad, K., Ellermann, T., Eeftens, M., Peeters, P.H., Meliefste, K., Wang, M., Bueno-de-Mesquita, B., Sugiri, D., Kramer, U., Heinrich, J., de Hoogh, K., Key, T., Peters, A., Hampel, R., Concin, H., Nagel, G., Ineichen, A., Schaffner, E., Probst-Hensch, N., Kunzli, N., Schindler, C., Schikowski, T., Adam, M., Phuleria, H., Vilier, A., Clavel-Chapelon, F., Declercq, C., Grioni, S., Krogh, V., Tsai, M.Y., Ricceri, F., Sacerdote, C., Galassi, C., Migliore, E., Ranzi, A., Cesaroni, G., Badaloni, C., Forastiere, F., Tamayo, I., Amiano, P., Dorronsoro, M., Katsoulis, M., Trichopoulou, A., Brunekreef, B., Hoek, G., 2014. Effects of long-term exposure to air pollution on natural-cause mortality: an analysis of 22 European cohorts within the multicentre ESCAPE project. Lancet 383, 785-795.

Blanchard, C.L., Hidy, G.M., Shaw, S., Baumann, K., Edgerton, E.S., 2016. Effects of emission reductions on organic aerosol in the southeastern United States. Atmos Chem Phys 16, 215-238.

Blanchard, C.L., Tanenbaum, S., Hidy, G.M., 2012. Source Contributions to Atmospheric Gases and Particulate Matter in the Southeastern United States. Environ Sci Technol 46, 5479-5488.

Blanchard, C.L.H., G. M.; Tanenbaum, S.; Edgerton, E. S.; Hartsell, B. E., 2013. The Southeastern Aerosol Research and Characterization (SEARCH) study: Temporal trends in gas and PM concentrations and composition, 1999-2010. J Air Waste Manage 63, 247-259.

Boothe, V., Dimmick, F., Haley, V., Paulu, C., Bekkedal, M., Holland, D., Talbot, T., Smith, A., Werner, M., Baldridge, E., 2006. A review of public health air surveillance evaluation project. Epidemiology 17, S450-S451.

Bowers, J., Bjorklund, J., Cheney, C., Schewe, G.J., 1980. Industrial source complex (ISC) dispersion model user's guide. US Environmental Protection Agency, Office of Air Quality Planning and Standards.

Brauer, M., Freedman, G., Frostad, J., van Donkelaar, A., Martin, R.V., Dentener, F., van Dingenen, R., Estep, K., Amini, H., Apte, J.S., Balakrishnan, K., Barregard, L., Broday, D., Feigin, V., Ghosh, S., Hopke, P.K., Knibbs, L.D., Kokubo, Y., Liu, Y., Ma, S.F., Morawska, L., Sangrador, J.L.T., Shaddick, G., Anderson, H.R., Vos, T., Forouzanfar, M.H., Burnett, R.T., Cohen, A., 2016. Ambient Air Pollution Exposure Estimation for the Global Burden of Disease 2013. Environ Sci Technol 50, 79-88.

Brauer, M., Lencar, C., Tamburic, L., Koehoorn, M., Demers, P., Karr, C., 2008. A cohort study of traffic-related air pollution impacts on birth outcomes. Environ Health Perspect 116, 680-686.

Brook, R.D., Rajagopalan, S., Pope, C.A., Brook, J.R., Bhatnagar, A., Diez-Roux, A.V., Holguin, F., Hong, Y.L., Luepker, R.V., Mittleman, M.A., Peters, A., Siscovick, D., Smith, S.C., Whitsel, L., Kaufman, J.D., Epidemiol, A.H.A.C., Dis, C.K.C., Metab, C.N.P.A., 2010. Particulate Matter Air Pollution and Cardiovascular Disease An Update to the Scientific Statement From the American Heart Association. Circulation 121, 2331-2378.

Byun, D., Young, J., Gipson, G., Godowitch, J., Binkowski, F., 1997. Description of the Models-3 Community Multiscale Air Quality(CMAQ) Modeling System.

Census Bureau, U.S., 2012. Summary Population and Housing Characteristics 2010 Census of Population and Housing. census.gov.

Cesari, D., Donateo, A., Conte, M., Contini, D., 2016. Inter-comparison of source apportionment of PM10 using PMF and CMB in three sites nearby an industrial area in central Italy. Atmos Res 182, 282-293.

Chan, Y.C., Cohen, D.D., Hawas, O., Stelcer, E., Simpson, R., Denison, L., Wong, N., Hodge, M., Comino, E., Carswell, S., 2008. Apportionment of sources of fine and coarse particles in four major Australian cities by positive matrix factorisation. Atmos Environ 42, 374-389.

Chang, S.Y., Vizuete, W., Valencia, A., Naess, B., Isakov, V., Palma, T., Breen, M., Arunachalam, S., 2015. A modeling framework for characterizing near-road air pollutant concentration at community scales. Sci Total Environ 538, 905-921.

Chen, C.H., Chan, C.C., Chen, B.Y., Cheng, T.J., Guo, Y.L., 2015. Effects of particulate air pollution and ozone on lung function in non-asthmatic children. Environ Res 137, 40-48.

Chen, H., Goldberg, M.S., Burnett, R.T., Jerrett, M., Wheeler, A.J., Villeneuve, P.J., 2013. Long-term exposure to traffic-related air pollution and cardiovascular mortality. Epidemiology 24, 35-43.

Chen, L.C., Lippmann, M., 2009. Effects of Metals within Ambient Air Particulate Matter (PM) on Human Health. Inhal Toxicol 21, 1-31.

Chow, J.C., Watson, J.G., Chen, L.W., Chang, M.C., Robinson, N.F., Trimble, D., Kohl, S., 2007. The IMPROVE_A temperature protocol for thermal/optical carbon analysis: maintaining consistency with a long-term database. J Air Waste Manag Assoc 57, 1014-1023.

Chow, J.C., Watson, J.G., Chen, L.W.A., Rice, J., Frank, N.H., 2010. Quantification of PM2.5 organic carbon sampling artifacts in US networks. Atmos Chem Phys 10, 5223-5239.

Chow, J.C., Watson, J.G., Kuhns, H., Etyemezian, V., Lowenthal, D.H., Crow, D., Kohl, S.D., Engelbrecht, J.P., Green, M.C., 2004. Source profiles for industrial, mobile, and area sources in the Big Bend Regional Aerosol Visibility and Observational study. Chemosphere 54, 185-208.

Chow, J.C., Watson, J.G., Pritchett, L.C., Pierson, W.R., Frazier, C.A., Purcell, R.G., 1993. The Dri Thermal Optical Reflectance Carbon Analysis System - Description, Evaluation and Applications in United-States Air-Quality Studies. Atmos Environ a-Gen 27, 1185-1201.

Cimorelli, A.J., Perry, S.G., Venkatram, A., Weil, J.C., Paine, R.J., Wilson, R.B., Lee, R.F., Peters, W.D., Brode, R.W., 2005. AERMOD: A dispersion model for industrial source applications. Part I: General model formulation and boundary layer characterization. J Appl Meteorol 44, 682-693.

Cohen, A.J., Anderson, H.R., Ostro, B., Pandey, K.D., Krzyzanowski, M., Kunzli, N., Gutschmidt, K., Pope, A., Romieu, I., Samet, J.M., Smith, K., 2005. The global burden of disease due to outdoor air pollution. J Toxicol Env Heal A 68, 1301-1307.

Colvile, R.N., Hutchinson, E.J., Mindell, J.S., Warren, R.F., 2001. The transport sector as a source of air pollution. Atmos Environ 35, 1537-1565.

Cressie, N., 1988. Spatial Prediction and Ordinary Kriging. Math Geol 20, 405-421.

Crooks, J.L., Ozkaynak, H., 2014. Simultaneous statistical bias correction of multiple PM2.5 species from a regional photochemical grid model. Atmos Environ 95, 126-141.

D'Onofrio, D., Kim, B., Kim, Y., Kim, K., 2016. Atlanta Roadside Emissions Exposure Study – Methodology & Project Overview. http://www.atlantaregional.com/environment/air/arees-near-road-emissions.

Dearth, M.A., Gierczak, C.A., Siegl, W.O., 1992. Online Measurement of Benzene and Toluene in Dilute Vehicle Exhaust by Mass-Spectrometry. Environ Sci Technol 26, 1573-1580.

Delfino, R.J., Staimer, N., Gillen, D., Tjoa, T., Sioutas, C., Fung, K., George, S.C., Kleinman, M.T., 2006. Personal and ambient air pollution is associated with increased exhaled nitric oxide in children with asthma. Environ Health Persp 114, 1736-1743.

Dominici, F., Peng, R.D., Barr, C.D., Bell, M.L., 2010. Protecting Human Health From Air Pollution Shifting From a Single-pollutant to a Multipollutant Approach. Epidemiology 21, 187-194.

Dons, E., Temmerman, P., Van Poppel, M., Bellemans, T., Wets, G., Panis, L.I., 2013. Street characteristics and traffic factors determining road users' exposure to black carbon. Sci Total Environ 447, 72-79.

Dunker, A.M., Yarwood, G., Ortmann, J.P., Wilson, G.M., 2002. The decoupled direct method for sensitivity analysis in a three-dimensional air quality model - Implementation, accuracy, and efficiency. Environ Sci Technol 36, 2965-2976.

Edgerton, E.S., Hartsell, B.E., Saylor, R.D., Jansen, J.J., Hansen, D.A., Hidy, G.M., 2005. The southeastern aerosol research and characterization study: Part II. Filter-based measurements of fine and coarse particulate matter mass and composition. J Air Waste Manage 55, 1527-1542.

Edgerton, E.S., Hartsell, B.E., Saylor, R.D., Jansen, J.J., Hansen, D.A., Hidy, G.M., 2006. The Southeastern Aerosol Research and Characterization Study, part 3: Continuous measurements of fine particulate matter mass and composition. J Air Waste Manage 56, 1325-1341.

Environmental Protection Agency, U.S., Air Quality System Data Mart [internet database] available at http://www.epa.gov/ttn/airs/aqsdatamart.

Environmental Protection Agency, U.S., 2011. Annual Data Summary Report for the Chemical Speciation of PM2.5 Filter Samples Project.

Environmental Protection Agency, U.S., 2012. Motor Vehicle Emission Simulator (MOVES) User Guide for MOVES2010b.

Environmental Protection Agency, U.S., 2013a. Use of ASOS meteorological data in AERMOD dispersion modeling. https://www3.epa.gov/scram001/metobsdata_procaccprogs.htm.

Environmental Protection Agency, U.S., 2013b. User’s Guide for R-LINE Model Version 1.2 A Research LINE source model for near-surface releases.

Environmental Protection Agency, U.S., 2016. National Emission Inventory. https://www.epa.gov/air-emissions-inventories/national-emissions-inventory.

EPA, 2000. Meteorological Monitoring Guidance for Regulatory Modeling Applications. EPA.

EPA, U.S.E.P.A., 1997. The STability ARray program. https://www3.epa.gov/scram001/metobsdata_procaccprogs.htm.

EPA, U.S.E.P.A., 2004a. EPA-CMB8.2 Usear's Manual.

EPA, U.S.E.P.A., 2004b. User's guide for the AERMOD Meteorological Preprocessor (AERMET).

EPA, U.S.E.P.A., 2009. Integrated science assessment for particulate matter.

EPA, U.S.E.P.A., 2011. Annual Data Summary Report for the Chemical Speciation of PM2.5 Filter Samples Project.

EPA, U.S.E.P.A., 2015. AERMINUTE User's Guide.

Fine, P.M., Cass, G.R., Simoneit, B.R.T., 2001. Chemical characterization of fine particle emissions from fireplace combustion of woods grown in the northeastern United States. Environ Sci Technol 35, 2665-2675.

Friberg, M.D., Zhai, X., Holmes, H.A., Chang, H.H., Strickland, M.J., Sarnat, S.E., Tolbert, P.E., Russell, A.G., Mulholland, J.A., 2016a. Method for fusing observational data and chemical transport model simulations to estimate spatiotemporally resolved ambient air pollution. Environ Sci Technol 50, 3695-3705.

Friberg, M.D., Zhai, X.D., Holmes, H., Chang, H.H., Strickland, M., Sarnat, S.E., Tolbert, P.E., Russell, A.G., Mulholland, J.A., 2016b. Method for Fusing Observational Data and Chemical Transport Model Simulations to Estimate Spatiotemporally-Resolved Ambient Air Pollution. Environ Sci Technol.

Friberg, M.D., Zhai, X.X., Holmes, H.A., Chang, H.H., Strickland, M.J., Sarnat, S.E., Tolbert, P.E., Russell, A.G., Mulholland, J.A., 2016c. Method for Fusing Observational Data and Chemical Transport Model Simulations To Estimate Spatiotemporally Resolved Ambient Air Pollution. Environ Sci Technol 50, 3695-3705.

Fujita, E.M., Campbell, D.E., Zielinska, B., Chow, J.C., Lindhjem, C.E., DenBleyker, A., Bishop, G.A., Schuchmann, B.G., Stedman, D.H., Lawson, D.R., 2012. Comparison of the MOVES2010a, MOBILE6.2, and EMFAC2007 mobile source emission models with on-road traffic tunnel and remote sensing measurements. J Air Waste Manage 62, 1134-1149.

Ganguly, R., Batterman, S., Isakov, V., Snyder, M., Breen, M., Brakefield-Caldwell, W., 2015. Effect of geocoding errors on traffic-related air pollutant exposure and concentration estimates. Journal of exposure science & environmental epidemiology 25, 490-498.

Garland, J.A., 1978. Dry and Wet Removal of Sulfur from Atmosphere. Atmos Environ 12, 349-362.

Gauderman, W.J., Vora, H., McConnell, R., Berhane, K., Gilliland, F., Thomas, D., Lurmann, F., Avol, E., Kunzli, N., Jerrett, M., Peters, J., 2007. Effect of exposure to

traffic on lung development from 10 to 18 years of age: a cohort study. Lancet 369, 571-577.

Gehring, U., Wijga, A.H., Brauer, M., Fischer, P., de Jongste, J.C., Kerkhof, M., Oldenwening, M., Smit, H.A., Brunekreef, B., 2010. Traffic-related air pollution and the development of asthma and allergies during the first 8 years of life. Am J Respir Crit Care Med 181, 596-603.

Georgia Department of Transportation, U.S., 2013. http://www.dot.ga.gov/DriveSmart/MapsData/Documents/Statewide/TrafficFlowMap_Interstate_AADT.pdf.

Gill, E.A., Curl, C.L., Adar, S.D., Allen, R.W., Auchincloss, A.H., O'Neill, M.S., Park, S.K., Van Hee, V.C., Roux, A.V.D., Kaufman, J.D., 2011. Air Pollution and Cardiovascular Disease in the Multi-Ethnic Study of Atherosclerosis. Prog Cardiovasc Dis 53, 353-360.

Gulliver, J., Briggs, D., 2011. STEMS-Air: A simple GIS-based air pollution dispersion model for city-wide exposure assessment. Sci Total Environ 409, 2419-2429.

Hagler, G.S.W., Thoma, E.D., Baldauf, R.W., 2010. High-Resolution Mobile Monitoring of Carbon Monoxide and Ultrafine Particle Concentrations in a Near-Road Environment. J Air Waste Manage 60, 328-336.

Hankey, S., Marshall, J.D., 2015. Land Use Regression Models of On-Road Particulate Air Pollution (Particle Number, Black Carbon, PM2.5, Particle Size) Using Mobile Monitoring. Environ Sci Technol 49, 9194-9202.

Hansen, D.A., Edgerton, E.S., Hartsell, B.E., Jansen, J.J., Kandasamy, N., Hidy, G.M., Blanchard, C.L., 2003. The southeastern aerosol research and characterization study: Part 1-overview. J Air Waste Manage 53, 1460-1471.

Hart, J.E., Garshick, E., Dockery, D.W., Smith, T.J., Ryan, L., Laden, F., 2011. Long-term ambient multipollutant exposures and mortality. Am J Respir Crit Care Med 183, 73-78.

Held, T., Ying, Q., Kleeman, M.J., Schauer, J.J., Fraser, M.P., 2005. A comparison of the UCD/CIT air quality model and the CMB source-receptor model for primary airborne particulate matter. Atmos Environ 39, 2281-2297.

Hidy, G.M., Blanchard, C.L., Baumann, K., Edgerton, E., Tanenbaum, S., Shaw, S., Knipping, E., Tombach, I., Jansen, J., Walters, J., 2014. Chemical climatology of the southeastern United States, 1999-2013. Atmos Chem Phys 14, 11893-11914.

Hidy, G.M., Pennell, W.T., 2010. Multipollutant Air Quality Management. J Air Waste Manage 60, 645-674.

Hoek, G., Beelen, R., de Hoogh, K., Vienneau, D., Gulliver, J., Fischer, P., Briggs, D., 2008. A review of land-use regression models to assess spatial variation of outdoor air pollution. Atmos Environ 42, 7561-7578.

Houyoux, M., Vukovich, J., Brandmeyer, J., Seppanen, C., Holland, A., 2000. Sparse Matrix Operator Kernel Emissions Modeling System-SMOKE User Manual. Prepared by MCNC-North Carolina Supercomputing Center, Environmental Programs, Research Triangle Park, NC.

Hu, S.S., Paulson, S.E., Fruin, S., Kozawa, K., Mara, S., Winer, A.M., 2012. Observation of elevated air pollutant concentrations in a residential neighborhood of Los Angeles California using a mobile platform. Atmos Environ 51, 311-319.

Hu, Y., 2014. HiRes2 Air Quality & Source Impacts Forecasting for Georgia, https://forecast.ce.gatech.edu/hires_about.php.

Hu, Y., Balachandran, S., Pachon, J.E., Baek, J., Ivey, C., Holmes, H., Odman, M.T., Mulholland, J.A., Russell, A.G., 2014. Fine particulate matter source apportionment using a hybrid chemical transport and receptor model approach. Atmos Chem Phys 14, 5415-5431.

Hu, Y., Chang, M.E., Russell, A.G., Odman, M.T., 2010. Using synoptic classification to evaluate an operational air quality forecasting system in Atlanta. Atmos Pollut Res 1, 280-287.

Ito, K., Xue, N., Thurston, G., 2004. Spatial variation of PM2.5 chemical species and source-apportioned mass concentrations in New York City. Atmos Environ 38, 5269-5282.

Ivey, C.E., Holmes, H.A., Hu, Y.T., Mulholland, J.A., Russell, A.G., 2015. Development of PM2.5 source impact spatial fields using a hybrid source apportionment air quality model. Geosci Model Dev 8, 2153-2165.

Jerrett, M., Arain, A., Kanaroglou, P., Beckerman, B., Potoglou, D., Sahsuvaroglu, T., Morrison, J., Giovis, C., 2005. A review and evaluation of intraurban air pollution exposure models. J Expo Anal Env Epid 15, 185-204.

Johns, D.O., Stanek, L.W., Walker, K., Benromdhane, S., Hubbell, B., Ross, M., Devlin, R.B., Costa, D.L., Greenbaum, D.S., 2012. Practical Advancement of Multipollutant Scientific and Risk Assessment Approaches for Ambient Air Pollution. Environ Health Persp 120, 1238-1242.

Kampa, M., Castanas, E., 2008. Human health effects of air pollution. Environ Pollut 151, 362-367.

Kelly, F.J., Fussell, J.C., 2012. Size, source and chemical composition as determinants of toxicity attributable to ambient particulate matter. Atmos Environ 60, 504-526.

Kim, J.Y., Burnett, R.T., Neas, L., Thurston, G.D., Schwartz, J., Tolbert, P.E., Brunekreef, B., Goldberg, M.S., Romieu, I., 2007. Panel discussion review: session two - interpretation of observed associations between multiple ambient air pollutants and health effects in epidemiologic analyses. J Expo Sci Env Epid 17, S83-S89.

Kim, Y.J., Kim, K.W., Kim, S.D., Lee, B.K., Han, J.S., 2006. Fine particulate matter characteristics and its impact on visibility impairment at two urban sites in Korea: Seoul and Incheon. Atmos Environ 40, S593-S605.

Kingham, S., Longley, I., Salmond, J., Pattinson, W., Shrestha, K., 2013. Variations in exposure to traffic pollution while travelling by different modes in a low density, less congested city. Environ Pollut 181, 211-218.

Kioumourtzoglou, M.A., Schwartz, J.D., Weisskopf, M.G., Melly, S.J., Wang, Y., Dominici, F., Zanobetti, A., 2016. Long-term PM2.5 Exposure and Neurological Hospital Admissions in the Northeastern United States. Environ Health Perspect 124, 23-29.

Knibbs, L.D., Coorey, C.P., Bechle, M.J., Cowie, C.T., Dirgawati, M., Heyworth, J.S., Marks, G.B., Marshall, J.D., Morawska, L., Pereira, G., Hewson, M.G., 2016. Independent Validation of National Satellite-Based Land-Use Regression Models for Nitrogen Dioxide Using Passive Samplers. Environ Sci Technol 50, 12331-12338.

Koppmann, R., Czapiewski, K.v., Reid, J., 2005. A review of biomass burning emissions, part I: gaseous emissions of carbon monoxide, methane, volatile organic compounds, and nitrogen containing compounds. Atmospheric chemistry and physics discussions 5, 10455-10516.

Lai, H.K., Kendall, M., Ferrier, H., Lindup, I., Alm, S., Hanninen, O., Jantunen, M., Mathys, P., Colvile, R., Ashmore, M.R., Cullinan, P., Nieuwenhuijsen, M.J., 2004. Personal exposures and microenvironment concentrations of PM2.5, VOC, NO2 and CO in Oxford, UK. Atmos Environ 38, 6399-6410.

Larson, T., Henderson, S.B., Brauer, M., 2009. Mobile Monitoring of Particle Light Absorption Coefficient in an Urban Area as a Basis for Land Use Regression. Environ Sci Technol 43, 4672-4678.

Lee, S., Kim, H.K., Yan, B., Cobb, C.E., Hennigan, C., Nichols, S., Chamber, M., Edgerton, E.S., Jansen, J.J., Hu, Y.T., Zheng, M., Weber, R.J., Russell, A.G., 2008a. Diagnosis of aged prescribed burning plumes impacting an urban area. Environ Sci Technol 42, 1438-1444.

Lee, S., Liu, W., Wang, Y.H., Russell, A.G., Edgerton, E.S., 2008b. Source apportionment of PM2.5: Comparing PMF and CMB results for four ambient monitoriniz sites in the southeastern United States. Atmos Environ 42, 4126-4137.

Lee, S., Russell, A.G., 2007. Estimating uncertainties and uncertainty contributors of CMB PM2.5 source apportionment results. Atmos Environ 41, 9616-9624.

Lelieveld, J., Evans, J.S., Fnais, M., Giannadaki, D., Pozzer, A., 2015. The contribution of outdoor air pollution sources to premature mortality on a global scale. Nature 525, 367-+.

Lena, T.S., Ochieng, V., Carter, M., Holguin-Veras, J., Kinney, P.L., 2001. Elemental carbon and PM2.5 levels in an urban community heavily impacted by truck traffic. Epidemiology 12, S38-S38.

Lim, S.S., Vos, T., Flaxman, A.D., Danaei, G., Shibuya, K., Adair-Rohani, H., Amann, M., Anderson, H.R., Andrews, K.G., Aryee, M., Atkinson, C., Bacchus, L.J., Bahalim, A.N., Balakrishnan, K., Balmes, J., Barker-Collo, S., Baxter, A., Bell, M.L., Blore, J.D., Blyth, F., Bonner, C., Borges, G., Bourne, R., Boussinesq, M., Brauer, M., Brooks, P., Bruce, N.G., Brunekreef, B., Bryan-Hancock, C., Bucello, C., Buchbinder, R., Bull, F., Burnett, R.T., Byers, T.E., Calabria, B., Carapetis, J., Carnahan, E., Chafe, Z., Charlson, F., Chen, H.L., Chen, J.S., Cheng, A.T.A., Child, J.C., Cohen, A., Colson, K.E., Cowie, B.C., Darby, S., Darling, S., Davis, A., Degenhardt, L., Dentener, F., Des Jarlais, D.C., Devries, K., Dherani, M., Ding, E.L., Dorsey, E.R., Driscoll, T., Edmond, K., Ali, S.E., Engell, R.E., Erwin, P.J., Fahimi, S., Falder, G., Farzadfar, F., Ferrari, A., Finucane, M.M., Flaxman, S., Fowkes, F.G.R., Freedman, G., Freeman, M.K., Gakidou, E., Ghosh, S., Giovannucci, E., Gmel, G., Graham, K., Grainger, R., Grant, B., Gunnell, D., Gutierrez, H.R., Hall, W., Hoek, H.W., Hogan, A., Hosgood, H.D., Hoy, D., Hu, H., Hubbell, B.J., Hutchings, S.J., Ibeanusi, S.E., Jacklyn, G.L., Jasrasaria, R., Jonas, J.B., Kan, H.D., Kanis, J.A., Kassebaum, N., Kawakami, N., Khang, Y.H., Khatibzadeh, S., Khoo, J.P., Kok, C., Laden, F., Lalloo, R., Lan, Q., Lathlean, T., Leasher, J.L., Leigh, J., Li, Y., Lin, J.K., Lipshultz, S.E., London, S., Lozano, R., Lu, Y., Mak, J., Malekzadeh, R., Mallinger, L., Marcenes, W., March, L., Marks, R., Martin, R., McGale, P., McGrath, J., Mehta, S., Mensah, G.A., Merriman, T.R., Micha, R., Michaud, C., Mishra, V., Hanafiah, K.M., Mokdad, A.A., Morawska, L., Mozaffarian, D., Murphy, T., Naghavi, M., Neal, B., Nelson, P.K., Nolla, J.M., Norman, R., Olives, C., Omer, S.B., Orchard, J., Osborne, R., Ostro, B., Page, A., Pandey, K.D., Parry, C.D.H., Passmore, E., Patra, J., Pearce, N., Pelizzari, P.M., Petzold, M., Phillips, M.R., Pope, D., Pope, C.A., Powles, J., Rao, M., Razavi, H., Rehfuess, E.A., Rehm, J.T., Ritz, B., Rivara, F.P., Roberts, T., Robinson, C., Rodriguez-Portales, J.A., Romieu, I., Room, R., Rosenfeld, L.C., Roy, A., Rushton, L., Salomon, J.A., Sampson, U., Sanchez-Riera, L., Sanman, E., Sapkota, A., Seedat, S., Shi, P.L., Shield, K., Shivakoti, R., Singh, G.M., Sleet, D.A., Smith, E., Smith, K.R., Stapelberg, N.J.C., Steenland, K., Stockl, H., Stovner, L.J., Straif, K., Straney, L., Thurston, G.D., Tran, J.H., Van Dingenen, R., van Donkelaar, A., Veerman, J.L., Vijayakumar, L., Weintraub, R., Weissman, M.M., White, R.A., Whiteford, H., Wiersma, S.T., Wilkinson, J.D., Williams, H.C., Williams, W., Wilson, N., Woolf, A.D.,

Yip, P., Zielinski, J.M., Lopez, A.D., Murray, C.J.L., Ezzati, M., 2012. A comparative risk assessment of burden of disease and injury attributable to 67 risk factors and risk factor clusters in 21 regions, 1990-2010: a systematic analysis for the Global Burden of Disease Study 2010. Lancet 380, 2224-2260.

Lin, Y.F., Huang, K., Zhuang, G.S., Fu, J.S.S., Wang, Q.Z., Liu, T.N., Deng, C.R., Fu, Q.Y., 2014. A multi-year evolution of aerosol chemistry impacting visibility and haze formation over an Eastern Asia megacity, Shanghai. Atmos Environ 92, 76-86.

Liu, B., Frey, H.C., 2015. Variability in Light-Duty Gasoline Vehicle Emission Factors from Trip-Based Real-World Measurements. Environ Sci Technol 49, 12525-12534.

Liu, Q.Y., Baumgartner, J., Zhang, Y., Schauer, J.J., 2016. Source apportionment of Beijing air pollution during a severe winter haze event and associated pro-inflammatory responses in lung epithelial cells. Atmos Environ 126, 28-35.

Liu, X.H., Zhang, Y., Cheng, S.H., Xing, J., Zhang, Q.A., Streets, D.G., Jang, C., Wang, W.X., Hao, J.M., 2010a. Understanding of regional air pollution over China using CMAQ, part I performance evaluation and seasonal variation. Atmos Environ 44, 2415-2426.

Liu, X.H., Zhang, Y., Xing, J., Zhang, Q.A., Wang, K., Streets, D.G., Jang, C., Wang, W.X., Hao, J.M., 2010b. Understanding of regional air pollution over China using CMAQ, part II. Process analysis and sensitivity of ozone and particulate matter to precursor emissions. Atmos Environ 44, 3719-3727.

Lv, B.L., Hu, Y.T., Chang, H.H., Russell, A.G., Bai, Y.Q., 2016. Improving the Accuracy of Daily PM2.5 Distributions Derived from the Fusion of Ground-Level Measurements with Aerosol Optical Depth Observations, a Case Study in North China. Environ Sci Technol 50, 4752-4759.

Maciejczyk, P., Chen, L.C., 2005. Effects of subchronic exposures to concentrated ambient particles (CAPs) in mice: VIII. Source-related daily variations in in vitro responses to CAPs. Inhal Toxicol 17, 243-253.

Malm, W.C., Schichtel, B.A., Pitchford, M.L., 2011. Uncertainties in PM2.5 gravimetric and speciation measurements and what we can learn from them. J Air Waste Manag Assoc 61, 1131-1149.

Mar, T.F., Ito, K., Koenig, J.Q., Larson, T.V., Eatough, D.J., Henry, R.C., Kim, E., Laden, F., Lall, R., Neas, L., Stolzel, M., Paatero, P., Hopke, P.K., Thurston, G.D., 2006. PM source apportionment and health effects. 3. Investigation of inter-method variations in associations between estimated source contributions Of PM2.5 and daily mortality in Phoenix, AZ. J Expo Sci Env Epid 16, 311-320.

Marmur, A., Mulholland, J.A., Russell, A.G., 2007. Optimized variable source-profile approach for source apportionment. Atmos Environ 41, 493-505.

Marmur, A., Park, S.K., Mulholland, J.A., Tolbert, P.E., Russell, A.G., 2006. Source apportionment of PM2.5 in the southeastern United States using receptor and emissions-based models: Conceptual differences and implications for time-series health studies. Atmos Environ 40, 2533-2551.

Marmur, A., Unal, A., Mulholland, J.A., Russell, A.G., 2005. Optimization-based source apportionment of PM2.5 incorporating gas-to-particle ratios. Environ Sci Technol 39, 3245-3254.

Mauderly, J.L., Chow, J.C., 2008. Health effects of organic aerosols. Inhal Toxicol 20, 257-288.

Melen, E., Nyberg, F., Lindgren, C.M., Berglind, N., Zucchelli, M., Nordling, E., Hallberg, J., Svartengren, M., Morgenstern, R., Kere, J., Bellander, T., Wickman, M., Pershagen, G., 2008. Interactions between glutathione S-transferase P1, tumor necrosis factor, and traffic-related air pollution for development of childhood allergic disease. Environ Health Persp 116, 1077-1084.

Miller, K.A., Siscovick, D.S., Sheppard, L., Shepherd, K., Sullivan, J.H., Anderson, G.L., Kaufman, J.D., 2007. Long-term exposure to air pollution and incidence of cardiovascular events in women. New Engl J Med 356, 447-458.

Moutinho, J.L., Liang, D., Weber, R., Sarnat, J., Russell, A.G., 2016. Characterization of Traffic Emissions Exposure Metrics in the Dorm Room Inhalation to Vehicle Emissions (DRIVE) Study, International Technical Meeting on Air Pollution Modelling and its Application. Springer, pp. 523-528.

Napelenok, S.L., Cohan, D.S., Hu, Y.T., Russell, A.G., 2006. Decoupled direct 3D sensitivity analysis for particulate matter (DDM-3D/PM). Atmos Environ 40, 6112-6121.

Nordling, E., Berglind, N., Melen, E., Emenius, G., Hallberg, J., Nyberg, F., Pershagen, G., Svartengren, M., Wickman, M., Bellander, T., 2008. Traffic-related air pollution and childhood respiratory symptoms, function and allergies. Epidemiology 19, 401-408.

Oakes, M., Baxter, L., Long, T.C., 2014a. Evaluating the application of multipollutant exposure metrics in air pollution health studies. Environ Int 69, 90-99.

Oakes, M.M., Baxter, L.K., Duvall, R.M., Madden, M., Xie, M.J., Hannigan, M.P., Peel, J.L., Pachon, J.E., Balachandran, S., Russell, A., Long, T.C., 2014b. Comparing Multipollutant Emissions-Based Mobile Source Indicators to Other Single Pollutant and Multipollutant Indicators in Different Urban Areas. Int J Env Res Pub He 11, 11727-11752.

Odman, M.T., Boylan, J.W., Wilkinson, J.G., Russell, A.G., Mueller, S.F., Imhoff, R.E., Doty, K.G., Norris, W.B., McNider, R.T., 2002. SAMI air quality modeling final report. Southern Appalachian Mountains Initiative, Asheville, NC.

Paatero, P., Tapper, U., 1994. Positive matrix factorization: A non‐negative factor model with optimal utilization of error estimates of data values. Environmetrics 5, 111-126.

Pachon, J.E., Balachandran, S., Hu, Y.T., Mulholland, J.A., Darrow, L.A., Sarnat, J.A., Tolbert, P.E., Russell, A.G., 2012. Development of outcome-based, multipollutant mobile source indicators. J Air Waste Manage 62, 431-442.

Pachon, J.E., Balachandran, S., Hu, Y.T., Weber, R.J., Mulholland, J.A., Russell, A.G., 2010. Comparison of SOC estimates and uncertainties from aerosol chemical composition and gas phase data in Atlanta. Atmos Environ 44, 3907-3914.

Parrish, D.D., 2006. Critical evaluation of US on-road vehicle emission inventories. Atmos Environ 40, 2288-2300.

Patton, A.P., Milando, C., Durant, J.L., Kumar, P., 2017. Assessing the Suitability of Multiple Dispersion and Land Use Regression Models for Urban Traffic-Related Ultrafine Particles. Environ Sci Technol 51, 384-392.

Pennington, A.F., Strickland, M.J., Klein, M., Zhai, X., Bates, J.T., Drews-Botsch, C., Hansen, C., Russell, A.G., Tolbert, P.E., Darrow, L.A., 2017a. Exposure to mobile source air pollution in early life and childhood asthma incidence: The Kaiser Air Pollution and Pediatric Asthma Study. Epidemiology.

Pennington, A.F., Strickland, M.J., Klein, M., Zhai, X.X., Russell, A.G., Hansen, C., Darrow, L.A., 2017b. Measurement error in mobile source air pollution exposure estimates due to residential mobility during pregnancy. J Expo Sci Env Epid 27, 513-520.

Pope, C.A., 3rd, Ezzati, M., Dockery, D.W., 2009. Fine-particulate air pollution and life expectancy in the United States. The New England journal of medicine 360, 376-386.

Poschl, U., 2005. Atmospheric aerosols: Composition, transformation, climate and health effects. Angew Chem Int Edit 44, 7520-7540.

Press, W.H., Rybicki, G.B., 1989. Fast Algorithm for Spectral-Analysis of Unevenly Sampled Data. Astrophys J 338, 277-280.

Querol, X., Viana, M., Alastuey, A., Amato, F., Moreno, T., Castillo, S., Pey, J., de la Rosa, J., de la Campa, A.S., Artinano, B., Salvador, P., Dos Santos, S.G., Fernandez-Patier, R., Moreno-Grau, S., Negral, L., Minguillon, M.C., Monfort, E., Gil, J.I., Inza, A., Ortega, L.A., Santamaria, J.M., Zabalza, J., 2007. Source origin of trace elements in PM

from regional background, urban and industrial sites of Spain. Atmos Environ 41, 7219-7231.

Reche, C., Querol, X., Alastuey, A., Viana, M., Pey, J., Moreno, T., Rodriguez, S., Gonzalez, Y., Fernandez-Camacho, R., de la Campa, A.M.S., de la Rosa, J., Dall'Osto, M., Prevot, A.S.H., Hueglin, C., Harrison, R.M., Quincey, P., 2011. New considerations for PM, Black Carbon and particle number concentration for air quality monitoring across different European cities. Atmos Chem Phys 11, 6207-6227.

Redman, J.D., Holmes, H.A., Balachandran, S., Maier, M.L., Zhai, X., Ivey, C., Digby, K., Mulholland, J.A., Russell, A.G., 2016. Development and evaluation of a daily temporal interpolation model for fine particulate matter species concentrations and source apportionment. Atmos Environ.

Riley, E.A., Banks, L., Fintzi, J., Gould, T.R., Hartin, K., Schaal, L., Davey, M., Sheppard, L., Larson, T., Yost, M.G., Simpson, C.D., 2014. Multi-pollutant mobile platform measurements of air pollutants adjacent to a major roadway. Atmos Environ 98, 492-499.

Riley, E.A., Gould, T., Hartin, K., Fruin, S.A., Simpson, C.D., Yost, M.G., Larson, T., 2016a. Ultrafine particle size as a tracer for aircraft turbine emissions. Atmos Environ 139, 20-29.

Riley, E.A., Schaal, L., Sasakura, M., Crampton, R., Gould, T.R., Hartin, K., Sheppard, L., Larson, T., Simpson, C.D., Yost, M.G., 2016b. Correlations between short-term mobile monitoring and long-term passive sampler measurements of traffic-related air pollution. Atmos Environ 132, 229-239.

Rowangould, G.M., 2013. A census of the US near-roadway population: Public health and environmental justice considerations. Transport Res D-Tr E 25, 59-67.

Sahinler, S., Topuz, D., 2007. Bootstrap and jackknife resampling algorithms for estimation of regression parameters. Journal of Applied Quantitative Methods 2, 188-199.

Salvi, S., 2007. Health effects of ambient air pollution in children. Paediatric respiratory reviews 8, 275-280.

Sarnat, J.A., Marmur, A., Klein, M., Kim, E., Russell, A.G., Sarnat, S.E., Mulholland, J.A., Hopke, P.K., Tolbert, P.E., 2008. Fine particle sources and cardiorespiratory morbidity: An application of chemical mass balance and factor analytical source-apportionment methods. Environ Health Persp 116, 459-466.

Schichtel, B.A., Husar, R.B., Falke, S.R., Wilson, W.E., 2001. Haze trends over the United States, 1980-1995. Atmos Environ 35, 5205-5210.

Seinfeld, J.H., Pandis, S.N., 2012a. Atmospheric chemistry and physics: from air pollution to climate change. John Wiley & Sons.

Seinfeld, J.H., Pandis, S.N., 2012b. Atmospheric chemistry and physics: from air pollution to climate change. John Wiley & Sons.

Shen, X.J., Sun, J.Y., Zhang, X.Y., Zhang, Y.M., Zhang, L., Che, H.C., Ma, Q.L., Yu, X.M., Yue, Y., Zhang, Y.W., 2015. Characterization of submicron aerosols and effect on visibility during a severe haze-fog episode in Yangtze River Delta, China. Atmos Environ 120, 307-316.

Shi, G.L., Li, X., Feng, Y.C., Wang, Y.Q., Wu, J.H., Li, J., Zhu, T., 2009. Combined source apportionment, using positive matrix factorization-chemical mass balance and principal component analysis/multiple linear regression-chemical mass balance models. Atmos Environ 43, 2929-2937.

Shi, G.L., Tian, Y.Z., Zhang, Y.F., Ye, W.Y., Li, X., Tie, X.X., Feng, Y.C., Zhu, T., 2011. Estimation of the concentrations of primary and secondary organic carbon in ambient particulate matter: Application of the CMB-Iteration method. Atmos Environ 45, 5692-5698.

Snyder, M.G., Venkatram, A., Heist, D.K., Perry, S.G., Petersen, W.B., Isakov, V., 2013. RLINE: A line source dispersion model for near-surface releases. Atmos Environ 77, 748-756.

Solomon, P.A., Crumpler, D., Flanagan, J.B., Jayanty, R.K.M., Rickman, E.E., McDade, C.E., 2014. US National PM2.5 Chemical Speciation Monitoring Networks-CSN and IMPROVE: Description of networks. J Air Waste Manage 64, 1410-1438.

Stanek, L.W., Sacks, J.D., Dutton, S.J., Dubois, J.J.B., 2011. Attributing health effects to apportioned components and sources of particulate matter: An evaluation of collective results. Atmos Environ 45, 5655-5663.

State of Georgia, U.S., 2013. Official Code of Georgia Annotated 40-6-51, 40.

Strickland, M.J., Darrow, L.A., Klein, M., Flanders, W.D., Sarnat, J.A., Waller, L.A., Sarnat, S.E., Mulholland, J.A., Tolbert, P.E., 2010. Short-term Associations between Ambient Air Pollutants and Pediatric Asthma Emergency Department Visits. Am J Resp Crit Care 182, 307-316.

Sturtz, T.M., Schichtel, B.A., Larson, T.V., 2014. Coupling Chemical Transport Model Source Attributions with Positive Matrix Factorization: Application to Two IMPROVE Sites Impacted by Wildfires (vol 48, pg 11389, 2014). Environ Sci Technol 48, 13021-13021.

Taylor, B.N., Kuyatt, C.E., 1994. Guidelines for evaluating and expressing the uncertainty of NIST measurement results, 1994 ed. U.S. Department of Commerce, Technology Administration, National Institute of Standards and Technology, Gaithersburg, MD.

United States, U., 1990. An Act to amend the Clean Air Act to provide for attainment and maintenance of health protective national ambient air quality standards, and for other purposes. US Government Printing Office.

Uysal, N., Schapira, R.M., 2003. Effects of ozone on lung function and lung diseases. Curr Opin Pulm Med 9, 144-150.

Venkatram, A., Isakov, V., Thoma, E., Baldauf, R., 2007. Analysis of air quality data near roadways using a dispersion model. Atmos Environ 41, 9481-9497.

Venkatram, A., Isakov, V., Yuan, J., Pankratz, D., 2004. Modeling dispersion at distances of meters from urban sources. Atmos Environ 38, 4633-4641.

Venkatram, A., Snyder, M.G., Heist, D.K., Perry, S.G., Petersen, W.B., Isakov, V., 2013. Re-formulation of plume spread for near-surface dispersion. Atmos Environ 77, 846-855.

Viana, M., Kuhlbusch, T.A.J., Querol, X., Alastuey, A., Harrison, R.M., Hopke, P.K., Winiwarter, W., Vallius, A., Szidat, S., Prevot, A.S.H., Hueglin, C., Bloemen, H., Wahlin, P., Vecchi, R., Miranda, A.I., Kasper-Giebl, A., Maenhaut, W., Hitzenberger, R., 2008. Source apportionment of particulate matter in Europe: A review of methods and results. J Aerosol Sci 39, 827-849.

Wang, L.T., Wei, Z., Yang, J., Zhang, Y., Zhang, F.F., Su, J., Meng, C.C., Zhang, Q., 2014. The 2013 severe haze over southern Hebei, China: model evaluation, source apportionment, and policy implications. Atmos Chem Phys 14, 3151-3173.

Wang, M., Sampson, P.D., Hu, J.L., Kleeman, M., Keller, J.P., Olives, C., Szpiro, A.A., Vedal, S., Kaufman, J.D., 2016. Combining Land-Use Regression and Chemical Transport Modeling in a Spatiotemporal Geostatistical Model for Ozone and PM2.5. Environ Sci Technol 50, 5111-5118.

Wang, X.L., Watson, J.G., Chow, J.C., Gronstal, S., Kohl, S.D., 2012a. An Efficient Multipollutant System for Measuring Real-World Emissions from Stationary and Mobile Sources. Aerosol Air Qual Res 12, 145-160.

Wang, Y.G., Hopke, P.K., Xia, X.Y., Rattigan, O.V., Chalupa, D.C., Utell, M.J., 2012b. Source apportionment of airborne particulate matter using inorganic and organic species as tracers. Atmos Environ 55, 525-532.

Watson, J.G., Chow, J.C., Lowenthal, D.H., Chen, L.W.A., Shaw, S., Edgerton, E.S., Blanchard, C.L., 2015. PM2.5 source apportionment with organic markers in the

Southeastern Aerosol Research and Characterization (SEARCH) study. J Air Waste Manage 65, 1104-1118.

Watson, J.G., Chow, J.C., Wang, X.L., Kohl, S.D., Chen, L.W.A., Etyemezian, V., 2012. Overview of Real-World Emission Characterization Methods. Dev Environm Sci 11, 145-170.

Watson, J.G., Cooper, J.A., Huntzicker, J.J., 1984. The Effective Variance Weighting for Least-Squares Calculations Applied to the Mass Balance Receptor Model. Atmos Environ 18, 1347-1355.

Weber, R.J., Guo, H.Y., Russell, A.G., Nenes, A., 2016. High aerosol acidity despite declining atmospheric sulfate concentrations over the past 15 years. Nat Geosci 9, 282-+.

Wesson, K., Fann, N., Morris, M., Fox, T., Hubbell, B., 2010. A multi-pollutant, risk-based approach to air quality management: Case study for Detroit. Atmos Pollut Res 1, 296-304.

West, J.J., Cohen, A., Dentener, F., Brunekreef, B., Zhu, T., Armstrong, B., Bell, M.L., Brauer, M., Carmichael, G., Costa, D.L., 2016. What We Breathe Impacts Our Health: Improving Understanding of the Link between Air Pollution and Health. Environ Sci Technol.

Wilton, D., Szpiro, A., Gould, T., Larson, T., 2010. Improving spatial concentration estimates for nitrogen oxides using a hybrid meteorological dispersion/land use regression model in Los Angeles, CA and Seattle, WA. Sci Total Environ 408, 1120-1130.

Zeger, S.L., Dominici, F., McDermott, A., Samet, J.M., 2008. Mortality in the Medicare Population and Chronic Exposure to Fine Particulate Air Pollution in Urban Centers (2000-2005). Environ Health Persp 116, 1614-1619.

Zhai, X., Mulholland, J.A., Russell, A.G., Holmes, H.A., 2017. Spatial and temporal source apportionment of PM 2.5 in Georgia, 2002 to 2013. Atmos Environ 161, 112-121.

Zhai, X., Russell, A., Sampath, P., Mulholland, J., Kim, B.-U., Kim, Y., D'Onofrio, D., 2016. Calibrating R-LINE Model Results with Observational Data to Develop Annual Mobile Source Air Pollutant Fields at Fine Spatial Resolution: Application in Atlanta. Atmos Environ.

Zhang, R.Y., Wang, G.H., Guo, S., Zarnora, M.L., Ying, Q., Lin, Y., Wang, W.G., Hu, M., Wang, Y., 2015. Formation of Urban Fine Particulate Matter. Chem Rev 115, 3803-3855.

Zhang, W., Capps, S.L., Hu, Y., Nenes, A., Napelenok, S.L., Russell, A.G., 2012. Development of the high-order decoupled direct method in three dimensions for

particulate matter: enabling advanced sensitivity analysis in air quality models. Geosci Model Dev 5, 355-368.

Zheng, M., Cass, G.R., Schauer, J.J., Edgerton, E.S., 2002. Source apportionment of PM2.5 in the southeastern United States using solvent-extractable organic compounds as tracers. Environ Sci Technol 36, 2361-2371.

Zou, Y., Wang, Y., Zhang, Y., Koo, J.H., 2017. Arctic sea ice, Eurasia snow, and extreme winter haze in China. Sci Adv 3, e1602751.